THIN FILM NANOFIBROUS COMPOSITE ELECTROSPUN MEMBRANE FOR SEPARATION OF SALTS

SATINDERPAL KAUR
(BSc (Hons), MEng, NUS)

A THESIS SUBMITTED
FOR THE DEGREE OF DOCTOR OF PHILOSOPHY
DEPARTMENT OF MECHANICAL ENGINEERING
NATIONAL UNIVERSITY OF SINGAPORE
2011

ACKNOWLEDGEMENTS

I would like to express my deepest gratitude and great respect to my supervisor Prof. Seeram Ramakrishna, for his inspiration, encouragement and most importantly his faith in me. I greatly appreciate his detailed and constructive comments, and for his important support throughout this work

I would also like to express my deep and sincere gratitude to Emeritus Prof. Takeshi Matsuura from the University of Ottawa. It is an honour for me to have worked with such an important and well known researcher in the field of membrane technology. He had foreseen the potential for electrospun material to make excellent membranes in liquid filtration. I have valued all of his suggestions and comments during our journal preparations. I am also deeply grateful and indebted to Dr. Subramanian Sundarrajan for his valuable and extensive discussions around my work. I would also like to thank Dr. Dipak Rana from the University of Ottawa for his discussions on Surface Modifying Macromolecules.

I am highly indebted to Dr. Renuga Gopal, a very dear friend whom I have known long before my PhD thesis. I have been blessed with a fantastic friend and she has been a true inspiration to my work. My PhD duration was made fun with the presence of Dr. Molamma Prabhakaran who became a close friend. I have thoroughly enjoyed our lunches and tea breaks. She has always motivated and encouraged me whenever I have hit a road block in experiments. I am also grateful to Teo Wee Eong whom I have enjoyed discussing my research and exciting findings. Steffen Ng, Charlene Wang and Karen Teo have made their administrative support available in a number of ways which I can't thank enough. It would be a pleasure to thank my other entire laboratory mates whom who have supported me through my PhD duration.

This thesis would not have been possible without the support and love of my parents Santokh Singh and Charanjit Kaur and my siblings Pal, John and Kiran. They have been extremely proud of my decision to commence this PhD and constantly encouraged me to complete it. I suspect they have been eagerly waiting for a family portrait with me in the PhD gown! And of course I have to thank my lovely nephews Jastin, Royceton and Triston whom I have enjoyed playing with after a hard day of experimental work.

This might sound outrageous but I would like to thank my scrambler bike, XLR HONDA FQ9572X that has 'ferried' me to and fro home and laboratory. Without it, I could not have carried out my many experiments which required me to stay late hours in the laboratory. I am deeply saddened that I had to part away with it on the 25th of November 2009 when I met with a terrible road accident which almost took my life and left me physically challenged for almost 5 months. It had been the toughest and most torturous part of my life. After this incident I never failed to thank god for every wonderful day.

This thesis would have been left incomplete after the accident without my husband, Rav Bola's, love, faith and encouragement. He was my pillar of support and strength through the most difficult part of my life. I must also thank my in laws Mr. and Mrs. Bola who have been such sweethearts as they looked after me throughout my dissertation writing. I concluded writing this thesis in England, a place totally new to me and they warmly embraced me in their home and never let me feel alone. I enjoyed our daily 4 pm Deal or No deal T.V programme which I used to digress my mind away from work. I also have to thank my sister-in-laws Suki and Chris for being very supportive and they were sincerely happy whenever I completed a journal paper.

I am extremely grateful to yoga.org.nz for supplying online DVDs on their carefully planned weekly exercises. The daily exercise routine was responsible for my revitalised energy, spiritual and calm mind which helped me conclude this thesis.

I wish to express my gratitude to the Environment and Water Industry (EWI) Development Council (Govt. of Singapore) and for the fellowship for research work at University of Ottawa.

Most importantly I would like to thank Waheguru (the almighty) for bringing me this far. Without HIM, I would not have been alive to complete this thesis.

TABLE OF CONTENTS

SUMMARY

Nanofibers offer unique properties like high specific surface area (ranging from 1-100 m^2/g depending on the diameter of fibers and intra-fiber porosity), good interconnectivity of pores and potential to incorporate active chemistry or functionality on nanoscale. They have been commercially utilised in air filtration for 20 years. However the use of nanofibers in liquid separation is still at its infancy and there is much anticipation of its usefulness as a liquid filter. Hence the motivation of this thesis was to explore the use of electrospun nanofibrous membrane (ENM) in liquid filtration. The main objective of this thesis was to investigate how polymeric material, surface architecture and subsequently pore-size of (ENMs) influence its separation performance specifically in nanofiltration.

Interfacial polymerization (IP) technique (formation of a thin film at the interface between two immiscible solvents, aqueous and organic phase, which contain the reactants) was carried out on the surface of ENM so as to introduce a thin polyamide layer. Through this modification, the microfiltration ENM now functions as a nanofilter. Two different polymeric materials were studied, namely poly(vinylidene) fluoride (PVDF) and polyacrylonitrile (PAN). When PVDF was electrospun, the conventional way of carrying out IP was a challenge (Chapter 4) as PVDF was hydrophobic. Several approaches to fabricate a polyamide layer on the surface of the self-supporting ENM were carried out. A uniform polyamide layer can be successfully produced by carrying out a reverse of the IP process. This approach allowed the separation of 81% $MgSO_4$ and 67% NaCl at a pressure of 70 psig under a dead-end filtration set up. The fluxes attained were low (0.5 L/m^2h). It was realised that a hydrophobic polymer influenced the formation of a thick polyamide layer (27 μm) which resulted in low flux and hence this was highly unattractive.

The design of the membrane structure was improved by adopting a three-tier composite structure (Chapter 5) and subsequent separations were performed on a cross-flow set up. This structure comprised of the polyamide layer which was formed over PAN ENM that has been electrospun directly on a backing material (BM). The conventional way of carrying out IP was feasible on PAN because it is hydrophilic. In addition, the polyamide layer produced was very thin such that imprints of the nanofibers beneath can be observed. Hot-pressing improved the adhesion between the PAN ENM and the BM before the IP process was carried out. Without this treatment, the membrane was able to reject 86.5% $MgSO_4$ at a flux of 102 L/m^2h at 70 psig. The membrane failed to perform at pressures greater than 130 psig. By hot-pressing the ENMs before the IP process, not only was the membrane able to separate the salt at higher pressures (up to 190 psig), the overall composite membrane had reduced surface roughness. A membrane with a smoother surface has less tendency to foul. The treated membrane had fluxes 3 folds greater than commercial membrane, NF 90 but with rejections compromised between 8-12%.

Further experiments were conducted to relate the surface architecture, pore-size and thickness of the ENM layer to separation of salt (Chapter 6). It was hypothesized that the fiber size of the electrospun membrane will play an important role in the separation efficiency of salt ions. This is based on the fact that separation efficiency is dependent on the membrane pores, which can be altered by varying the nanofiber size. Different fiber sizes were obtained by varying the concentration of PAN solution (namely 4, 6, 8 and 10 wt%) to explore the interplay between electrospun fiber size and rejected salt ions. As the fiber size decreases, the rejection of electrolytes improved but with a reduction of flux. At 10 wt% of PAN (ENM-10) the membrane failed to separate at higher pressures, indicating that larger fiber size ENM was not able to support the thin film. However, one can consider to use this membrane at

lower pressures to separate slightly higher molecular weight solutes. At 8 wt% of PAN (ENM-8), the developed thin film nanofibrous composite (TFNC) membrane, TFNC-8, was able to separate 89% of $MgSO_4$ with a flux of 220 L/m^2h at 190 psig. By decreasing the concentration further to 6 wt% (TFNC-6) and 4 wt% (TFNC-4), the rejection of $MgSO_4$ improved by 3% and 6% respectively but the flux values dropped by half. This was because as the fiber size decreased, the packing density of the fibers increased which led to a decreased pore-size and pore-size distribution. This subsequently resulted in a flux drop. Closed packed fibers favoured the uniform formation of the thin film, which may adopt a more cross-linked and packed (chain stiffness) structure with decreased chain mobility, thereby contributing to an improved rejection but a decrease in the permeate flux.

When the overall cross-sectional thickness of the nanofiber in contact with the polyamide layer (TFNC-E) was reduced together with the fiber size (42 nm), the average permeate flux and rejection of 2000 ppm NaCl was determined as 102.3 L/m^2h and 83.4% respectively at 190 psig. The permeate flux and rejection values of TFNC-E improved by 38.3% and 6.6% respectively when compared to TFNC-4. This was due to a decrease in the hydraulic resistance of the nanofibrous support with the polyamide layer. The separation efficiency of TFNC-E was also compared to a commercial membrane NF 270. The rejection of NaCl on TFNC-E was 30.5% higher than NF 270 but the flux was 48.5% lower. However by increasing the fiber size in the case of TFNC-8, it has NaCl rejection comparable to NF 270 and its flux was 24.4 % higher than NF 270.

Besides separation results, surface roughness, morphology and mechanical properties of the various membranes were also studied. Contrary to popular belief in membrane science, IP could take place on ENM surface even though the top layer possesses comparatively large

pores as compared to conventional supports. Conventional supports (such as asymmetric phase inverted membranes) should have pore-sizes less than 0.20 µm so as to adequately hold the polyamide layer. This study shows that besides pore-size, the surface architecture and surface area also plays an important role in supporting the polyamide layer. In addition, the type of polymer used in fabricating the ENM had a major influence in the way IP was carried out. Hydrophobic material prevented the membrane to easily retain the reagent present in the aqueous phase during the IP process and hence a hydrophilic ENM is preferred. By carefully optimising the fiber size and thickness of the ENM layer as well as the reagents used to form the thin film, both high fluxes and rejection rates can be achieved at low pressures - hence the development of energy efficient membranes. In addition, a chapter (Chapter 7) has been dedicated to convert a hydrophobic material into a hydrophilic by introducing surface modifying macromolecules on the surface of ENM. This modified membrane achieved high flux at low pressure.

This study shed new insight on the role of ENMs as a support membrane and overall performance of the composite membranes, which may contribute significantly towards the development of better nanofiltration membranes. This thesis would pave way for many scientist and engineers in the water filtration domain.

LIST OF PUBLICATIONS

Journal Publications:

1) **S.Kaur**, D. Rana, T. Matsuura, S. Sundarajjan, B. Subramanian, S. Ramakrishna

Preparation and characterization of surface modified electrospun membranes for higher filtration lux

J.Membr.Sci., 2012, 390, p. 235-242

2) **S.Kaur**, S.Subramaninan, S.Ramakrishna

Influence of electrospun fiber size on the separation efficiency of thin film nanofiltration composite membrane

J.Membr.Sci., 2012, 392, p.101-111

3) **S. Kaur**, S.Subramanian, R.Gopal, S.Ramakrishna

Characterization of polyamide composite membranes based on electrospun non-woven porous support for salt separation

J.Appl.Poly.Sci., DOI: 10.1002/app.36375

4) **S. Kaur**, B. Barhate, S.Subramanian, T.Matsuura, S.Ramakrishna

Hot-pressing of electrospun membrane composite and its influence on separation performance on thin film composite nanofiltration membrane

Desalination, 2011, 279 (1-3), p. 201-209

5) T. Matsuura, C. Feng, D. Rana, G.Singh, R.Gopal, **S.Kaur**, R.S. Barhate, S.Ramakrishna

Development of novel membranes based on electro‐spun nanofibers and their application in liquid filtration, membrane distillation and membrane adsorption

Membrane, 2010, 35 (3), p. 119-127

6) C. Feng, K.C. Khulbe, T. Matsuura, R.Gopal, **S.Kaur,** S.Ramakrishna, M.Khayet

Production of drinking water from saline water by air-gap membrane distillation using polyvinylidene fluoride nanofiber membrane

J.Membr.Sci., 2008, 311, p.1–6

7) **S. Kaur**, R. Gopal, W.J. Ng, S. Ramakrishna, T. Matsuura

Next generation fibrous media for water treatment

MRS bulletin, 2008, 33, p. 21-26

Book Chapter:

1) W.E. Teo, **S. Kaur**, S.Ramakrishna

Chapter 19: Electrospun polymer nanocomposites fibres: fabrication and physical properties

In Physical properties and applications of polymer nanocomposites

Edited by S C Tjong and Y-W Mai, Woodhead Publishing Limited, 2010

Conferences (Oral):

1) **S. Kaur**, S. Ramakrishna

   Electrospun nanofibrous nanofiltration membrane

   Network Young Membrains (NYM 2009), Sept. 3-4, Meze – Montpellier, France

2) **S.Kaur**, D.Rana, G.Singh, B.A. Taboush, T. Matsuura, S.Ramakrishna

   Modified electrospun membranes for higher filtration flux

   North American Membrane Society (NAMS) 2009, June 20-24, Charleston, South Carolina USA

3) S. Ramakrishna, T. Matsuura, W.J. Ng, **S. Kaur**, G. Singh, R. Balamurugan

   Development of low-pressure, high-flux UF and NF membranes based on electrospun nanofibers for water treatment

   EWIDC-IAP, June 27, Pan Pacific, Singapore

4) S. Ramakrishna, D. Pliszka, A.N.S. Nair, **S. Kaur**, W.E. Teo

   Quest for cleaner water and energy using nature's basic building blocks

   International Nanofiber Symposium 2009, June 18-19 Tokyo Institute of Technology, Tokyo, Japan

5) T. Matsuura, C. Feng, K.C. Khulbe, D. Rana and G. Singh, R. Gopal, **S. Kaur**, S. Ramakrishna

   Development of novel membranes based on electro-spun nanofibers and their application in liquid filtration, membrane distillation and membrane adsorption

The 7th International Conference on Membrane Science & Technology, May 12-15, Kuala Lumpur, Malaysia

6) S. Ramakrishna, W.E. Teo, L Teng, G. Singh, R.S. Barhate, J. Rajan, D. Pliszka, **S. Kaur**

Electrospinning what is new? Nanofibers for the 3rd Millenium

Nano For Life, Liberec: Elmarco (Keynote paper),11 - 12 Mar 2009, Prague, Czech Republic

7) G. Singh, **S. Kaur**, S. Ramakrishna, Ng W.J., T. Matsuura

Properties and Potential of Polymeric Nanofiber Membranes for Liquid Filtration Applications

ICOM 2008, July 12-18, 2008, Honolulu, Hawaii USA

8) S. Ramakrishna, W.J. Ng, T. Matsuura, G. Singh, **S. Kaur**

Electrospun Nanofiber Membranes for Water Treatment

SIWW-International Advisory Panel Presentation, June 27, 2008, Singapore

Conferences (poster):

1) **S.Kaur**, G.Singh, T. Matsuura, S.Ramakrishna

Composite membranes based on electrospun non-woven porous support for salt separation

Euromembrane 2009, Sept. 6-10, Montpellier, France – **Received the best technical poster award**

List of Figures

List of Tables

CHAPTER 1

INTRODUCTION

1.1. Fibrous media in separation technology

Throughout the history of filtration and separation processes, many variants of fibrous media have been used to improve the quality of water. Fibrous filter media can take the form of fine synthetic, mineral or natural fibers and can be classified further as woven (ordered) and non-woven (non-ordered) filters where non-wovens are more commonly used in filtration technology [Dickenson 1992]. Non-wovens are uniquely engineered fibrous materials, designed to offer high filtration performance and permeable media. The fibers in a non-woven structure, compared to a woven, are arranged in a more open structure which allows effective use of individual fibers for filtration. The demand for high performance, energy saving, recyclability and light weight gave non-wovens an advantage over other filter media [Bitz 2001]. Non-wovens have two main functions in liquid filtration: (1) to filter and/or separate phases/components of a fluid, or (2) as a backing material during liquid filtration.

Non-woven filters are used for liquid filtration in water treatment, water desalination, and water discharge treatment plants. They also have applications in drinking water filtration, medical filtration processes, pharmaceutical processes, and as swimming pool filters [Hutten 2007].

1.2. Methods of fabrication

These structures can be made using two distinct methods: dry formed and wet laid. There are four major dry formed techniques used to create fibrous filters and they are air laid, dry laid, spunbonded and melt-blown processes [Hutten 2007]. Air laying process disperses fibers into a fast moving air stream and by means of pressure or vacuum these fibers are condensed onto a moving screen to form a fibrous web while dry laying utilizes a carding machine. Spunbonding involves the extrusion of molten polymer through a die block comprising of a spinneret with several thousand drilled holes. Conversely in melt-blowing molten polymer is extruded and drawn with heated high velocity air.

1.3. Advantages of non-woven filter media

The main attraction of non-woven filter media is its extensive fibrous network, absent in other forms of filter media such as phase-inversed membranes. The fibrous network provides non-woven media with a high internal surface area and hence enormous dirt loading capacity compared with phase-inversed membranes. This makes them ideal candidates for high efficiency filter media, both in liquid and air filtration applications.

In water treatment, non-woven filter media are predominantly used as a pre-filter, which aids to take most of the load off downstream separation units, such as Nanofiltration (NF) and Reverse Osmosis (RO) membranes. Most of the contaminants are removed by the prefilter whereas the final membrane serves as the ultimate barrier trapping all particles leaking through the prefilter-including fibers which “sluff-off” the fibrous media due to “media-

migration". The smaller the fiber diameter used in the prefilter, the greater the surface area for adsorption of particles and the better the retention of small particles.

1.4. Limitations of non-woven filter media

Despite having advantages of low cost, high dirt holding capacity and high filtration efficiency, non-woven media have certain limitations. The present non-woven media can only reject particles of a larger size range. This is because the overall average pore-size generated by the micron size fiber is considerably large. Hence this filter is limited to the removal of particles between 10 and 200 μm in diameter. In addition, particles are easily trapped and lodged within the tortuous path of the non-woven media. They are not easily cleaned and generally reusability is not an option. Non-woven filter media are not as effective as asymmetric membranes in removing particles less than 10 μm. Furthermore, the particle retention rates are not defined as precisely as with membranes or woven filters due to the random structure of the depth media[1] [Vogt 2005].

In addition, if a fibrous media is used to separate particles less than 10 microns in diameter, a thicker fibrous layer is required to reduce the overall average pore-size of the media. However, having a thicker layer may lead to compaction with prolonged use and will ultimately result in a decline in flux. Thus the beneficial intrinsic porous network is compromised. Nevertheless these fibrous media is mechanically robust and hence it is usually used as a substrate to support porous membranes.

[1] Depth media means filter cross section structure is utilized throughout the filtration process

1.5. Next generation fibrous media: electrospun fibers

The main driving force in the filtration industry is the requirement for finer and finer degrees of filtration whatever the application [Sutherland 2006]. In air filtration, the requirement for finer filtration is already being met by media with finer fibers. In liquid filtration a leading application is the ability to separate bacteria, viruses and particulate. In liquid filtration, this need is being increasingly met by membrane processes which have expanded their range of applications in the microfiltration range to meet the need. Low throughputs from the membrane based filtration processes driving the material scientists to explore highly porous media with finer fibers.

With the advent of nanotechnology, it is now possible to produce polymeric nanofibers and it is expected that the shortcomings of non-woven filter media discussed previously can be reduced or overcome [Kaur 2008]. Nanofiber has become a very popular term today and is rapidly reaching 'buzz-word' status in filtration technology. In a broad sense, nanofibers are fibers with diameters less than 1 micron. It is best to make comparison with different types of fibers to realize the size scale of nanofiber. For instance, cotton fiber has a diameter of 18,000 nm, human hair is approximately 30,000 nm, ordinary meltblown fibers are 5,000 nm, spunbonded fibers are 25,000 nm, bacteria are typically around 900 nm, while viruses are around 20 nm [Ward 2005]. In comparison, nanofibers are one-tenth the size of the smallest meltblown fibers and bigger than components such as ions and viruses. Nanofibers can be produced by a simple and versatile technique called electrospinning, which will be discussed in depth in the next chapter.

1.6. Nanofibers in air filtration

It has been shown, in air filtration applications, that under the same operating conditions, a thin layer of nanofibers has far superior filtration efficiency compared to larger fiber size. The Donaldson Company was the first to realize the commercial value of electrospinning by taking advantage of the enormous availability of the specific surface of electrospun fibers and the ultrafine nature of the fibers. They introduced the Ultra-Web® cartridge filter for industrial dust collection in 1981 and more recently the Hollingsworth & Vose Company introduced the Nanoweb® for automotive and truck filter applications [Frank 2006]. Nanofibers have been extensively used for air filtration in commercial, industrial and defense applications for more than 20 years. They have been shown to deliver improved filter life, increased contaminant holding capacity and enhanced filtration efficiency [Kosmider 2002]. However the use of nanofibers in liquid separation is still at its infancy and there is much anticipation of its usefulness as a liquid filter [Seeram 2005, Thavasi 2008].

1.7. Stumbling block

As this PhD quest begun, it was conceived that the use of ENMs in liquid filtration was limited as they have been classified only as microfiltration membranes. Their use beyond this stage has yet to be explored, with attractive attributes to tap on. It will take the next decade or two to realize if nanofiber liquid filter media is a fantasy or the future. More fundamental research on this filter has to be performed to realize its full potential and may undoubtedly reveal more surprises of its function as a filter. It is the interest of this thesis to bring this filter to the next membrane process stage such as nanofiltration.

To realize the potential of electrospun fibers in liquid separation technology an in depth knowledge is needed to evaluate and relate its structural properties to separation performance. When the fiber size is reduced by several hundred to thousand times—higher filtration efficiency is anticipated. This has been evident in air filtration applications where nanofibers have already been commercially used. However the use of nanofibers in liquid filtration (at the higher end of the filtration scale) at a commercial level is not realized as there is limited study of its property and efficiency in this field. Will the fiber size have similar influence in separation efficiency as an air filter? The structure of the filter influences the separation and permeation mechanism and hence a fundamental understanding of the influence of fiber size as well as thickness of the membrane layer on separation performance is essential and imperative. With this understanding, it will be easier to predict filter performance for a particular water treatment application and perhaps offer solutions to current state- of- art membrane technology. It is in this light that the proposal is made.

1.8. Objective

The main objective of this study is to:

Investigate how the polymeric material, surface architecture and subsequently pore-size of electrospun nanofibrous membrane influences its separation performance in nanofiltration.

This will be achieved based on the following approach:

- Suitable polymeric materials used in the membrane field are selected for electrospinning

- Electrospinning parameters are optimized to generate different fibers and architectures
- Interfacial polymerization is carried out on the surface of ENM to transform it into a nanofiltration membrane i.e thin film nanofibrous composite (TFNC) membranes. This was performed to explore the feasibility of using the ENMs beyond their microfiltration stage and also to tap onto the ENMs intrinsic and advantages features.
- Characterization of ENMs to evaluate its properties and performance and to relate process parameter-structure-performance relationship.
- The nanofiltration performances of the developed TFNC membranes were determined by salt rejections and flux throughput of NaCl, Na_2SO_4, $CaCl_2$ and $MgSO_4$ at different applied cross flow filtration pressure.

1.9. Significance of this research

The direct impact of this study is to the field of non-woven technology and membrane science. If successful this membrane can be considered as a new or alternative material for liquid separation and would pave way for further research and scale up. The thesis also contributes to the electrospinning field by demonstrating the use of surface modification techniques in creating a desired application. Collectively, this research will provide valuable insights into the influence of electrospun nanofiber architecture in water separation technology which will be instrumental in the successful implementation of ENMs for water treatment applications.

CHAPTER 2

LITERATURE REVIEW

2.1. Electrospinning

Conventional fiber synthesis techniques of wet, dry, melt and gel- spinning are capable of producing polymer fibers with diameters down to the micrometer range only [Sawicka 2006]. With the emergence of nanotechnology, it was realized that electrospinning, also known as electrostatic spinning, is capable of fabricating fibers from sub-micron to nanoscale. Its relatively non-material specific process makes it highly versatile. It is a century old technique that went through a series of discoveries, understanding and technological developments which eventually led it to a commercial success in 1981 through the invention of an air filter Ultra-Web® by Donaldson.[2] This filter comprised of electrospun nylon nanofibers (200-500 nm) sandwiched in traditional non-woven support. The history of how electrospinning started is rather interesting and a brief overview is shared in the next section.

2.1.1. History of electrospinning

William Gilbert, a British natural philosopher, made the first systematic observation of the deformation of a drop of liquid in an electric filed [Gilbert 1600]. He observed that when a charged piece of amber[3] was held next to a water drop, it will take a conic form. It was Geroge Mathias Bose who observed that drops of water would disperse under the influence of electrostatic forces, the phenomenon which these days referred as electrostatic spraying or

[2] www.ultrawebisalwaysbetter.com

[3] a pale yellow fossil resin of vegetable origin generally translucent, brittle, an excellent insulator and capable of gaining a negative electrical charge by friction.

electrospraying [Bose 1745]. The term electrospinning was then coined when viscous solutions were used and formation of jets was observed rather than small drops from a liquid. In 1902 John F. Cooley patented an apparatus for dispersing fluids [Cooley 1902] where an electrode was employed which indirectly charged a fluid running out from a small nozzle and eventually causing the fluid to disperse. In 1882 Lord Rayleigh predicted the amount of charge needed to overcome the surface tension of a drop of fluid [Peters 1980]. This study enabled John Zeleny [Zeleny 1914] to perform a series of systematic studies that further led to the understanding that the electrospraying process can be further divided into several domains depending on the applied voltage. Amongst one of these domains, a jet would form at the apex of a conic drop. His use of an electrode in direct contact with the solution completed the development of the basic electrospinning apparatus.

Anton Formhals subsequently patented electrospinning as a possible fiber fabrications process (production of artificial yarns) [Formhals 1934]. Charles L. Norton patented electrospinning from a polymer melt during the same period [Norton 1936]. However, it did not gain significant industrial importance due to poor understanding and control of the process. Also the development of new polymers like nylon and other fiber production techniques made electrospinning as unimportant. It took another 30 years and the pivotal works of Taylor [Taylor 1964] to spark interest into this field again. He provided a theoretical explanation for the formation of the cone shaped drop, since known as the Taylor cone.

2.1.2. Electrospinning process

A typical electrospinning set up is illustrated in Figure 2.1. The process, in its simplest form, is comprised of a syringe which is filled with the polymer solution and attached to a syringe

pump, a spinneret with a tiny nozzle attached to the syringe, a collector, a DC voltage supply in the kV range, an electrode attached to the polymer solution or the nozzle and an electrode attached to the collector; the collector is grounded in most cases. The electrospinning process comprises of four stages namely: (a) initiation of the jet by Taylor cone formation, (b) thinning of the straight jet, (c) jet propagation in the bending instability region and (d) solidification and collection of fibers.

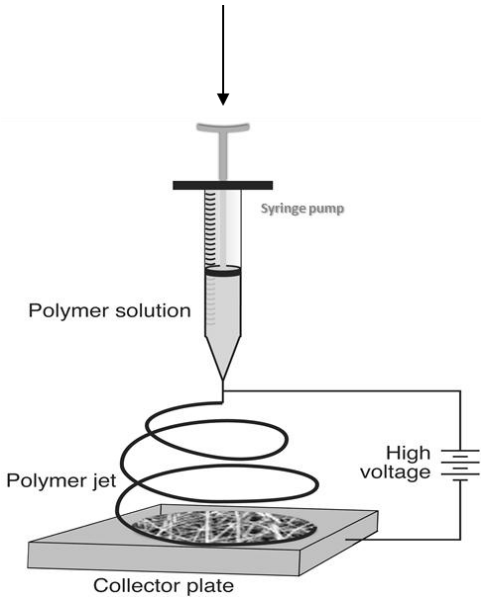

Figure 2.1. Schematic diagram of electrospinning setup

As understood from the history above, charge repulsion is the main driving force in electrospinning to stretch the polymer solution or melt from the tip of the spinneret into nanofibers. A high voltage (typically more than 10 kV) is applied directly to the solution via the use of an electrode so as to transfer sufficient charges into the solution for stretching to occur. A metallic spinneret may serve as the electrode or a separate electrode may be immersed directly into the solution. Once a critical voltage is reached which varies for different solutions and spinning conditions, a highly charged electrospinning jet (initiated by the formation of a Taylor cone) will erupt from the tip of the spinneret. The polymer solution initially propagates along a straight line. At a distance from the Taylor cone the jet becomes

instable and starts bending from the axis of the straight jet causing the jet to form increasingly long (growing) and thin (stretching) loops as the loop diameter and circumference increases. Smaller loops form around the path charted by the first level of looping. This cycle continues, with diminishing scale, as long as the charge on the jet has sufficient force to overcome the surface tension and viscoelastic forces. The uniqueness of this process as compared to mechanical drawing is that bending allows for very large elongation to occur in a small region of space.

As the electrospinning jet continuously stretches and accelerates towards a collector, the solvent evaporates to form solidified nanofibers. The repulsive forces between the charges carried with the jet causes every segment of the jet to lengthen continuously along a changing path until the jet solidifies. Due to the charges carried by the spinning jet, it will accelerate towards a region of neutral charges or of an opposing charge where it finally ceases and deposit as fibers. Generally, an electrically earthed target or collector is used to collect the resultant fibers. A point to note is that the solution must have sufficient viscosity for it to be stretched without breaking up into droplets.

2.1.3. Electrospinning parameters

There are three main parameters that affect the formation of fibers from the polymer solutions: (a) solution properties, (b) processing conditions and last but not least (c) ambient conditions. Each of these categories is influenced by several other factors where each parameter is closely related to each other. For example, the change of polymer concentration, molecular weight and solvent composition affects solution viscosity [Huang 2003]. A complete understanding of all factors and the interactions between them is necessary and

important. By controlling the process parameters one can optimize the fiber size and can create a variety of morphologies such as beaded fibers, yarns, porous fibers, hollow fibers, ribbon fibers, branched fibers, helical fibers etc. Some of these structures are represented in Figure 2.2.

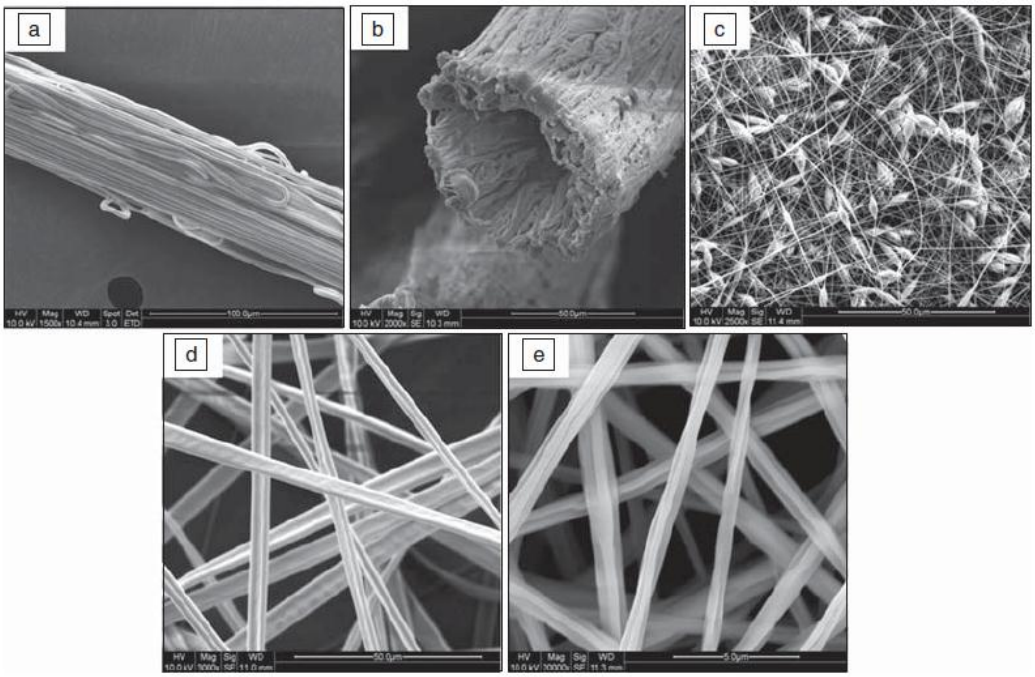

Figure 2.2. SEM micrographs of (a) yarn, (b) hollow yarn, (c) beaded fibers, (d) smooth ribbon fibers, (e) rough fibers [Kaur 2008]

These set of parameters influence the formation of various polymer fibers differently. One set of processing conditions of a particular polymer cannot be used for another polymer. Hence the processing parameters have to be optimized separately for each polymer [Seeram 2005]. A few key process parameters in each category that are known to have significant impact on the fiber morphology will be discussed.

2.1.3.1. Solvent conditions

Parameters of solution properties include polymer molecular weight, polymer concentration, polymer solubility in solvent, solution conductivity, solution viscosity and solvent surface tension, dielectric properties and boiling point.

A suitable solvent is required to dissolve the polymer and the viscosity and surface tension of the resultant solution must neither be too large to prevent the jet from forming nor too small to allow the polymer solution to simply drain from the needle tip. The vapour pressure of the solvent should be high enough to allow quick evaporation before dry fibers are collected and not too high, such that the fibers harden before it reaches the nanometer range. Solution viscosity is a function of polymer concentration as well as molecular weight (the number of chain entanglements within a polymer). A higher viscosity is associated with a greater interaction between the solvent and polymer molecules and when the solution is stretched under the influence of the charges, the solvent molecules tend to spread over the entangled polymer molecules thus reducing the tendency for the solvent molecules to come together under the influence of surface tension.

The applied charges on the polymer solution must be high enough to overcome the surface tension of the solution. Surface tension has the effect of decreasing the surface area per unit mass of a fluid. As the jet accelerates from the tip of the needle to the collector, the solution is stretched. During the stretching of the polymer solution, it is the entanglement of the molecule chains that prevents the electrically driven jet from breaking up thus maintaining a continuous solution jet. If the viscosity is not high enough then the surface tension of the solution may cause the solution to breakup into droplets and this process is called

electrospraying [Morozov (1998), Christanti (2001), Shummer, 1983]. Surface tension has also been attributed to the formation of beads on the elecrospun fibers. Surface tension of a polymer solution can be reduced by employing solvents such as ethanol [Fong 1999] which has low surface tension or adding surfactants to the solution [Zeng 2003].

Too low a polymer concentration leads to lower viscosity and surface tensions on the solution jet increases and consequently results in beaded fibers [Megelski 2002, Fong 1999]. If the molecular weight of the polymer is too low, it leads to a low viscosity of the solution and does not encourage formation of fibers but instead results in formation of droplets / particles [Shenoy 2005]. On the other end, if the solution is too viscous, clogging results at the tip of spinneret [Kameoka 2003]. When sufficient viscosity of polymer solution is attained, uniform fibers are produced. In the appropriate viscosity region which results in uniform fibers, an increase in polymer concentration results in an increase in fiber diameter [Deitzel 2001, Demir 2002, Megelski 2002].

Higher solution conductivity influences the formation of smaller fiber diameters [Zhong 2002]. During electrospinning the charges at the jet surface would be repulsed, resulting in stretching of the solution jet. The level of charges is increased with higher conductivity which may induce highly stretched jet. The smaller diameter of fibers spun from highly conductive solution might be a result of high stretching of the jet. Although solution conductivity has been reported to affect fiber diameter, some researchers claimed that a reduction of fibers is due to dielectric constant [Lee 2003, Son 2004]. When solvent with either higher electrical conductivity or dielectric constant is added, the solubility of a polymer in the solvent must be paid attention to. If the solubility of a polymer is decreased due to excessive solvent added,

beaded fibers are formed [Wannatong 2004]. It is noted that additional solvent into the polymer solution also changes total solution viscosity and surface tension.

2.1.3.2. Processing conditions

Processing conditions such as voltage, feed rate of polymer solution, distance between needle and collector and diameter of needle influences the electrospun fiber morphology. The applied voltage should be adequate to overcome the viscosity and surface tension of the polymer solution to form and sustain the jet. Since the electrical charges are the basis of electrospinning, the solution must be dielectric or electrically conducting. Fortunately, most solvents such as methanol, N,N-dimethyl formamide and water are able to carry charges. Solvents with higher charge carrying capacity are often doped with salt to facilitate fiber spinning from the polymer solution. With most polymers having correspondent solvents and with the right doping, most polymers can be electrospun to form nanofibers.

Applied voltage is associated with the amount of charges on a solution jet. Higher voltage results in higher charges on a solution jet and the resultant solution jet will be highly stretched during electrospinning due to the charge-induced repulsive force. The stretching of the solution jet is further encouraged by interaction with an external electric field. Hence, higher voltage is found to induce electrospinning of fibers with smaller diameter [Megelski 2002, Buchko 1999]. Low viscosity solution shows relatively high mobility of polymer chains within polymer solution and when a higher voltage is applied to such a solution it causes more solution to be released from the spinneret. If this influence is dominant over that of stretching, a higher voltage may result in a larger fiber diameter. At even higher range of applied voltage, beaded fibers were produced and the beads adopt a more spherical shape

rather than spindle-like shape which is generally prominent at lower voltage [Demir 2002, Deitzel 2001, Zhong 2002].

The distance between the needle tip and the grounded collector is affected by the electric field strength and a jet traveling time which reflects solidification or stretching time for a solution jet. This distance should not be too small to generate sparks between the electrodes but should be sufficiently large for the solvent to evaporate in time for the fibers to form. If the influence of jet traveling time is dominant, wet / interconnected fiber membranes are produced with a decreased distance due to insufficient solidification time for a solution jet [Buchko 1999]. An increase in the distance results in electrospinning of smaller diameter fibers due to the relatively longer time to stretch the solution jet [Zhao 2004, Reneker 2000, Ayutsede 2005]. However if this distance becomes too large, the fibers tend to 'fly' all over the place rather than being collected only on the grounded surface [Suthar 2001]. The distance between the spinneret and the collector may be as short as 5 cm but this depends on the rate at which the solvents evaporate and whether the polymer solution is sufficiently stretched into the nano-dimension before deposition. Although it may seem unlikely that such a short distance is adequate to dramatically stretch the solution from a microliter droplet to nanofibers, this is made possible by the chaotic and helical path which the electrospinning jet takes to reach the collector. Interestingly, if the influence of the electric field strength is dominant, beaded fibers are electrospun at too short spinneret and collector distance due to the instable jet initiation [Megelski 2001, Deitzel 2001], while fibers with larger diameter are electrospun at long spinneret to collector distance due to the weak electric field [Lee 2004].

It is economical to collect fibers at a faster rate but feed rate has implications on the fiber size. When other parameters held constant, higher feed rate results in larger fiber diameter,

with a limit to increase in fiber diameter. In addition feed rate affects the solidification time for a solution jet and may result in wet / interconnected fibers if not thoroughly dried in time.

2.1.3.3. Ambient conditions

Ambient conditions are difficult to control. Humidity was found to affect surface features of fibers electrospun from polymers dissolved in volatile solvents [Megelski 2002, Bognitzki 2001]. Porous surface of fibers can be electrospun at higher humidity level and the size of pores is dependent on the humidity level [Casper 2004].

Besides fiber morphology, different fiber architectures can be achieved. In a conventional electrospinning setup, the collected nanofibers are in the form of a non-woven mat. By changing the collector design, different fiber architectures such as aligned fibers that can be stacked on each other, yarns and hollow yarns can be obtained. This makes the technique highly advantageous as desirable architecture can be achieved.

2.2. Advantages of ENMs for liquid filtration

The key advantage of having a non-woven structure is its extensive fibrous network which provides a large dirt loading capacity due to its large internal surface area. Non-woven filters are highly efficient as they have a better capacity to remove pollutants in both gas and liquid environments. Thus electrospun nanofibrous membranes (ENMs) should be suitable to be used as prefilters. The current state of art of pre-filters is that they help to take the load off the final membranes which are costly. The load readily fouls the membranes downstream such as

the reverse osmosis (RO) membrane and hence the efficiency of the downstream membrane is greatly affected.

In addition ENMs are highly porous due to their interconnected structure. They have a porosity of 10-20% greater than phase inverted membranes [Kaur 2007]. Higher porosity generally leads to higher fluxes. Besides filtration efficiency, flux is an important factor in determining the membrane performance.

During the electrospinning process, the fiber dimension can be optimized to the nano-range by varying process variables such as polymer concentration, applied voltage, fluid flow rate, surface tension, etc. [Seeram 2005]. This improves the overall surface area to volume ratio of the membrane and hence making them suitable for several types of separation especially when the surface interaction is the dominant driving force for particulate separation such as in air and affinity separations [Yoon 2008], their large surface area for capturing certain foulants or functionalization of a specific chemical group which subsequently captures a specific undesirable chemical that has to be removed. When compared to larger fibers, smaller fibers in the submicron range are well known to provide better filter efficiency at the same pressure drop in the interception and inertial impaction regimes [Hinds, 1982]. The large surface-to-area ratio of nano-and microfibers has improved the performance in a variety of applications such as chemical and biological sensors, tissue engineering, protective clothing and affinity separation [Ramaseshan 2006].

Last but not least, the fibers generated during the electrospinning process are generally long (up to hundreds of kilometres if the process is not disrupted) despite their small diameters. Thus it is extremely difficult for them to become airborne and enter the body [Yoon 2008].

Hence the safety concerns on producing ENMs are minimal as compared to asbestos fibers (0.01 μm) that were popular pre-filters during the 1960s and they posed a health hazard risk [Porter 1990].

The preceding section provides a brief introduction of membranes before the section of applications of ENMs in liquid filtration is revealed.

2.3. Membranes

A membrane acts as a selective barrier separating two distinct phases. Its main function is to discriminate species it comes into contact with on one phase (feed) and transport them across to the other (permeate). Species migrate from one phase to another under the influence of a driving force.

However membrane technologies are energy intensive [Furukawa 1997] and hence a continuous need of new membrane technologies that make use of low pressure systems that significantly reduce energy use, operation and maintenance costs is needed.

2.3.1. Membrane structure

A membrane can be homogenous or heterogeneous, symmetric (isotropic) or asymmetric (anisotropic) in structure. It may be a solid or liquid in nature. It may be neutral or carry either positive or negative charges or it may carry bipolar charges. Its thickness may vary between less than 100 nm to more than a cm [Mark 1990]. Membrane structure is very important as it dictates not only the separation and permeation mechanism but also as a

consequent the application. Figure 2.3 shows the various cross-section structures of a membrane.

2.3.1.1 Symmetric membrane

Symmetric membranes have the same chemical and physical structures across the cross-section of the membrane. The thickness of such membranes ranges from 10-200 µm [Mark 1990]. The resistance to mass transfer is determined by the total membrane thickness, for example a decrease in membrane thickness results in an increased permeation rate.

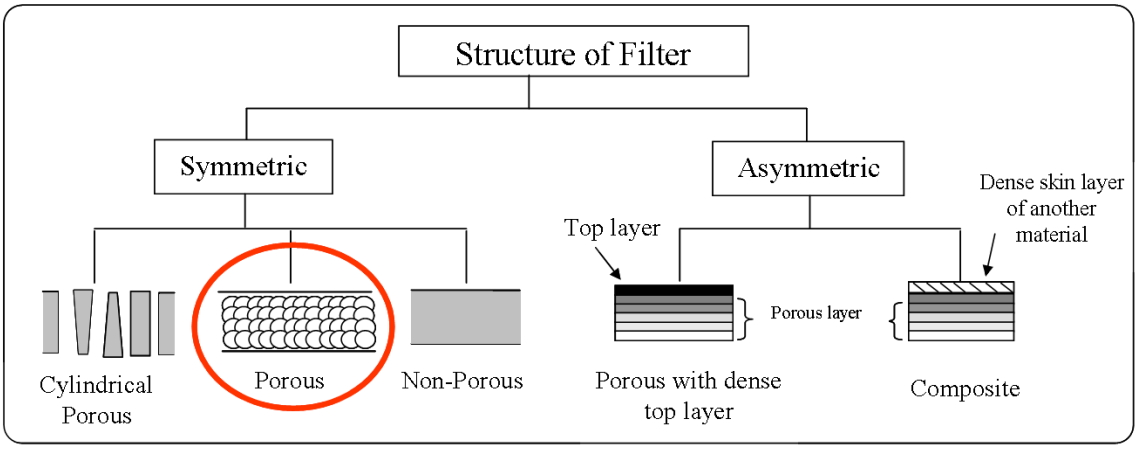

Figure 2.3. Cross-section illustration of membranes. The circled picture reflects the cross-section of ENM [Kaur 2008].

A typical example for this type is phase inversion membranes which are produced by casting a film from a polymer solution and immersing the cast film in a non-solvent for the polymer. Most of the polymers used in such applications are hydrophobic, so water is the most common non-solvent. The polymer precipitates out of the solution upon contact with water to form the membrane. Another type of microporous membrane is the track-etched membrane. This type of membrane is prepared by irradiating a polymer film with charged particles that

attack the polymer chains, leaving damaged molecules behind. The film is then passed through an etching solution, and the damaged molecules dissolve to produce cylindrical pores, many of which are perpendicular to the membrane surface. Symmetric membranes can also be dense films which either lack pores or contain pores that are so small as to render the membrane effectively non-porous. These films in turn are prepared by solution casting followed by solvent evaporation or melt extrusion.

2.3.1.2 Asymmetric membrane

Asymmetric membranes have a non-uniform cross-section. They typically consist of layers which vary in structure and/or chemical composition. There are two main types of asymmetric membranes: phase separation membranes and thin film composite membranes. Phase-separated membranes are homogeneous in chemical composition, but not in structure. These membranes are produced via phase inversion techniques such as those described above, except that the pore-sizes and porosity differs across the membrane thickness. The membranes often consist of a rather dense layer of polymer on the surface of an increasingly porous layer.

Thin film composite membranes are both chemically and structurally heterogeneous. It is characterized by a thin "skin" on the surface of the membrane with a thickness of generally 0.1 to 0.5 μm. This dense layer is supported by a porous structure with thickness of 50 to 150 μm. The top and sub layer originate from different polymeric materials. The top is a thin dense polymer skin formed over a microporous support film. Each layer can be optimized independently.

Due to its unique ultrastructure, rejection only occurs at the surface and retained particles do not enter the main body of the membrane. As such, these asymmetric membranes rarely get "plugged". The resistance to mass transfer is determined largely by the thin top layer. This layer has insufficient mechanical strength and hence requires some support. The support layer does not add any significant hydraulic resistance to the flow of solvent through the membrane [Peterson 1993]. The resultant membrane formed after modification is termed as a composite membrane. They can be made via several methods including interfacial polymerization, solution coating and plasma polymerization or surface treatment [Baker 2004]. As-spun ENMs are classified as symmetric membranes and a pictorial view is shown in Figure 2.3.

2.3.2. Performance of a membrane

The permeation performance of a membrane is governed by two key factors: selectivity and flux. Selectivity relates to the discrimination of the type of species that can pass through the membrane. On the other hand flux relates to the rate (diffusivity) at which species are transported across the membrane and how much gets into the membrane (solubility). These parameters are generally influenced by several features of the membrane such as porosity, pore-size and distribution, wetabillity, pressure drop across the membrane and thickness.

2.3.3. Operation mode

The operation of membrane processes are classified in two modes: dead-end filtration and cross flow filtration. They are schematically shown in Figure 2.4. Dead-end filtration results in a build-up of product on the membrane surface that may damage product, lower recovery and "foul" the membrane. Fouling impedes the filtration rate until it eventually stops. Cross

flow Filtration involves the recirculation of the retentate across the surface of the membrane. This gentle "cross flow" feed acts to minimize membrane fouling and concentration polarization, maintains a high filtration rate and provides higher product recovery since the sample remains safely in solution.

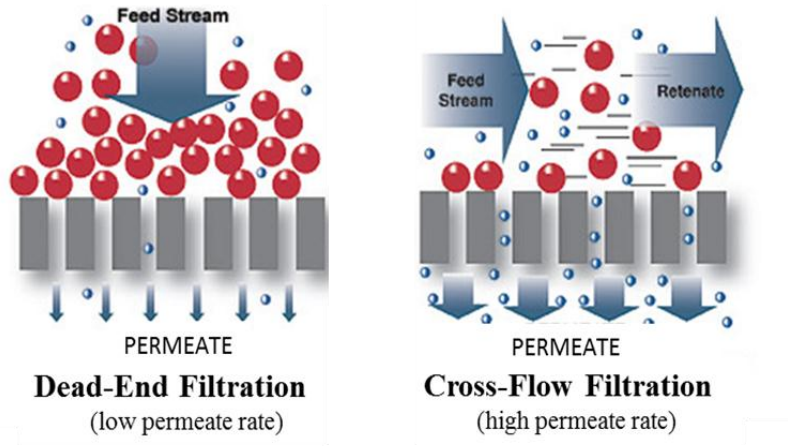

Figure 2.4. Different filtration styles/mode.

2.3.4. Concentration polarization

When a membrane is used for a separation, the concentration of any species being removed is higher near the membrane surface than it is in the bulk of the stream. This condition is known as concentration polarization. The result of concentration polarization is the formation of a boundary layer of substantially high concentration of substances being removed by the membrane. The thickness of the layer and its concentration depend on the mass transfer conditions that exist in the membrane system. Membrane flux and feed flow velocity are both important in controlling the thickness and the concentration in the boundary layer. The boundary layer impedes the flow of water through the membrane and the high concentration of species in the boundary layer produces permeate of inferior quality and hence relatively

high fluid velocities are maintained along the membrane surface to reduce the concentration polarization effect.

2.3.5. Fouling

Membrane fouling is the process in which solute or particles deposit onto a membrane surface or into membrane pores such that membrane performance is degraded. Fouling is the major cause for flux decline. This phenomenon depends on many factors including feed characteristics, membrane apparatus type, membrane characteristics and operational procedures. Many approaches have been examined to minimize the impact of membrane fouling. One way of reducing it is through cross flow filtration. Another way to minimise membrane fouling is using the appropriate membrane material for a specific operation. For aqueous filtration, a hydrophilic membrane is preferred. This can be achieved by blending tailor-made surface active polymers into the polymer solutions. During the casting process the surface active additives migrate to the membrane surface, thus creating asymmetric membranes with modified surface via a single manufacturing step [Ho 2000, Suk 2002].

Flux and trans-membrane pressure (TMP) are the best indicators of membrane fouling. Under constant flux operation, TMP increases to compensate for the fouling. On the other hand, under constant pressure operation, as membrane fouling increases flux decreases.

2.3.6. Pore-size, Pore-size Distribution and Porosity

Pore-size refers to the diameter of the pores present in the membrane. Such information can discriminate between the type (size or molecular weight) of species than can permeate

through and which will be retained. However, pores in membrane, especially polymeric membrane, do not have identical pore-size but rather a range of sizes. This is known as the pore-size distribution. Whereas, porosity is the fraction of the membrane volume occupied by the pores (void volume). While the pore-size and its distribution discriminates the type of species that can permeate, it is the porosity that determines the flux.

2.3.7. Pressure driven membranes

A driving force is essential for the transport of species across a membrane. The transport through the membrane only occurs when a driving force is applied on the individual components in the feed solution. The flux is determined by the driving force acting on the permeating species and their mobility and concentration within the interphase [Strathmann 1981]. There are four different categories of driving forces, namely, pressure, temperature, concentration and electric potential differences across the membrane [Matsuura 1994]. Since pressure-driven systems are the most commonly used membrane systems, the preceding paragraph will be based on it.

Pressure-driven processes use hydraulic pressure to force water molecules through the membranes. Impurities are retained and concentrate in the feed water, which becomes the reject water or concentrate stream. The permeate - the water that passes through the membrane- is recovered as product or pure water [Keith 1995].

Pressure driven membranes include in order of decreasing permeability: microfiltration (MF), ultrafiltration (UF), nanofiltration (NF), and reverse osmosis (RO). The range of sizes of

selected constituents in water and wastewater and the performance capabilities of the different membranes are illustrated in Table 2.1.

Table 2.1. Comparison of different membrane processes

Parameters	**Membrane system**			
	MF	**UF**	**NF**	**RO**
Particle size, µm	0.03 to 10	0.005 to 0.2	0.001 to 0.01	0.0001 to 0.001
Retained compounds	Very small suspended particles, some colloids, most bacteria	Organics > 1000 MW, pyrogens, viruses, bacteria, colloids	Organics > 300 MW. THM precursors, some dissolved solids, divalent> monovalent	Ions, organics > 100 MW
Operating pressure, psi	1 to 15	10 to 100	80 to 125	125 to 1,000
Maximum temperature, ^{o}F (^{o}C)	80 (27)	80 (27)	80 (27)	100(38)
Recovery rate %	100	75	85	50 to 85
Note: Recovery rate is the percent of product recovered from the feedwater.				

MF and UF often serve to remove large organic molecules, large colloidal particles, and many microorganisms**.** MF performs as a porous barrier to reduce turbidity and some types of colloidal suspensions. UF offers higher removals than MF, but operates at higher pressures.

RO membranes are effectively non-porous and, therefore, exclude particles and even many low molar mass species such as salt ions, organics, etc. [Perry 1997]. NF is an intermediate between RO and UF and it rejects molecules which have a size in the order of one nanometer. They are sometimes called “loose” RO membranes [Baker 2004]. It was introduced in the late 1980s, mainly aiming at combined softening and organics removal. Since then, the application range of NF has extended tremendously. New possibilities were discovered for drinking water production, providing answers to new challenges such as arsenic removal, removal of pesticides, endocrine disruptors and chemicals and partial desalination [Bruggen 2008].

In wastewater reclamation, MF or UF might provide a suitable level of treatment. In drinking-water treatment, MF or UF might be used in tandem with NF or RO to remove coarser material so that fouling of the less permeable membranes is minimized. The most commonly used process for the production of drinking water is RO, but NF is now emerging as a viable alternative to conventional water treatment because it can operate at lower pressures and higher recovery rates than RO systems. NF is also cost-effective in many groundwater softening applications where the incoming turbidity is low.

2.3.8. Interfacial polymerization (IP)

Interfacial polymerization (polycondensation reaction of polyfunctional amine and acid chloride monomers at the interface of two immiscible solvents) is the preferred route to the synthesis of thin-film composite (TFC) membranes for RO and NF membrane filters. In fact the breakthrough in NF took place with the invention of a thin film composite (TFC) structure which comprises of three essential layers (1) top ultra-thin selective barrier layer

(which bridges and overcoats the surface pores of the middle porous layer), (2) middle porous support and (3) bottom non-woven fabric. Layers (1) and (2) could be carefully altered to produce the optimal separation performance. Concomitantly layer (3) does not influence the separation characteristics but rather it offers handling strength [Peterson 1993].

Over the years, improvements in performance of TFC membranes for aqueous applications have taken place mainly in terms of selectivity (solute rejection) without any appreciable change in membrane productivity (flux). It has become imperative in developing membranes, which provide higher fluxes or productivities without severely affecting membrane selectivity. In particular, the demand for developing membranes with high water flux is enormous for applications to industrial wastewater treatment and ultra-pure water production [Rao 2003].

The top ultra-thin selective barrier layer is commonly prepared by interfacial polymerization technique. In forming the interfacial layer commonly referred as polyamide thin film, a polyfunctional amine is dissolved in water and polyfunctional acid chloride is dissolved in apolar organic solvents like hexane. When the two monomer solutions are brought into contact, both monomers partition across the liquid-liquid interface and react to form a polymer. The performance (solute rejection and flux) of the barrier layer is generally improved by the addition of additives during polymerization, post treatments (for e.g. by-product removal) and pre-treatment conditions. Most of the research has been devoted in optimizing the top barrier layer to achieve a desired combination of solvent flux and solute rejection. Since this layer is rather thin it is therefore always supported by structures (the middle microporous layer) having a moderate hydrodynamic resistance and surface pores small enough to be bridged by the selective film. The salt rejection depends critically on the

mechanical integrity of this thin layer as any break in this film will lead to a failure in salt rejection.

The middle microporous layer is typically prepared by phase-inversion process and possesses a dense surface skin and the pore-size increases rapidly across the membrane thus adopting an asymmetric structure. It generally offers maximal mechanical strength and compression resistance, combined with a minimal resistance to permeate flow. The porous support also plays a pivotal role in the formation of the barrier layer and hence influencing the selectivity of the top barrier layer [Schafer 2005].

The effect of pore-size (70 nm and 150 nm, designated as type 1 and type 2 membrane, respectively) of a phase inverted polysulfone support layer on the morphology and performance of thin film polyamide membrane has been studied [Singh 2006]. Larger pores of type 2 membrane favours effective formation of polyamide inside in the pores and thereby reduced the thickness of thin polyamide film, whereas in type 1 membrane surface defects and two fold enhancement in the thickness were observed. NaCl (2000 ppm) rejection efficiency of 95-96 % and permeate flux of 0.14 – 0.16 L/(m^2.h.psi) for the type 1 membrane was achieved; while rejection efficiency of 45-66 % and permeate flux of 0.32 L/(m^2.h.psi) for type 2 membrane was obtained.

2.4. Applications of ENMs in liquid filtration

Nanofibrous membranes are increasingly being looked at as a solution for providing water at lower energy costs. It is anticipated that due to their higher porosities and interconnected pore structures (hence a shorter path for the passage of water), nanofibers would offer a higher

permeability to water filtration over conventional materials being used. The following sub-sections highlights the different applications ENMs used in the various pressure driven processes namely microfiltration, ultrafiltration and nanofiltration.

2.4.1. Microfiltration ENMs

Few lab scale liquid separation studies have been performed on ENMs to demonstrate its applicability in particulate removal and subsequently to relate its structural properties to membrane separation properties and performance.

The very first study was conducted on Polyvinylidene fluoride (PVDF) ENMs and characterization of these ENMs revealed that they have similar properties to that of conventional microfiltration membranes [Gopal 2006]. The electrospun membranes were used to separate 1, 5 and 10 μm polystyrene (latex) particles. The electrospun membranes were successful in rejecting more than 90% of the micro-particles from solution and no fouling was observed for 5 and 10 μm particles. Interestingly the separation of 1 μm particles was the highest and the flux was not recovered at the end of the separation indicating a certain extent of fouling. A layer of particle deposition on the surface of the ENM was observed. As the micro-particles are small, they were able to pack closely together, reducing the effective pore-size of the ENM significantly at the surface. This dense 'cake' acted as the separating layer for the ENM. This accounts for the unusually high rejection of 98%. This separation does not correlate with any of the membrane characterization data obtained previously. This work opened up the avenue of exploring the use of ENMs for more mainstream application in the separation technology. It was through this work that it was realized that ENMs could be a potential membrane for pre-treatment of water prior to reverse

osmosis or as pre-filters to minimize fouling and contamination prior to ultra- or nano-filtration.

A more thorough separation study (dead end) was conducted on PSU ENMs. The membranes were subjected to separation of a fuller range polystyrene (PS) micro-particles of sizes 0.1, 0.5, 1, 2, 3, 7, 8 and 10 μm dispersed in water at 0.5 psig. The fiber diameter of PSU ENM was 470 nm and the thickness of the ENM was 135 μm. When an attempt was made to separate micro-particles larger than the bubble-point (largest pore) of the ENM, it acted as a screen filter, with high micro-particle rejection rate and no fouling observed. However, when the study was performed to separate micro-particles with a diameter close to the mean pore-size of the nanofibrous media, severe and irreversible fouling occurred. When sub-micron particles were separated, they tend to get attracted to the surface of the nanofibers and thus the media became a depth filter [Gopal 2007b]. The following paragraph gives a detailed insight of the separation profile.

The separation for 10, 8 and 7 μm particles was well above 99%. The flux in fact dropped during the separation experiments of these particles but there was 100% recovery by washing. Since the particles were larger than 4.6 μm, the largest pore-size of the ENM, the size prevented the particles from entering and/or passing through the pores or openings. Hence, the minimum washing was enough to completely regenerate the ENM. From the onset of the 3 μm separation experiment a drop in flux recovery was observed. The separation factor for 3 μm particles was 92 %. Some of the particles passed through the membrane pores because the particle size was smaller than 4.6 μm. The drop in flux observed was probably due to entrapment of the particles within the larger pores. The most severe drop in flux was noted during the 2 μm particle separation experiments. The flux reduction was instantaneous at the

onset of the experiment and a permanent drop in flux at the end of the experiment was observed. This indicates the permanent fouling of the ENM, most probably due to the cake-layer formation on the membrane surface. There was another significant drop in flux after the 1 μm separation as well. This implied that the bottle-neck for the PSU-ENM was in the 1-2 μm region. The velocity of particle migration seems to be the lowest for 1 and 2 μm. It is well known that the least migration of the particles away from the surface by the Brownian diffusion and the particle lift force caused the severest particle precipitation to the surface and it occurs when the particle size is about 1 μm.

Motion of 1 μm particle was also most probably affected by the presence of 2 μm particles left on/within the membrane in the previous run and hence it shows a higher separation than the 2 μm particles, even though all the pores in the ENM were found to be larger than 1 μm. Consequently, the subsequent separation of 0.5 and 0.1 μm particles were affected by the permanent fouling on the ENM by the 2 and 1 μm particles and thus are not reflective of the true nature of the selectivity of the ENM to particles smaller than 1 μm. The formation of dense cake layer of 2 and 1 μm particles resulted in unusually high separation of 0.5 and 0.1 μm particles, even though they are much smaller than the membrane pore-sizes.

In a similar study, nylon-6 ENM was used for the removal of micron to sub-micron particles from aqueous media. A similar conclusion was drawn. The membrane was capable of effectively removing micro-particles above the membrane average pore-size without fouling. However the membrane was severely fouled with sub-micron particles. It was recommend by the authors that in order to improve the understanding of separation behaviour a cross-flow pattern is highly encouraged. In addition it was suggested that it would be interesting to

perform more work on the effect of nitrogen flow rate on the separation factor [Aussawasathien 2008].

Subsequently the influences of nanofiber diameter, morphology and the thickness on the pore-size distribution of polysulfone (PSU) ENMs were studied [Gopal 2007a]. The media had excellent flux performance and low pressure drop compared to conventional membranes. As anticipated it was found that the presence of beads on fibers and the thickness of the media had a significant influence on the pore-size distribution, mean flow pore-size and largest pore-size (bubble point). The presence of beads, if numerous, affects the packing of the media, leading to reduced pore-sizes as well as porosity and thus flux. Likewise, as the thickness of the media increased, the mean pore-size decreased which is due to more layers of nanofibers deposited that give rise to more hindrance to the flow path.

The above findings highlight both the potential and the drawbacks of using electrospun media in their natural state as barrier materials for separation technology. Unlike for air filtration, a thin layer of these nanofibers will not suffice for liquid filtration but instead a thicker mesh is required to decrease the overall average pore-size of the filter (as evident from above). However, a thick media composed of these thinner fibers results in smaller interspatial void volume, affecting the flux performance. In addition the ENM has a symmetrical structure and the pores of the membrane can be easily plugged by particles.

To overcome this bottleneck and to expand the application of nanofibrous media in liquid separation, researchers have functionalized the surface of nanofibrous media. This can be done in two different ways. Either a top layer of the membrane is modified such that the

overall filter becomes asymmetric or each fiber in the membrane throughout is modified with particles that aid in the separation process based on an affinity mechanism.

Plasma induced graft copolymerization[4] has been used to modify and reduce the surface pores of nanofibrous filter media to below 1 micron. Through graft copolymerization, the bubble point of the self -supporting ENM reduced from 3.6 μm to 0.9 μm. Most significantly, water flux permeation studies revealed that the grafted nanofibrous media had a better flux (by approximately 150-200% more) throughput than a commercially viable phase-inverted membrane of the same pore-size [Kaur 2007]. This showed that the nanofiber architecture is better than the phase inverted and could result in energy saving membranes.

2.4.2. Ultrafiltration ENMs

A high flux and low fouling ultrafiltration membrane based on ENM has also been achieved on a lab scale [Yoon 2006]. A water permeable coating of chitosan (a hydrophilic biopolymer that has anti-fouling enhancement properties) of thickness ~ 1 μm was applied over the surface of ENM. The membranes so fabricated were tested for the separation of oil/water emulsion. The feed solution was prepared by mixing of vegetable oil (1350 ppm), surfactant (150 ppm, Dow Corning 193 fluid) and deionized water. The effective membrane area was 65.2 cm^2 and the transmembrane pressure drop was 130 psig.

The performance of the ENM based composite membranes is compared with that of a commercial nanofiltration membrane. Two ENM based composite membranes; one with a thickness of about 1.3 μm made by coating of 1.37 wt% chitosan solution and the other with

[4] Plasma is a complex gaseous state of matter, consisting of free radicals, electrons, photons and ions. The surface of the membrane is exposed to plasma followed by exposure to oxygen to form peroxides and subsequently polymerized.

a thickness of ~1 μm made by coating of 1.2 wt% solution, were used for comparison with a commercial NF 270 membrane. Although all membranes showed certain degrees of fouling the fluxes of both ENM based composite membranes were much higher than the commercial NF membrane. The oil rejection was more than 99.9 % for the ENM based composite membranes while it was 99.4 % for the commercial NF membrane during 24 h of operation.

Although not yet fully optimized, the media exhibited a flux rate that is an order of magnitude higher than commercial phase-inverted membranes during 24 h of operation, while maintaining the same rejection efficiency of 99.9% for oily waste-water filtration.

A novel class of high flux ultrafiltration membrane consisting of UV-cured polyvinyl alcohol (PVA) hydro-gel barrier layer introduced on PVA ENM has been investigated [Tang 2008]. It was found that UV curing of a 5-wt% UV-PVA solution coating over 20-s time period yielded a high flux (60.8 L/m^2h), high rejection (99.5%) UF membrane with good fouling resistance for separation of oil and water emulsion.

2.4.3. Nanofiltration ENMs

Cellulose acetate (CA) was successfully used as a support for subsequent coating with polyelectrolyte multilayers for polycation (chitosan, CHI)/polyanion (sodium alginate SA or poly(styrene sulfonate) sodium salt, PSS). These composite membranes were characterized for water permeability where the water flux decreased with an increase in the number of the bilayers. The water flux was in the range of 40-60 L/m^2h for 15 and 25 bilayered membranes, respectively. The sodium chloride (NaCl) solution flux was lower than the pure water flux due to the effect of osmotic pressure and it decreased with an increase in the NaCl

concentration. The rejection of NaCl increases substantially with the number of the bilayers of the polyelectrolyte multilayers. The level of NaCl rejection from this work was in the range of 6% and 15% for 15 and 25 bilayered membranes, respectively [Ritcharoen 2008].
In this work, the authors have not reported the pressure used and the rejection of monovalent salt was low. A separation of divalents salts such as magnesium sulphate ($MgSO_4$) would have given a clearer understanding on the separation characteristic of the membrane.

2.5. Motivation

Through these application studies and subsequently through a basic study from the start of this research as demonstrated in Chapter 3, it was realized that it will be feasible to coat or introduce a thin semi-permeable polymeric layer on the surface of ENMs, despite its large pore-size, so as to facilitate the separation of finer or even smaller solutes.

Through this understanding this thesis was directed to introducing a polymeric layer on the surface of ENMs and to understand its separation characteristics. This polymeric layer can be introduced by interfacial polymerization. The layer supporting the interfacial polymerized layer plays an essential role in the flux and rejection of salt [Singh 2006]. Hence it will be noteworthy to understand how ENMs will influence the separation performance. This thesis is thus geared in developing, a thin film nanofibrous composite structure (TFNC) and relating the fiber size and architecture of ENM to separation performance. The separation performance is evaluated by using monovalent (NaCl) and divalent salts ($MgSO_4$, $MgCl_2$, Na_2SO_4, $CaCl_2$) as the feed. It is thus anticipated that fiber size and morphology might have an influence on separation of solutes once the TFNC is developed.

Overall this thesis will open up a new avenue for the use of ENMs in liquid separation specifically in nanofiltration. This is a huge undertaking and the author hopes that this understanding will propel more interest to use these membranes as main stream product.

CHAPTER 3

REMOVAL OF HUMIC ACID FROM ELECTROSPUN NANOFIBER MEMBRANES

3.1. Introduction

The preliminary work done here was the driving force of deriving the main objective of this thesis. The author felt that it was imperative to show this initial work which was instrumental in realising the potential of ENM. It is to be emphasised that since the finding of this work led to the main objective of this thesis, optimization of the filtration efficiency was not carried out.

3.2. Polymer selection

Selecting the right material is very critical in separation technology. It is important to understand the influence of a material's intrinsic properties to the separation mechanism. By far the most versatile group of materials for membrane synthesis is polymers. Polymers can be tailored to meet specific requirements such as mechanical, thermal, hydraulic, chemical stability and high biodegradability. However, the chemical and physical properties differ so much that only few have achieved commercial status [Kroschwitz 1990].

The selection of a material for a certain application involves different criteria. For example for a porous MF membrane, the choice of the material does not directly determine the separation characteristics since the pore-size and the pore-size distribution are the main

factors influencing the separation of particles. However the choice of polymer definitely affects the chemical and thermal stability and surface characteristics such as adsorption and wettability [Mulder 1996]. Additionally the choice of polymer is crucial when certain cleaning agents are employed. For example polyamides are strongly attacked by chlorine-containing cleaning agents and hence should not be selected when such agents are required for sterilizations. The materials of MF generally consist of crystalline polymer generally engineering plastics including cellulose and its derivatives. Hydrophilic materials are not suitable for MF membranes that require mechanical strength and thermal stability [Toyomoto 1992].

Hydrophobic materials such as polytetrafluorethylene (PTFE), poly(vinylidene fluoride) (PVDF) and isotactic polypropylene (PP) are often used for MF membranes. PTFE is highly crystalline and possesses excellent thermal stability and is chemically resistance. Because of its chemical inertness, this polymer was not chosen to be electrospun since one of the requirements of electrospinning is to dissolve the polymer in a suitable solvent. Similarly PP is an excellent solvent resistant polymer and hence not suitable to be subjected to electrospinning. On the other hand PVDF exhibits good thermal and mechanical properties. Vinylidene fluoride ($-CH_2=CF_2-$) is polymerized readily by free-radical initiators to form a high molecular weight, partially crystalline polymer. The spatial symmetrical disposition of the hydrogen and fluorine atoms along the polymer chain gives rise to unique polarity influences that affect solubility, dielectric properties and crystal morphology. It has a melting point range of 155-192 ^{o}C. It can be autoclaved and its resistance to common solvents is good. It is chemically resistant but it is soluble in aprotic solvents such as N,N-dimethylformamide (DMF) and N,N-dimethylacetamide (DMAC). Because of its good solubility in solvents that possess a high dielectric constant and its resistance to severe

environmental stresses, PVDF has been selected for this research work to be electrospun. The membrane generated is generally hydrophobic and surface modification would provide a means to generate a hydrophilic surface. They have better resistance to chlorine than PS family. As such PVDF is an excellent choice for this study. In addition, it is highly resilient to many solvents but yet its ease in solubility in solvents with high dielectric constants and conductivity makes it an ideal candidate for electrospinning.

Traditionally, polymers with the best solvent resistance or those which provide the most convenient pore structure (as stated above) are too hydrophobic for use as a filter in aqueous media [Nunes 2001]. Conversely, polymers with the desired active surfaces do not possess adequate mechanical stability and hence cannot be used as a support or base membrane [Gopal 2006b]. Thus surface modification is frequently employed to combine the attributes of a desirable surface chemistry and adequate mechanical stability.

3.3. Surface modification techniques

The control of surface properties is of scientific and technological importance in many academic and industrial research areas. One such area is the modification of the membrane surfaces as they have an important role in membrane separation processes. There are several techniques to modify the surface: blending, coating, grafting, chemical modification, plasma treatment, etc [Gopal 2006 b]. Blending and coating are by far the simplest and easiest methods employed to functionalize a polymer. Both these techniques are physical approaches, whereby there is no chemical bonding or attachment involved between the polymer material and the functionalized species. It is a simple mixing of two or more

materials (blending) or using another material of desired properties to "cover" the surface of the polymer (coating).

3.4. PVDF electrospun nanofibrous membranes

This chapter focuses on introducing surface modifying macromolecules on the surface of ENM. This was achieved by blending the SMMs with PVDF before electrospinning. Some literature studies have shown that SMM blended phase-inverted membranes had a better separation performance and were less susceptible to fouling in oil-water separation [Rana 2005]. The membrane was then subjected to separation of 50 ppm of Humic acid (HA), a natural organic matter (NOM) foulant in drinking water, on a dead end filtration set up. The initial intention was to produce a hydrophilic membrane from PVDF, however during the separation of HA it was realised that the surface of the ENM could be modified with a thin polymeric layer which will be capable to separate small molecules/solutes.

3.5. Experimental section

All experimental findings were performed at the University of Ottawa.

3.5.1. Materials

Acetone (Chromasolv grade for HPLC, >99.9% purity, Sigma-Aldrich Company, St. Louis, MO, USA), N,N-Dimethylacetamide (DMAc, anhydrous, 99.8% purity, Aldrich Chemical Company, Inc., Milwaukee, WI, USA) were purchased and used as received. Poly(vinylidene fluoride) (PVDF, average molecular weight 4.41×10^5) was purchased from

Arkema Singapore, Singapore. Humic acid (Sigma-Aldrich Company, St. Louis, MO, USA) was prepared in de-ionised water (50 ppm) and subsequently filtered on a filter paper to remove any un-dissolved particles. SMM was made at the University of Ottawa.

3.5.2. Electrospinning conditions

PVDF solution of 20 % (w/v) concentration was prepared in a mixture of DMAc and acetone at a ratio of 2:3. A syringe pump (74900 series, Cole-Parmer Instrument Company, Vernon Hills, IL) was utilized to supply the polymer solution at a constant flow rate of 1 mL/h during electrospinning. A voltage of 15 kV was applied by a transformer (DW-P503-1C, Beijing Shining Technical & Commercial Centre, Xisanqu, Tiantongyuan, Changping District, Beijing, PR China) to draw nanofibers from the prepared solution. The fibers were collected on a grounded 100 cm^2 aluminium plate. The relative humidity was approximately 15 % and the temperature was 15 ^oC. After the ENMs were formed, they were heated at 60 ^oC for 1 h. Subsequently, the membranes were heated up to 157 ^oC to improve the structural integrity of the membrane. The fiber diameters were determined from the SEM image using the ImageJ software (http://rsb.info.nih.gov/ij/). The SMM blended ENMs were prepared by adding SMM (8 wt% of PVDF) to the 20 % (w/v) PVDF solution. Non-blended membranes will be labelled as ENM-control while the blended membrane will be labelled as ENM-SMM.

3.5.3. Pore-size distribution determination

The pore-size distribution, bubble point and mean flow pore of ENMs were determined using a capillary flow porometer (Porous Materials Inc, USA). The membranes were completely wetted with wetting liquid Galwick^{TM} (Porous Materials Inc, USA) and pressure was applied

on one side. Pressure (typically air) is applied on the sample to remove the wetting liquid from pores and permit gas flow. The change in flow rate is measured as a function of pressure for both dry and wet processes. All the required pore structure characteristics such as pore-size at bubble point, mean flow pore and pore-size distribution can be computed from the measured differential pressures and gas flow rates. The relationship between the pore-size and the corresponding pressure is given by the Young-Laplace equation:

$$R = \frac{2\gamma}{\Delta P}\cos\theta \qquad (1)$$

where, R is radius of the pore, ΔP is differential gas pressure, γ is surface tension of wetting liquid, Galwick™ (γ = 15.9 dynes/cm) and θ is wetting angle.

The pressure at which the capillary action of the fluid within the largest pore is overcome is termed the bubble point pressure. This bubble point pressure is used to determine the largest pore the ENM possesses using equation (1). The mean flow pore diameter is computed from mean flow pressure.

3.5.4 Separation of humic acid

Circular ENMs of 25 mm in diameter with an effective area of 4.1 cm^2 were stamped out and subsequently used for filtration studies. The filtration set up is shown below. It was observed that very little pressure was needed for the ENMs used. The pressure was much less than 1 bar. It was essential that the air flow is regulated effectively at low pressures. To achieve more control and allow for small incremental increase of pressure, the filtration set-up includes a reservoir gas tank, as shown in Figure 3.1. This set-up was successful in determining the flow rate effectively with sufficient control. Both membranes were compacted at 10 psi for 1 hour. An initial feed solution of 50 ppm humic acid (HA) was used

for each salt separation. For each separation experiment, the first 5 ml of permeate was discarded. The next 2 ml of permeate was collected and analyzed. The percentage of solute rejection was determined using the following equation (2):

$$Rejection\ (\%) = \left| 1 - {C_p}/{C_f} \right| \times 100\% \qquad (2)$$

Where C_p is the concentration of the permeate (ppm), C_f is the concentration of the final feed (ppm) that was retained in the cell after separation.

The absorbance of the solution was measured at 254 nm on a UV-VIS spectrophotometer. The separation experiment was repeated with a fresh membrane.

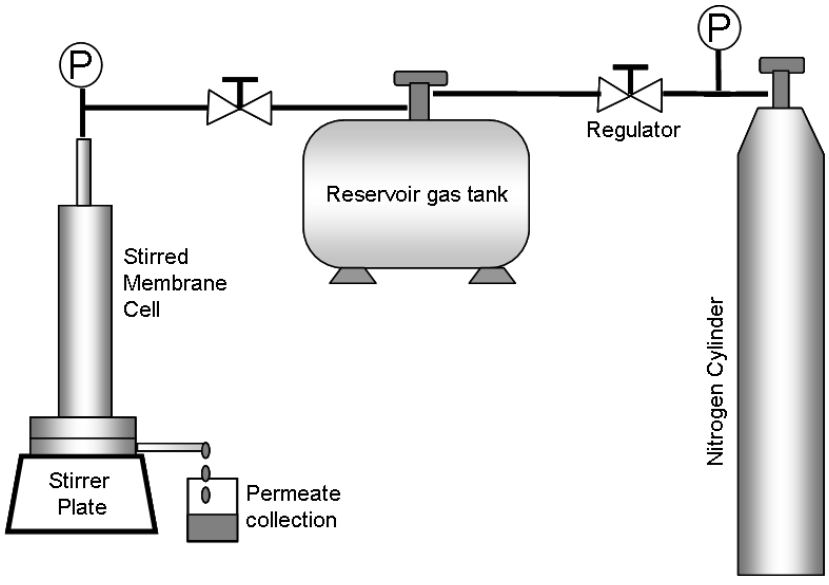

Figure 3.1. Schematic representation of cell used for LEPw and separation of HA.

3.6. Results and discussion

Separation of HA was performed on ENM-control and ENM-SMM. It is worthwhile to take note that separation of HA is typically done on MF membranes of pore-size cut -off value of 0.45 µm. Table 3.1 gives the pore-size distribution data of ENM-SMM and ENM-control. ENM-control has a bubble point of 4.7 µm while ENM-SMM has a bubble point of 5.1 µm. The large pore-size (in comparison to commercial membrane of cut-off value 0.45 µm) of the ENMs suggests that the membrane might not be able to separate the small molecules of HA. Nevertheless separation was still carried out as the architecture of the ENMs is different from commercial membranes.

The slight increase in bubble point for ENM-SMM when compared to ENM-control could be explained in terms of fiber size. The fiber size of ENM- control was 559 nm while that of EM-SMM was 665 nm. This is a 19% increase in size which is attributed to the addition of SMM. The SEM images of these membranes are shown in Figure 3.2. ENM-SMM had a slightly lower contact angle compared to ENM-control and its liquid entry pressure of water (LEPw) value was 46% lesser (see Table 3.2). However it is not clear if the lower LEPw is due to its larger pore-size or the effect of SMM (Chapter 7 is dedicated to investigating the influence and role of SMM). LEPw is the minimum pressure, the membrane can withstand prior to flow of permeate/water and hence where the first permeate/water is collected. With a lower LEPw, the blended membrane can work at a lower pressure for the same flux.

Table 3.1. Pore-size distribution of ENM-SMM and ENM-control.

Membrane	**Fiber size (µm)**	**Bubble Point (psi)**	**Small pore (µm)**	**Bubble point (µm)**	**Mean flow pore (µm)**
ENM-control	0.559 ± 0.302	1.408	0.8758	4.68717	1.9182
ENM-SMM	0.665 ± 0.300	1.297	1.3004	5.08782	2.6079

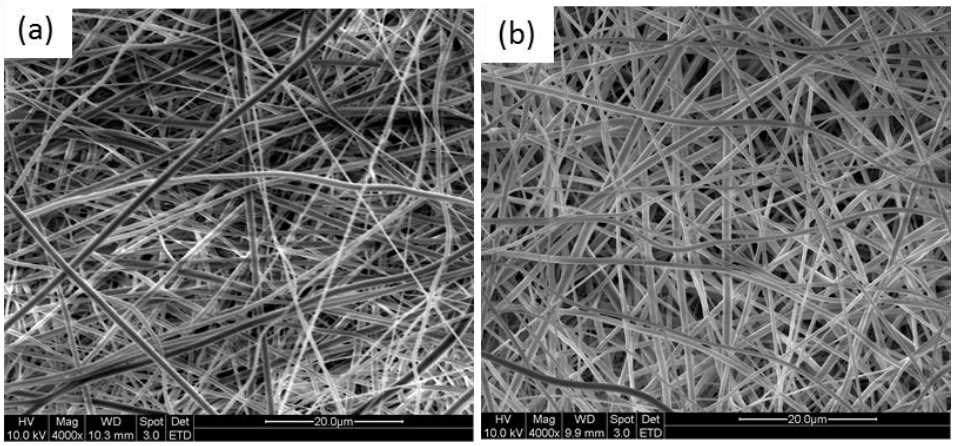

Figure 3.2. SEM images of (a) ENM-control, (b) ENM-SMM

Table 3.2. LEPw and contact angle of ENM-control and ENM-SMM.

Conditions	**LEPw (psi)**	**Right Contact Angle**	**Left Contact Angle**
ENM-control	2.85	121.6±2.5	119.6±5.6
ENM-SMM	1.55	111.3±1.7	108.6±2.4

Separation of 50 ppm HA was carried out on these membranes. The separation of HA was carried out at 5.05 psig for ENM-control while the separation of HA was carried out at 0.25 psig for ENM-SMM. The reason for this difference in applied pressure was to obtain the same initial flux. This was to keep the passage of permeate constant rather than pressure.

Since both of them have different contact angle and LEPw, naturally the rate of permeate flow will be different at the same pressure. Hence it was essential to adjust the same flux rate. The separation of HA on ENM-SMM increases with increasing time while that of ENM-control remained constant. It reached ~50 % rejection at 56 min. Both membranes had a similar flux profile as shown in Figure 3.4. After separation, the membrane was washed

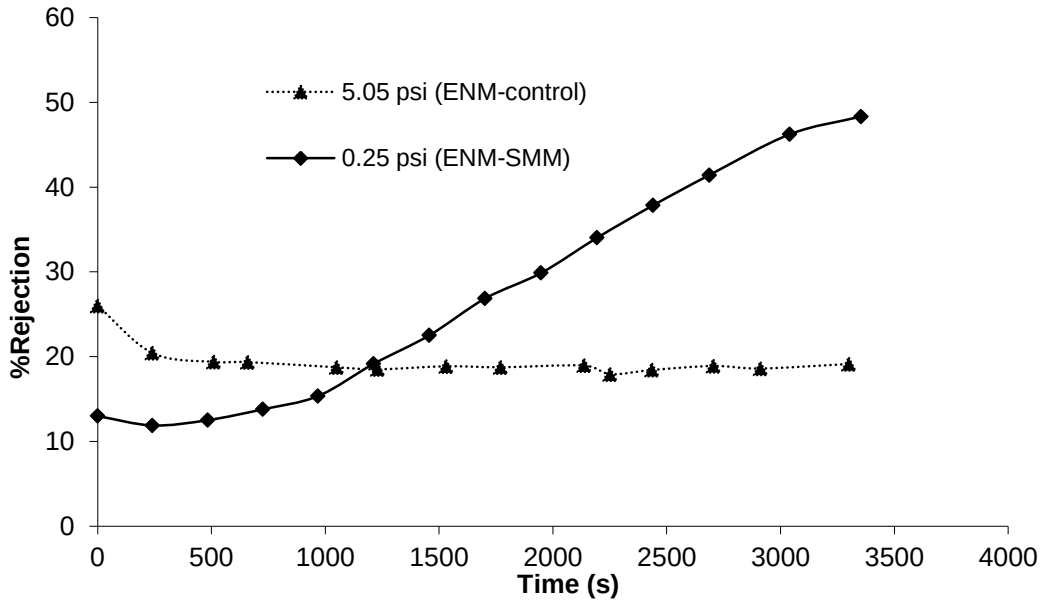

Figure 3.3. Separation of humic acid on ENM-control and ENM-SMM

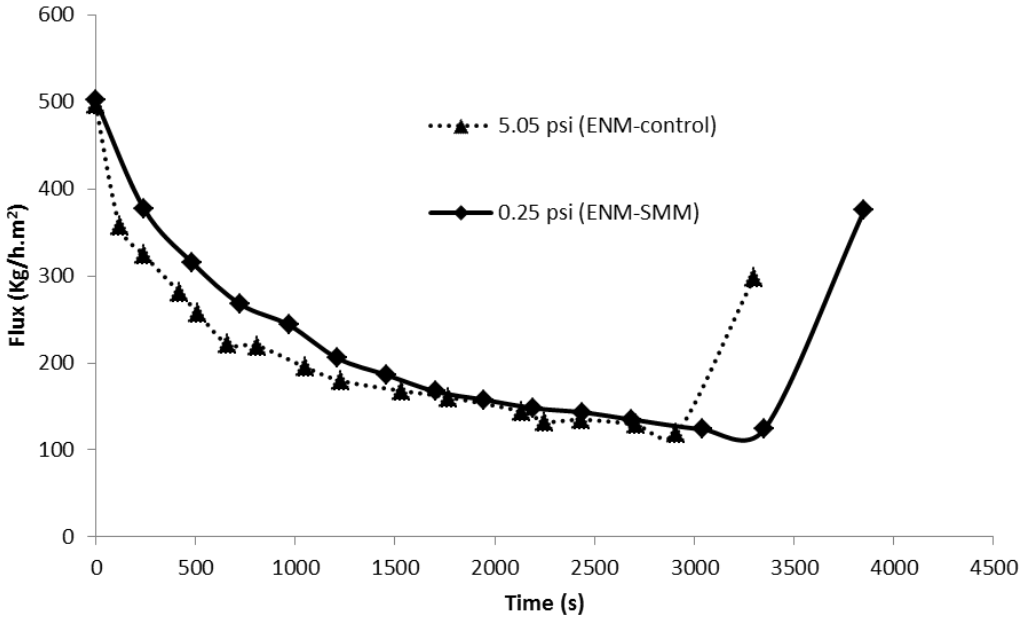

Figure 3.4. Flux of ENM-control and ENM-SMM during HA separation

once with water and the pure water flux was measured. This data is indicative in Figure 3.4 by the sudden jump in flux at the end of each graph. This shows that the membrane was not fouled severely since a certain amount of flux was retained at the end of the experiment. The separation profile as seen in Figure 3.3 did not show any tendency to plateau. Hence the cell was filled with fresh 50 ppm HA (since the cell has been depleted of feed after 56 min) and separation of HA was continued. This was done so as to understand the rejection pattern with time. Figure 3.5 reflects the rejection of HA for an additional hour at the same pressure of 0.25 psi. The rejection of HA increased drastically to 92 %. This rejection is considered economical in contrast to current published data, where HA separation was carried out at 10 psi, with 95% rejection using commercial MF membranes [Yuan 1999]. This shows that SMMs-blended ENMs are more energy efficient for water treatment and the separation performance is very similar to that of commercial MF membranes. The increase in rejection with time is due to accumulation of HA on the surface of ENM-SMM. SEM images support this claim. Figure 3.6 shows a very thin layer of HA formed on the surface of ENM-SMM. Interestingly, no plugging of pores occurred throughout the membrane as evinced from Figure 3.6 c.

This preliminary research inferred that the top of ENM might be capable in supporting a thin film despite its large pore-size. However it is not clear if the ENM is still able to support the film at higher pressures because of its large pore-size? This led the author in introducing a thin polymeric film on the surface of the ENM and maintaining the base porous structure so as to be able to separate solutes including salts and finally understanding the membrane stability at higher pressures. This thin film nanofibrous composite ENM can be achieved by a surface modification technique called interfacial polymerization (IP).

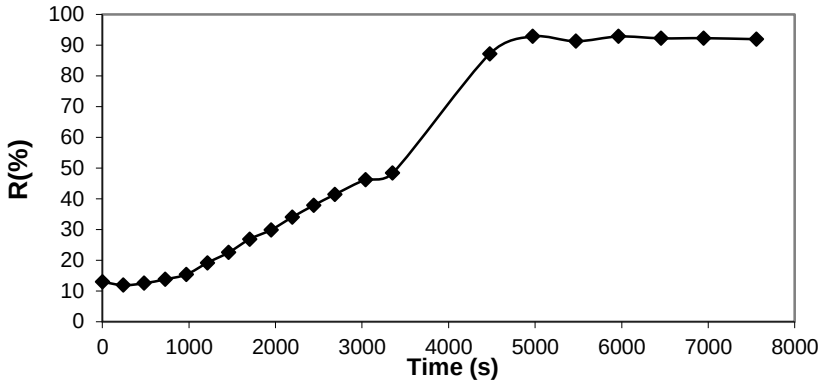

Figure 3.5. Rejection of HA on ENM-SMM for an additional hour.

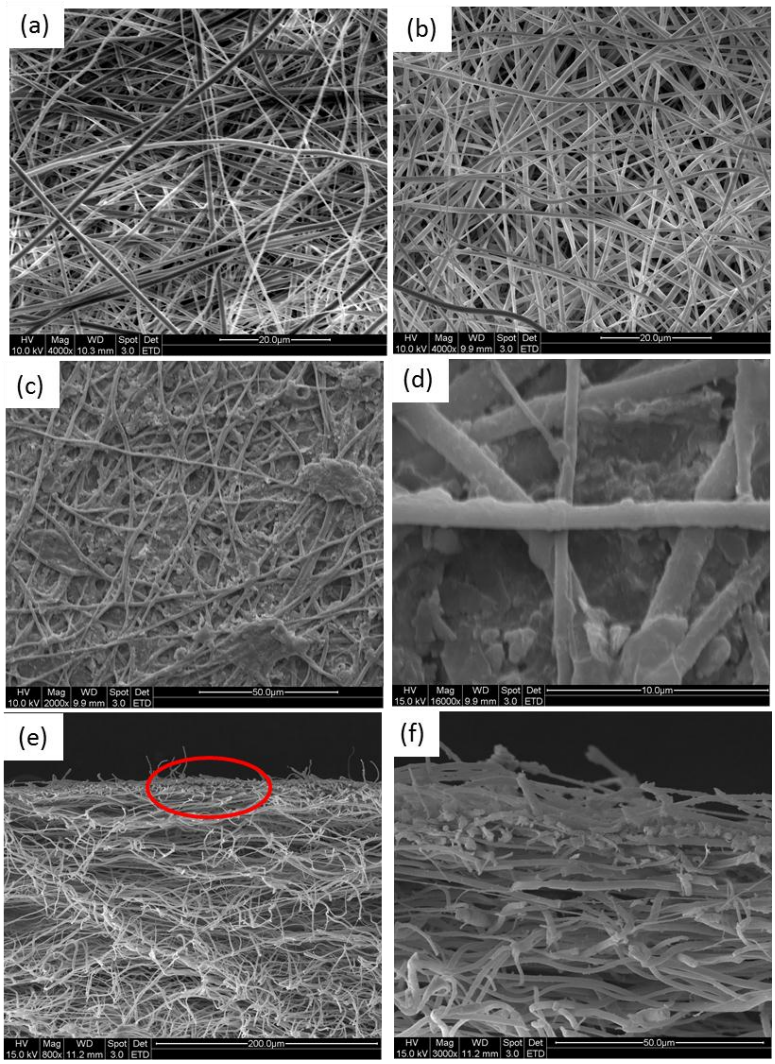

Figure 3.6. SEM micrographs of (a) ENM-control, (b) ENM-SMM, (c) HA separation on membrane b, (d) higher magnification of c, (e) cross section of c, (f) higher magnification of e.

3.7. Conclusion

The pioneering work reflected here was the key driving force for the main objective of this thesis, which was to develop thin film nanofibrous composite (TFNC) ENM via interfacial polymerization.

SMMs consisting of segment-blocked polyurethane were blended with PVDF solution and electrospun into membranes which were subsequently used to separate natural organic matter (NOM) composed of humic substances, typically present in surface water. The modified ENMs were able to attain 92% rejection of humic acid with an applied pressure of only 0.25 psi. Despite its large pore-size, it was able to separate solute. This was because with time, HA formed a layer (aggregated) on the surface of the ENM without clogging the pores. This observation implied the feasibility of fabricating nanofiltration (NF) membranes based on ENM via interfacial polymerization. Through this technique, a thin film might be introduced on the surface of ENM. This sounds impractical as literature shows that interfacial polymerization has to be carried out on a membrane with pore-sizes between 0.01 to 0.22 μm and membranes of pore-size rated at 0.45 μm led to failure of the thin film interfacially produced [Peterson 1993]. However the findings here indicate that the surface of ENM might be able to support a thin layer despite its large pore-size. Besides pore-size there might be another important parameter that influences the formation and consequently the stability of the interfacial layer- which in this case is the surface architecture. It is anticipated that TFNC-ENM should be able to separate solutes and salts. This thesis will explore in finding the essential parameters of ENM that will influence the development of a successful NF membrane and subsequently the separation of solutes/salts. Collectively, this research will provide valuable insights into the influence of ENMs (architecture) in water separation

technology which will be instrumental in the successful implementation of ENMs for NF applications.

CHAPTER 4

FORMATION AND CHARACTERIZATION OF POLYAMIDE COMPOSITE ELECTROSPUN PVDF MEMBRANES

4.1. Introduction

ENMs can be applied to nanofiltration (NF) range for the separation of monovalent and multivalent ions applications by reducing the surface pore-sizes further. This can be accomplished by the introduction of a thin film coating over ENMs via interfacial polymerization technique [Peterson 1993].

The thin film is the critical layer that aids in the removal of small contaminants e.g. dissolved salts. The film on its own is very fragile and weak and hence it is necessary to form this film in-situ on a support layer. This involves, immersing the membrane in an aqueous solution containing a monomer of known concentration and for some time. The wet membrane is then drained as much as possible leaving only a thinly adsorbed layer of solution on the surface of the membrane. The membrane is then placed in an organic solution containing another monomer. Due to the phase differences, the monomer in the aqueous phase will diffuse to the organic phase and react with the other monomer. This diffusion and reaction chemical processes result in the formation of a layer of polymer over the membrane. The thickness of this polymeric layer can be controlled through the reaction time as well as the concentration of the monomers, among other factors.

Commonly used monomers for the organic phase are trimesic acid chloride, tolylene-2,4-diisocyanate (TDI), trimesoyl chloride (TMC). Popular monomers used in the aqueous phase are m-phenylenediamine (MPD), p-dipehenylenediamine (PPD) and polyethylene imine (PEI).

The organic solvent is generally an aliphatic hydrocarbon and it is selected based on the following criteria: 1) ability to dissolve the polyacyl halide to a useful concentration, preferably 0.1 to 1%, 2) it does not interfere during the IP process by reacting or chemically combining with the diamines or polyacyl halides 3) it does not damage the microporous substrate used. Examples of useful aliphatic hydrocarbon solvents are hexane, heptane, naptha, octane and the like but are not limited to this range. Cyclohexane is also deemed useful. Generally hexane and cyclohexane is preferred [USA Patent 5258203]. Since harsh organic solvents are used during interfacial polymerization, the support layer is generally solvent resistant like polysulphone (PSU), polyethersulfone, cellulose, cellulose esters, polyvinyl chloride, polyamide, polyimide and polyvinylidene fluoride (PVDF). Once again PVDF was again selected as it is insensitive to several solvents [Schafer 2005, Sforca 1997].

The intention of this chapter was to prove that interfacial polymerization can successfully be performed on the surface of ENM. PVDF was once again selected (without any SMM) for convenience.

In the present study, PVDF electrospun nanofibrous membranes (ENMs) were surface modified with polyamide layer through interfacial polymerization technique utilizing two different approaches. The polyamide layer was formed through the reaction of p-phenylenediamine (PPD) and Trimesoyl chloride (TMC). PPD is an aromatic diamine and

generally aromatic diamines show better rejections but lower fluxes than aliphatic diamines [Oh 2001]. TMC has a triple functionality and can thus form cross-linked polymer chains. The unreacted groups can also be partially hydrolysed, the degree of which determines the hydrophilicity of the membrane and the density of the polymer film [Kim 2000, Roh 1998]. The aqueous phase reagent selected here is PPD and the organic phase reagent selected here is TMC. The author has also evaluated approach dependent behavior on the quality of film formation and demonstrated the separation efficiency of the membrane for monovalent and divalent salts. The intention of this chapter is to prove that a stable film is able to form on the surface of ENM and is capable of separating salts.

4.2 Experimental section

This part of the experiment was carried out at the National University of Singapore except for the fabrication and separation of NF-UF (1) and NF-UF (2).

4.2.1 Materials

Analytical grade hexane (99%), heptane, ethanol, N.N-dimethylacetamide (DMAC) and acetone were purchased from Sigma Aldrich (USA). Reagents p-phenylenediamine (PPD), Trimesoyl chloride (TMC), sodium hydroxide (NaOH) and sodium carbonate (Na_2CO_3) were also purchased from Sigma Aldrich (USA). Poly (vinylidene fluoride) (PVDF), Kynar 760 was obtained from Arkema, Singapore. Sodium chloride (NaCl) and calcium chloride ($CaCl_2$) were purchased from Merck (Germany) and magnesium sulphate hydrate was purchased from Sino Chemical (China). Insulating tape (DENKA, Vini tape) was manufactured in Japan. Commercial UF polysulfone (PS) membranes of molecular weight cut-off (MWCO)

500 kD used as the support membrane were obtained from the TriSep Corporation, Goleta, CA, USA. NF90 and NF270 were supplied by The FilmTec Corporation (Edina, MN, USA). NF 90 is an aromatic polyamide, which contains carboxylic acid and primary amines ($-NH_2$), whereas NF 270 is a mixed aromatic, aliphatic polyamide (polypiperazine amide) with secondary amine (-NH) and carboxylic acids [ArtuÄŸ 2007].

4.2.2. Preparation of ENM

As mentioned in the literature review, there are several factors that influence the formation of fibers and their morphology during electrospinning. Changing the concentration, molecular weight, solvent and humidity level can lead to different morphology such as thin or fat fiber, branched fibers, flat ribbons, beaded fibers and last but not least, porous fibers [Casper (2004), Bognitzki (2001), Koombhongse, (2001), Fong (1999)]. However not all the parameters are the same for every polymer. Hence the electrospinning conditions have to be optimized for a particular polymer. The easiest way of obtaining different fiber sizes is through the manipulation of concentration of PVDF solution.

Two different polyvinylidene fluoride (PVDF) concentrations, 9% (w/v) and 15% (w/v) were prepared in a mixture of DMAC and acetone at a ratio of 2:3.

A syringe pump (Fisher Scientific, USA) was utilized to supply a constant flow of 4mL/h polymer solution during electrospinning. A voltage of 15kV (Gamma High Voltage Research Inc., USA) was applied to draw nanofibers from the prepared solution. The fibers were collected on a grounded 10 cm square aluminum plate. After the membranes were formed, they were heated from room temperature to 60 ^{o}C for 1 h at a rate of 1 ^{o}C/min. The

membranes were then heated up to 157 ^{o}C at the same rate and subsequently heated at this temperature for 3 h to improve the structural integrity of the membrane. Membranes developed from 9% (w/v) PVDF solution will be referred to as ENM-A and membrane from 15% (w/v) PVDF solution will be referred to as ENM-B.

The fiber diameters were determined from the FE-SEM image using the ImageJ software (http://rsb.info.nih.gov/ij/). All data were expressed as mean ± standard deviation (SD). Levels of significance were calculated using Student's *t*-test (n=30). Differences were considered statistically significant at $p \leq 0.05$.

4.2.3. Preparation of TFNC-ENM

An aqueous solution containing 1% (w/v) of PPD and an organic solution of 0.25% (w/v) TMC in hexane were prepared. All reagents were purchased from Sigma-Aldrich (USA). Two approaches were studied. After interfacial polymerization, the membranes were annealed at 80 ^{o}C for 10 min to complete the reaction. Subsequently, they were washed with copious amounts of water to remove un-reacted reactants and loose film.

4.2.3.1 Approach A: Immersion in aqueous phase first.

PVDF ENM-A and ENM-B were first taped with an insulating tape onto a glass plate and immersed in 1% (w/v) PPD/water (aqueous phase) for 1, 3 or 5 min. The membranes were subsequently tilted in a vertical position for 5 min and any excess solution on the surface was removed by gently dabbing with lint free paper. Subsequently these membranes were

immediately immersed in a 0.25% (w/v) of TMC/hexane (organic phase) solution for 1, 5 or 10 min.

Three additional variations to the IP process stated above were carried out. In the first variation, pre-treatment of the ENM was carried out with 70 % (v/v) ethanol and washed several times with water to wet the membrane and subsequently dipped in 1% (w/v) PPD/water solution for 3 or 60 min. Thereafter, the membrane was placed in 0.25% (w/v) of TMC/hexane solution for 10 mins. In the second variation, the membrane was exposed to plasma (March Instruments), 15 W, 13.56 MHz for 10 s before IP was performed. The third variation involves the preparation of aqueous PPD solution with 0.1 M NaOH and 0.2 M Na_2CO_3 solution (1:1). Table 1 provides an overview of the different membrane conditions used in approach A.

4.2.3.2 Approach B: Immersion in organic phase first.

The reverse of approach A was performed here. Without taping down the support membranes onto a glass plate, they were soaked in 0.25% (w/v) TMC/hexane solution for 3 min, immediately followed by gentle placement of the membranes on the surface of the PPD/water solution (1% (w/v)). The concentrations of the organic and aqueous phase were further manipulated (see Table 4.3). Four different ratios of reactant solutions were prepared and the ratio within bracket indicates the weight % TMC and PPD: TMC/PPD (1:1), TMC/PPD (1:2), TMC/PPD (1:4) and TMC/PPD (1:16). The membrane floats in the aqueous solution and hence only one side of the membrane was being modified. The contact with the aqueous PPD phase was fixed at 10 min.

Successful composite membranes made from ENM-A and ENM-B will be labelled as TFNC-A and TFNC-B.

A schematic representation of these two different approaches is illustrated in Figure 4.1.

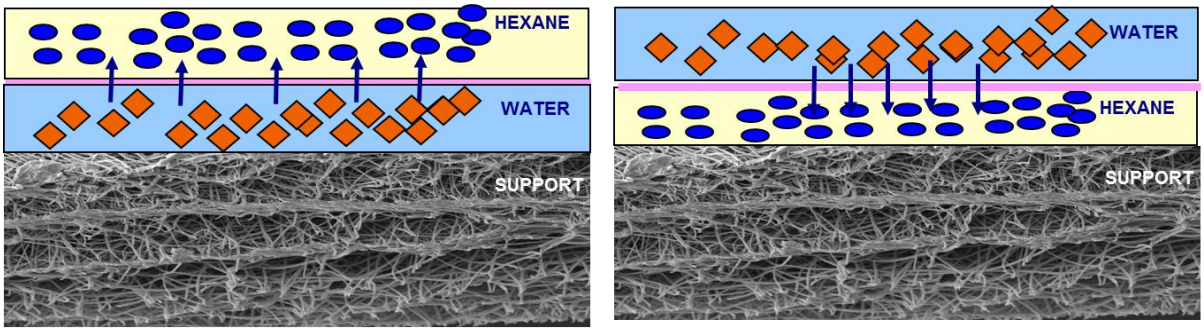

Figure 4.1. Interfacial polymerization techniques on (a) hydrophilic membrane (approach A) and (b) hydrophobic membrane (approach B).

4.2.4. Characterization

The surface and the cross-section of the membranes were observed by the field emission scanning electron microscopy (SEM, FEI-QUANTA 200F, The Netherlands). For cross-section, samples were prepared with a sharp blade. The samples were coated by platinum in the auto fine coater (JFC-1600, JEOL, Japan) before taking SEM images. Diameter of the nanofibers was determined from the FESEM image using the ImageJ software (http://rsb.info.nih.gov/ij/) and a value of $p \leq 0.05$ was considered statistically significant.

The pore-size distribution of the support membrane was evaluated using a capillary flow porometer (Porous Materials Inc., U.S.A).

Permeation tests were performed on an Amicon stirred cell (model 8010 and able to withstand a maximum operating pressure of 75 psig) at an operating condition of 70 psig. Circular composite ENM 25 mm in diameter were stamped out and placed in the test cell with the active layer facing the incoming feed. The effective membrane area was 4.1 cm^2. The membranes were initially pressurized at 70 psig until the constant flux was achieved at least for 3 h consecutively prior to any salt separation experiments. This was done to condition the membrane for the pure water permeation and salt separation runs that followed.

An initial feed solution of 2000 ppm was used for each salt separation. For each separation experiment, the first 1 ml of permeate was discarded. The next 2 ml of permeate was collected and analyzed. The percentage of solute rejection was determined using the following equation (3):

$$\text{Rejection (\%)} = \left(1 - \frac{2\lambda_p}{\lambda_{fo} + \lambda_{fi}}\right) \text{x } 100\% \qquad (3)$$

where λ_p is the conductivity of the product ($m\Omega^{-1}cm^{-1}$), λ_{fo} is the conductivity of the initial feed ($m\Omega^{-1}cm^{-1}$) and λ_{fi} ($m\Omega^{-1}cm^{-1}$) is the conductivity of the final feed that was retained in the cell after separation. The conductivity of the solution was determined using a conductivity meter (Orion 3star, Thermo Scientific, USA) and the values are directly used in equation (3). The separation experiment was repeated thrice for each salt. Statistical analysis was carried out and a value of $p \leq 0.05$ was considered statistically significant.

Table 4.1. Summary of membrane preparation conditions in approach A.

ENM Pre-treatment before interfacial polymerization	PPD* immersion time (min)	TMC** immersion time (min)
Nil	1	1
Nil	1	5
Nil	1	10
Nil	3	1
Nil	3	5
Nil	3	10
Nil	5	1
Nil	5	5
Nil	5	10
Nil	60	10
Nil	120	10
ENM pre-wetted with 70% (v/v) aq. ethanol	3	10
ENM pre-wetted with 70% (v/v) aq. ethanol	60	10
ENM not pretreated but soaked in PPD solution prepared with 0.1 M NaOH and 0.2 M Na_2CO_3 (1:1)	3	10
ENM was exposed to plasma	3	10

*PPD concentration of 1 % (w/v); ** TMC concentration of 0.25 % (w/v).

Static water contact angle (WCA) measurements were performed on the surface of ENMs using an Advanced Surface Technologies, Inc., VCA2000 (USA) video contact angle system. A thin strip of the membrane material ~ 0.7 cm by 4 cm was pasted on a clean glass slide with a double sided tape. A water drop of 0.5 µL was dispersed on the membrane surface and the contact angle was determined using the system software.

The change in the surface chemistry of ENMs were detected using a multi bounce (Germanium crystal) horizontal Attenuated Total Reflectance-Fourier Transform Infrared Spectroscopy (ATR-FTIR, Thermo Nicolet Avatar 360, USA). Each spectrum was obtained by accumulating 64 scans at a resolution of 8 cm^{-1}.

4.3. Results and Discussion

4.3.1 Electrospun nanofiber support membrane

When the solution of 9% (w/v) polymer concentration was electrospun and its morphology inspected under the FE-SEM, presence of beads along with the fibers was observed (Figure 4.2a). The fiber diameter was found to be 249 ± 80 nm. When the concentration of the polymer was increased to 15% (w/v), the formation of bead-free fibers with increased average fiber diameter (353 ± 153 nm) was observed (Figure 4.2b). This is because of the fact that polymer solution concentration is one of the important factors in determining the fiber size and morphology [Ramakrishna 2005]. The formation of beads and beaded fibers is driven by the surface tension [Magarvey 1962]. Generally at a low polymer concentration, the viscosity of the solution is not sufficient enough to form a stable jet. There is capillary breakup of the electrospinning jet by surface tension thus leading to formation of beads [Fong

1999]. As the polymer solution concentration increases, the polymer solution viscosity subsequently increases and the deformation forces in the solidification process are greatly reduced thus leading to the formation of uniform fibers [Xinhua 2002].

Even though the membrane thickness (approximately 120 µm) was constant for both ENM-A and ENM-B, but the difference in the two membrane architectures gave rise to different pore-size distribution. An overview of the membrane's characteristics is listed in Table 4.2.

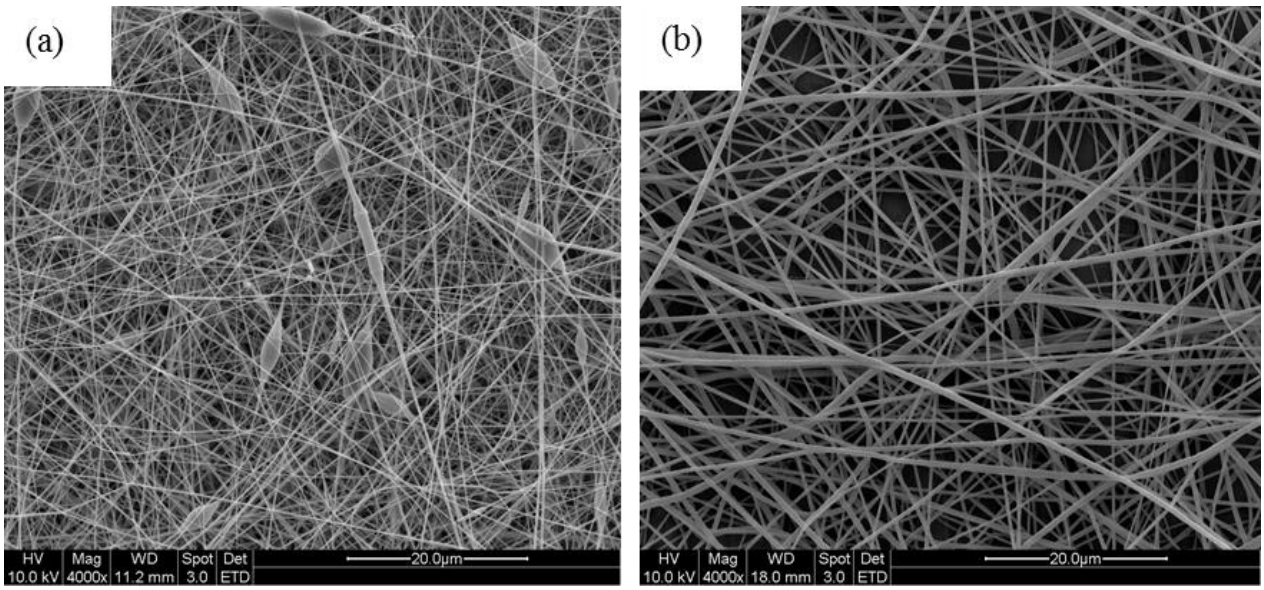

Figure 4.2. Surface architecture of (a) ENM-A (9 % (w/v)) and (b) ENM-B (15% (w/v)).

Table 4.2. Summary of membrane characteristics.

Membrane	PVDF solution (w/v)	Fiber diameter (nm)	Largest pore (µm)	Smallest pore (µm)	Membrane thickness (µm)
ENM-A	9 %	249± 80	1.8	0.2	~120
ENM-B	15%	353±153	3.4	0.7	~120

The difference in the pore-size distribution (range of 0.2 µm to 1.8 µm, Figure 4.3) in ENM-A was attributable to the presence of beads and finer fiber diameters gave rise to a higher packing density and hence smaller pores in ENM-A when compared to ENM-B pore-size (range 0.7 µm to 3.4 µm, Figure 4.4) and fiber diameters.

4.3.2 Composite membrane fabrication- Approach A

Figure 4.5 (a), (b) and (c) depict the extent of the thin surface layer formed on the ENM using the approach A with immersion periods of 3, 60 and 120 min, respectively, in the aqueous PPD solution. As can be seen from the micrographs, no film was formed after 3 min of immersion (Figure 4.5 (a)) while some film starts to be formed between the pores after 60 min immersion (Figure 4.5 (b)). Although some clear thin film formation occurred after the extended immersion period (for 120 min), the film formation was not homogeneous across the ENM and the presence of pin-holes or defects on the surface were observed, which are undesirable for subsequent filtration.

This non-uniformity was due possibly to the hydrophobic nature of the ENMs (surface contact angle of 135^{o}) and its postulated here that the aqueous PPD solution could not penetrate into the pore of the hydrophobic ENM. This may have led the PPD not to be retained uniformly on the surface of ENM, which reacted with TMC in the organic phase in the second stage. Similar results were observed in the case of ENM-A as well. It is to be noted here that the hydrophobic nature of ENM was due to its inherent surface roughness and trapped air pockets. The Wenzel and Cassie models [Wenzel 1936, Cassie 1944] provide an explanation for the relation between the surface morphology and the wetting behavior. The Wenzel model hypothesizes that an increase in surface roughness causes an increase in

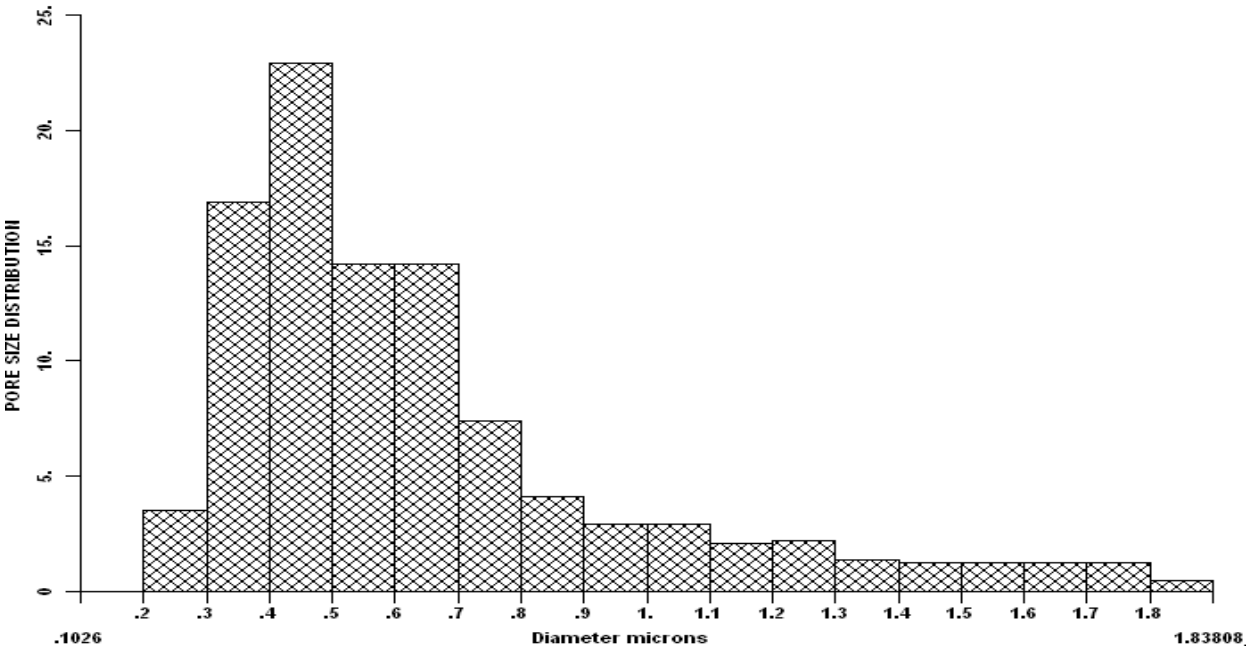

Figure 4.3. Pore-size distribution of the support ENM-A electrospun from 9% (w/v) PVDF solution.

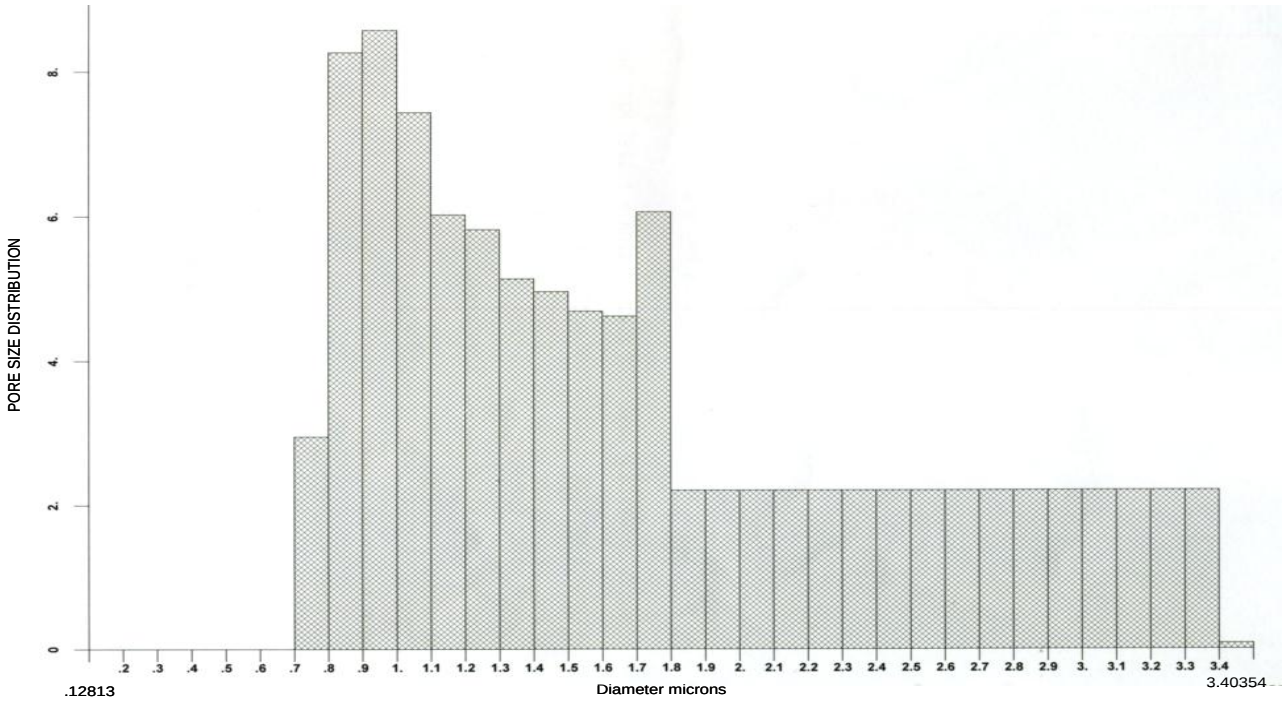

Figure 4.4. Pore-size distribution of the support ENM-B electrospun from 15% (w/v) PVDF solution.

surface area which leads to enhanced hydrophobicity. Since the liquid fills up the spaces on the rough surface leading to a better pinning, these types of surfaces show a high hysteresis. The Cassie model suggests that a rough surface will lead to the creation of grooves with trapped air. Liquid droplets remain suspended on these air trapped grooves and thus are not pinned to the surface leading to a low hysteresis. ENMs possess both rough surfaces and huge air pockets between each fiber as easily evident in the SEM micrographs of the ENM.

To overcome the problem of the high hydrophobicity of the ENMs and to make them uniformly wettable by aqueous PPD solution three variations were carried out: (1) pre-wet the ENM with 70% (v/v) ethanol, (2) preparing the PPD solution with NaOH and Na_2CO_3 and (3) exposing the ENM to plasma.

4.3.3 Enhancement in wettability by aqueous ethanol treatment

In the first variation, the PVDF ENM was pre-wetted with 70% (v/v) aqueous ethanol solution followed by interfacial polymerization leads to a formation of deep purple film on the surface of the ENM. By pre-wetting the membrane with ethanol, the contact angle of the membrane was reduced from 135^o to 0^o. When the PVDF ENM was soaked in PPD phase for 3 min followed by a 10 min reaction with TMC phase, a coarse and rough surface with globule like structures was observed with the formation of polyamide film (Figure 4.6 (a)).

When the immersion time was increased from 3 min to 60 min, the film adopted a honeycomb structure (Figure 4.6 (b)). This could be due to the formed globule like structure for the lower immersion time burst to give the honeycomb appearance and/or directing

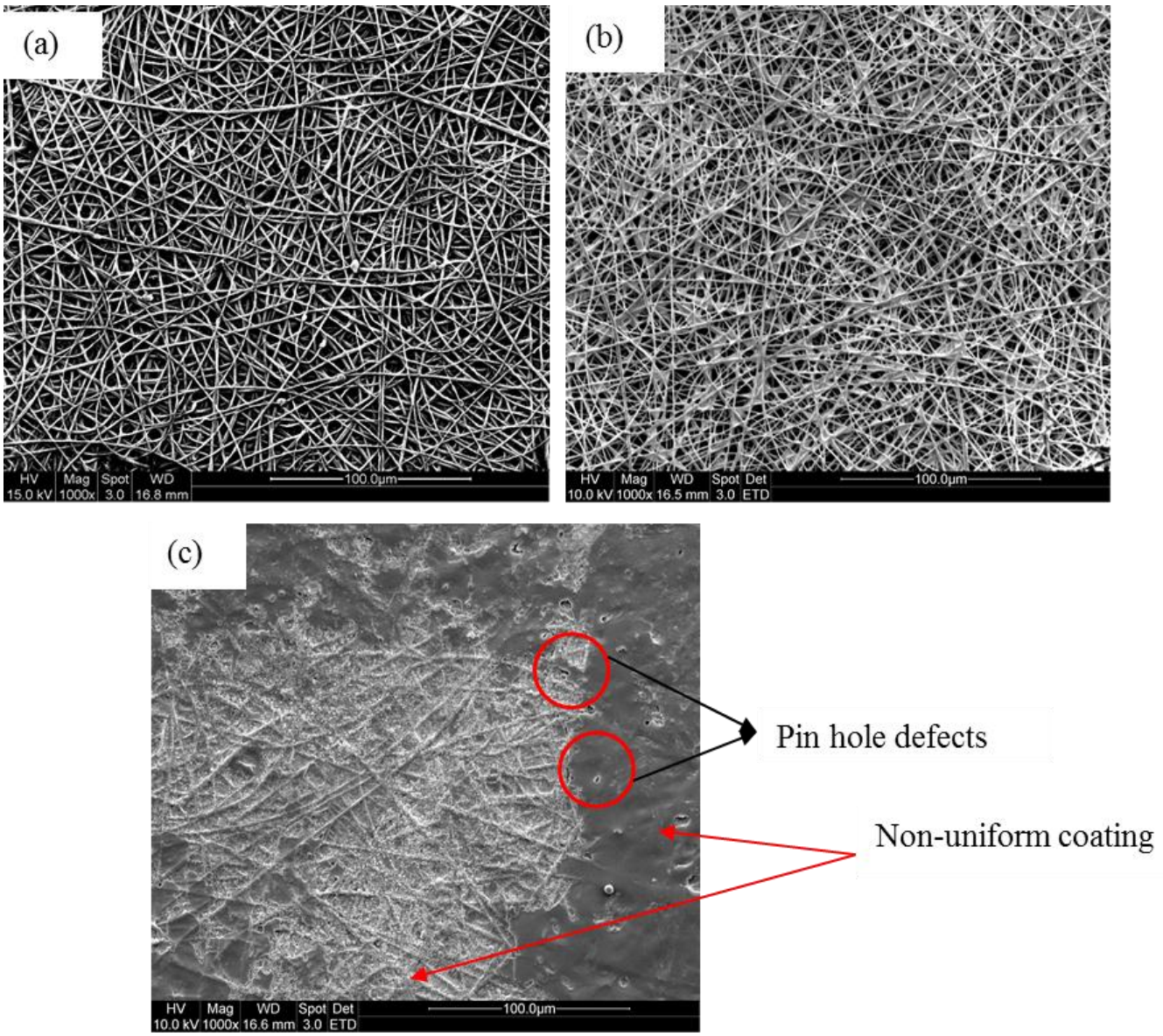

Figure 4.5. Approach A: Surface architecture of ENMs-B after they were immersed in the aqueous phase (a) 3 min and (b) 60 min (c) 120 min followed by 10 min soaking in the organic phase.

capability of more available PPD molecules at a higher immersion time for reaction with TMC.

Although film was formed on the ENM surface, these membranes were not able to reject any salt. On closer inspection of the honeycomb structure (Figure 4.6 (c)), indicates that many "holes" were observed on the surface, which most probably resulted in the unsuccessful rejection of salts.

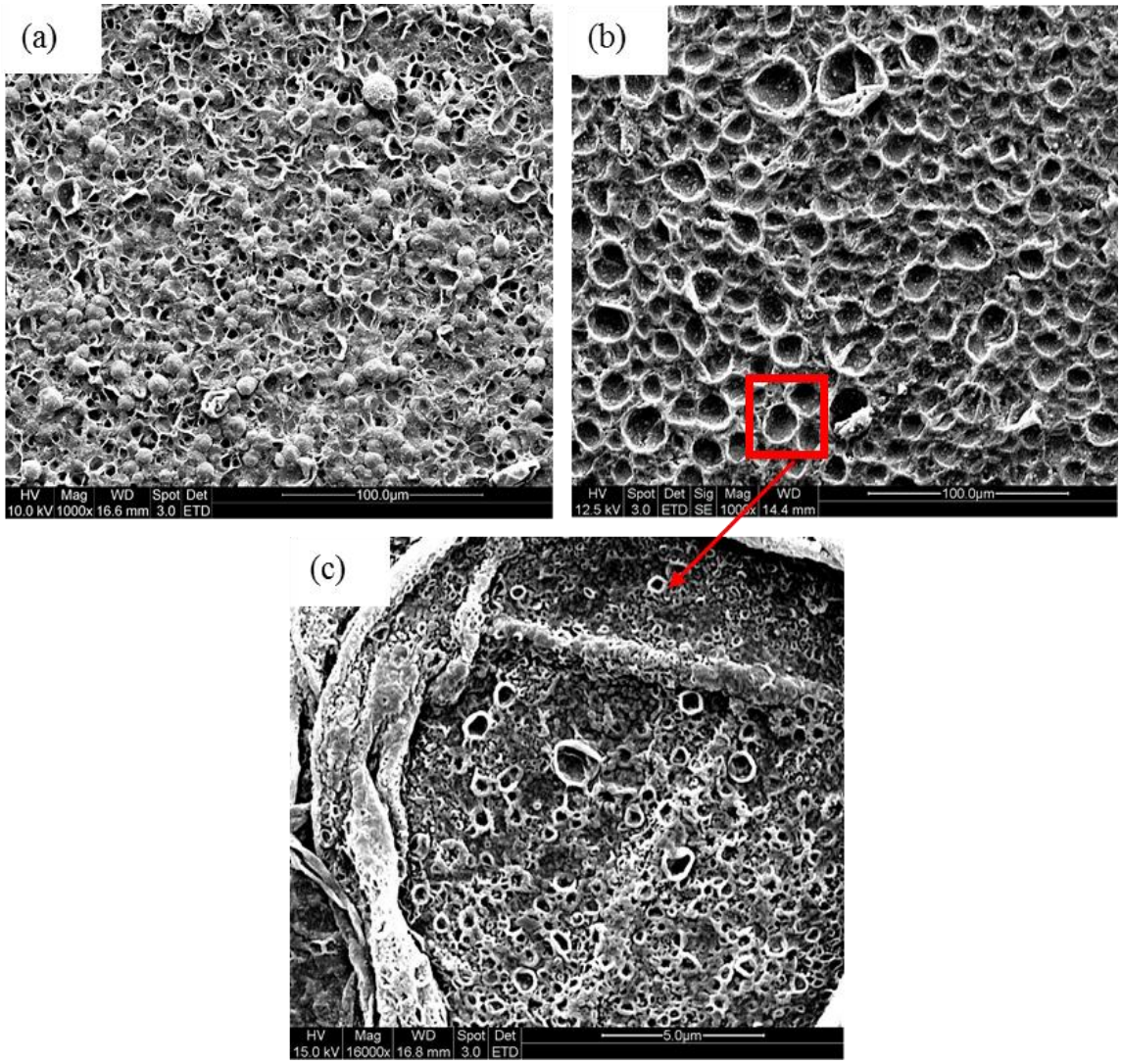

Figure 4.6. Surface architectures of ENMs-B after they were wetted with aqueous ethanol first followed by immersion in aqueous phase (approach A) for (a) 3 min, (b) 60 min and subsequent soaking in organic phase for 10 min. Micrographs (c) is a higher magnification of (b).

Figure 4.7 shows a pictorial difference when the membrane was wetted with ethanol and without ethanol indicating a difference in chemistry of the film formed. Also, the interfacial layer of membrane (a) in Figure 4.7 (a) was very brittle and peeled easily. Since there was no separation achieved, the chemistry of this difference was not further evaluated.

Figure 4.7. Pictorial view of a) membrane wetted with ethanol, b) membrane without ethanol wetting

4.3.4 Immersion in basic solution

PPD solution was prepared with NaOH and Na_2CO_3 solution to wet the membrane easily. Also, they have been added as acid receptors to neutralize the hydrogen chloride generated during formation of the polyamide via reaction of the acid halide and the amine solution [Zupancic 1987].

The film formed on the surface of the support ENM can be observed in Figure 4.8 and looked completely different when the membrane was pre-wetted with 70% (v/v) ethanol instead. The added additives have played an important role in the way the film was formed and also tend

to influence monomer solubility, diffusivity, hydrolysis, or protonation or to scavenge inhibitory reaction by-products. It has been reported in the literature that any factors alter the solubility and diffusivity of the amine monomer in the organic phase affect the reaction rate and thus the morphology and structure of the resulting polyamide film [Gosh 2008]. Although the membranes morphologies were different, they were not influencing the separation tendency and they were also not able to separate any monovalent and divalent salts. The magnification of the surface under SEM (Figure 4.8 (b)) clearly indicates that there were many holes on the film and this may have prevented the separation of salts.

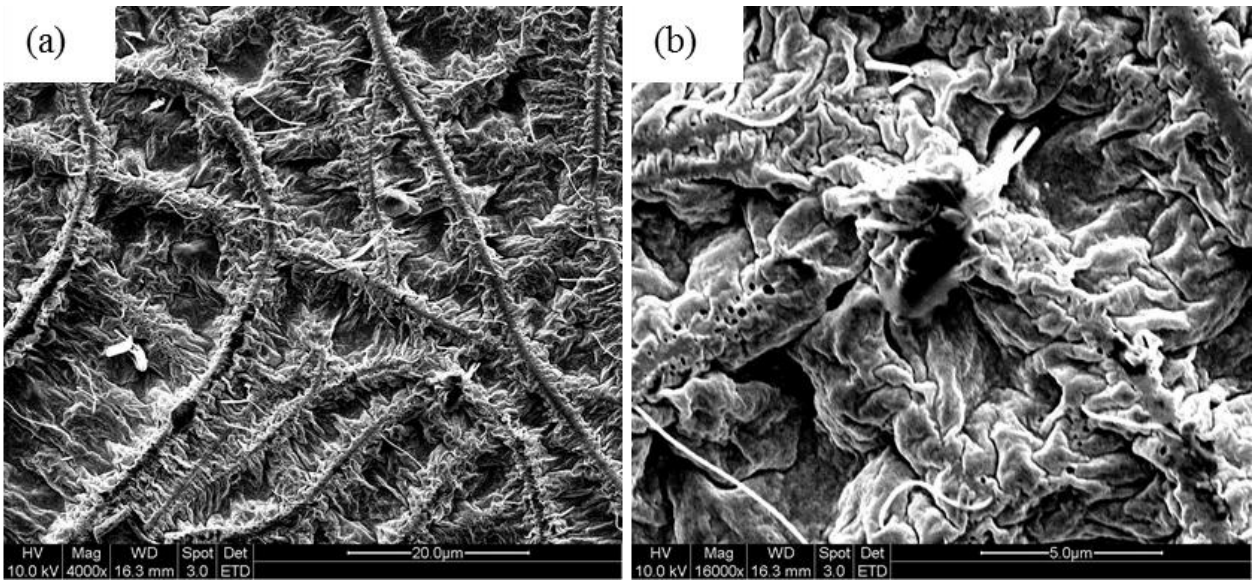

Figure 4.8. Surface architecture of the film formed on the surface of ENM-B when the aqueous PPD solution was prepared with 0.1M NaOH solution and 0.2M Na_2CO_3. (a) 4000x, (b) 160000x.

4.3.5. Plasma treatment

When the support ENM was exposed to plasma, the membrane surfaces were easily wetted by the aqueous phase, however, there was no film formed on the surface of the membrane

[Figure 4.9]. This might be because the radicals formed on the surface were insufficient to retain the aqueous solution.

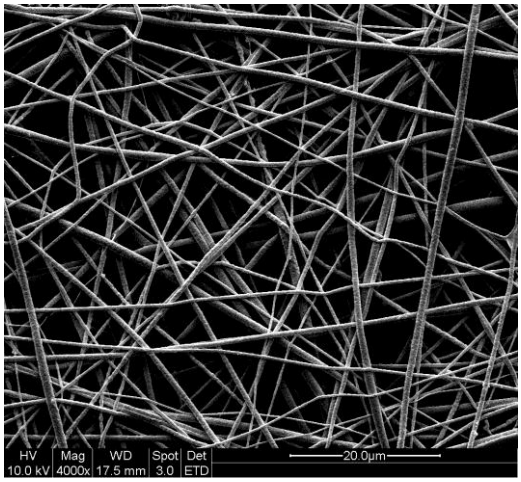

Figure 4.9. Surface morphology of ENM-B after being exposed to plasma and subsequently to interfacial polymerization using approach A.

4.3.6. Composite membrane fabrication- Approach B

Using Approach B, a composite polyamide film on both ENM-A and ENM-B without any defects was successfully made. The surface topography of the composite-ENMs is shown in Figure 4.10. One advantage of this approach was that IP could be carried out without fixing the membrane on a glass plate, hence saving time. We believe this approach is generally not preferred for conventional phase-inverted membranes as the membranes are coagulated in water bath and stored in water. It was obvious that the application of approach B required drying of the support. It would add another step in membrane preparation; hence approach A is generally used for conventional phase-inverted membranes. However, in this instance, PVDF was hydrophobic and hence it is more suitable to immerse the membranes in an organic phase first followed by IP.

Separation of $MgSO_4$ was carried out on both TFNC-A and TFNC-B. When 2000 ppm $MgSO_4$ was used as a feed solution, TFNC-A was able to achieve a salt rejection of 70.2% at a flux of 0.62 L/m^{2}h, while the TFNC-B achieved a salt rejection of 75.3% at a flux of 0.66 L/m^{2}h. TFNC-B showed better separation efficiency in terms of flux and rejection, which can be explained as follows. Firstly, ENM-B had a larger bubble point than ENM-A and hence resulting in a higher flux than ENM-A. Secondly, ENM-A had beaded fibers which might have affected the packing nature of the polymer chain in the polyamide film. This could have subsequently reduced the percentage rejection of $MgSO_4$ in ENM-A.

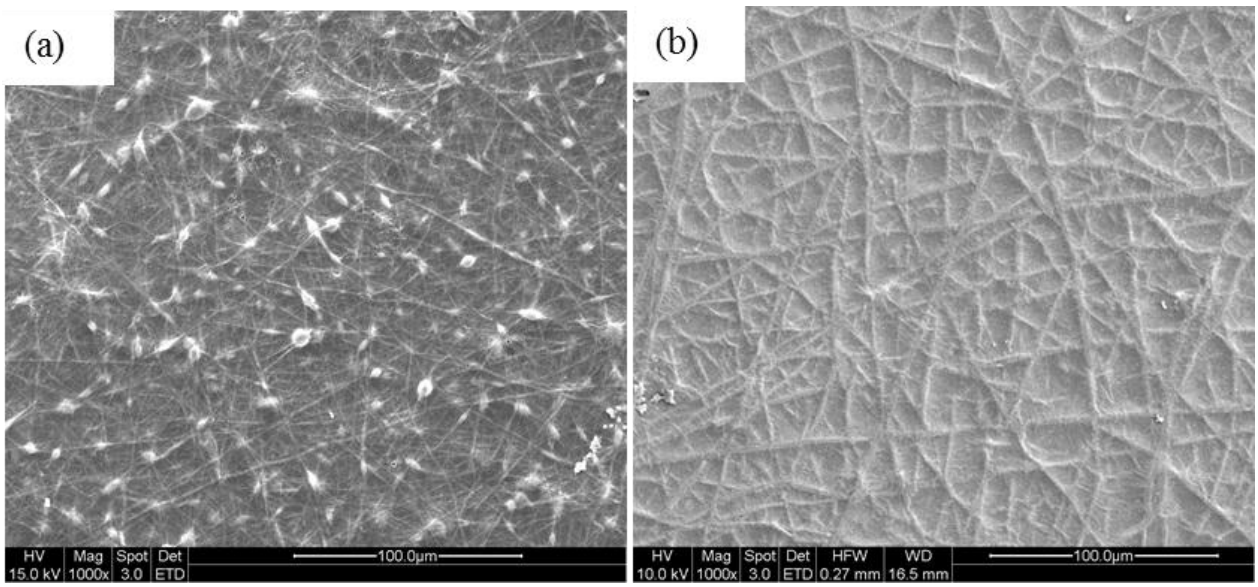

Figure 4.10. Polyamide film on the surface of (a) ENM-A (b) ENM-B.

The results obtained for the separation of various salts for ENM-B are shown in Figure 4.11. A NaCl rejection of 61.6% at a flux of 0.56 L/m^{2}h was obtained for 2000 ppm NaCl. In addition, the rejection of 2000 ppm $CaCl_2$ was 70.2% and the flux attained was 0.77 L/m^{2}h. The rejection and flux of $MgSO_4$ was significantly higher than NaCl and $CaCl_2$ ($p \leq 0.05$). The observed order of solute rejection for various salts are NaCl<$CaCl_2$<$MgSO_4$. This can be explained as follows. The hydration numbers (or related measures of hydrated ion size)

measured for the sodium, calcium and magnesium ions in water are 1.66, 5.29, and 7.06, respectively [David 2001] and hence higher amount of $MgSO_4$ was rejected than NaCl. Apart from this, if we compare the hydrated radius of anions between chloride and sulphate ions, the hydrated radius of chlorine and sulphate are 0.19 and 0.30 nm, respectively [Kiriukhin 2002].

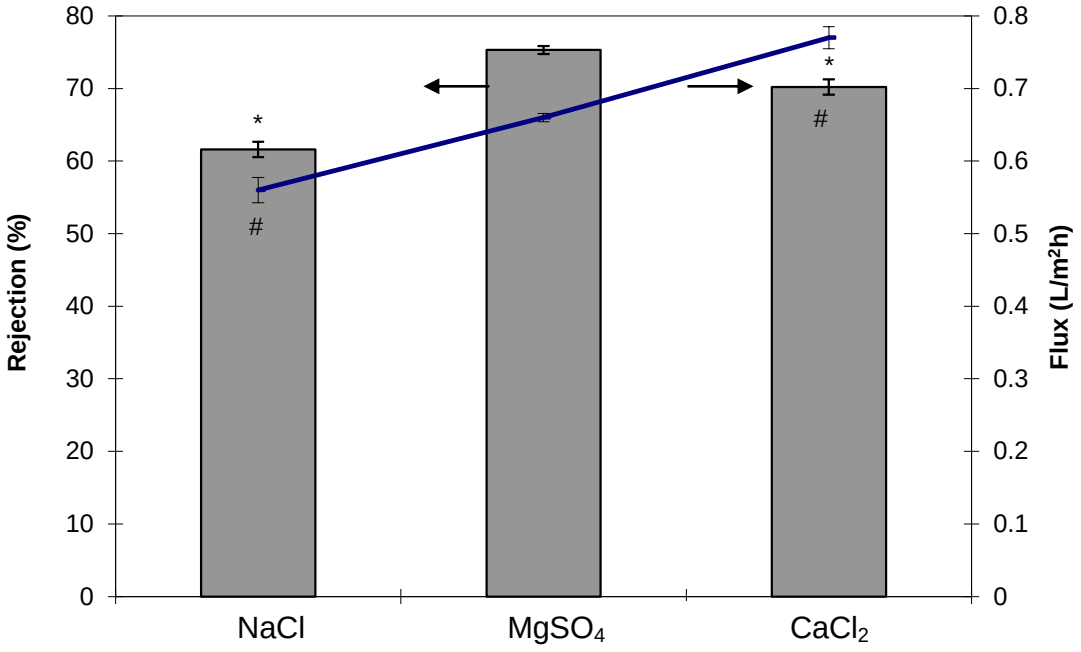

*Figure 4.11. Performance of the membrane prepared by approach B where the support ENM-B was soaked in 0.25% (w/v) TMC solution in hexane for 3 min and then one surface contacted with 1% (w/v) aqueous PPD solution for 10 min. * Significant against $MgSO_4$ rejection at $p \leq 0.05$ and # significant against $MgSO_4$ flux at $p \leq 0.05$.*

Since a successful film was formed using 0.25% (w/v) TMC and 1% (w/v) PPD, the ratio of the monomers were varied to study the effect on film formation and separation. The resulting concentrations studied are reflected in Table 4.3. The rejection and separation profile of the TFNC that was formed from different TMC and PPD concentration ratios is shown in Table 4.4.

The surface architecture of the modified membrane, when the concentration of both PPD and TMC solution was 1% (w/v), is shown in Figure 4.12. The salt rejection was zero per cent, which was due to incomplete formation of the thin film on the surface of the membrane. When the ratio was 1:2; i.e., TMC concentration was 0.5% (w/v) and PPD concentration was 1 % (w/v), $MgSO_4$ and NaCl rejections were 43.7% and 42.5%, respectively.

The ratio of TMC to PPD was modified to 1:16 to ensure that there is excess PPD to react completely with TMC to form a better cross-linked film. When the ratio was changed to 1:16 while maintaining the same soaking time of 3 min in TMC and 10 min in PPD, a $MgSO_4$ rejection of 80 % with a flux of 0.51 L/m^2h and NaCl rejection of 67% with a flux of 0.52 L/m^2h were achieved. By increasing the concentration of PPD with respect to the concentration of TMC, better separation results were achieved. This is because of the tri-functional nature (which is 3) of TMC molecule, which is more than that in PPD molecule. Stoichiometrically, a larger number of PPD is necessary to complete the cross-linking of polyamide chains and/or higher concentration may prevent the hydrolysis of TMC by a competing reaction and thereby to favor the formation of polymers. Also, when the concentration of the reactant (PPD) used are low, it may not be adequate to cover such a relatively big pores present in the ENM. However, at higher concentration of the reactant, the possibility of covering the pores by thin film of polymer may be high. Hence the separation is relatively good for high concentration reactant used membrane than lower concentration one. It is to be noted here that generally higher solution concentration of reactants favors the formation of polymers over the oligomer formation [Sundarrajan 2003]. The cross-section of the membrane that was modified with TMC and PPD in the ratio of 1:16 is shown in Figure 4.13. The polyamide layer was uniform throughout the cross-section of the membrane and

had an approximate thickness of 27 µm. This layer occupied approximately 20% of the entire ENM.

Table 4.3. Effect of concentration for the formation of IP.

Approach B	Ratio of TMC conc.: PPD conc.	TMC conc. (% (w/v))*	PPD conc. (% (w/v))**
i	1:1	1	1
ii	1:2	0.5	1
iii	1:4	0.25	1
iv	1:16	0.25	4

*TMC immersion time, 3 min; **PPD immersion time, 10 min.

Table 4.4. Flux and separation profile of TFNC-B made from different ratio of monomer concentrations.

Approach B (TFNC-B)	$MgSO_4$ experiment*		NaCl experiment*	
	Rejection (%)	Flux (L/m^2h)	Rejection (%)	Flux (L/m^2h)
i	0	-	0	-
ii	43.7	1.25	42.5	1.20
iii	75.3	0.66	61.6	0.56
iv	80.7	0.51	67	0.52

* Solute concentration in feed 2000 ppm, operating pressure 70 psig

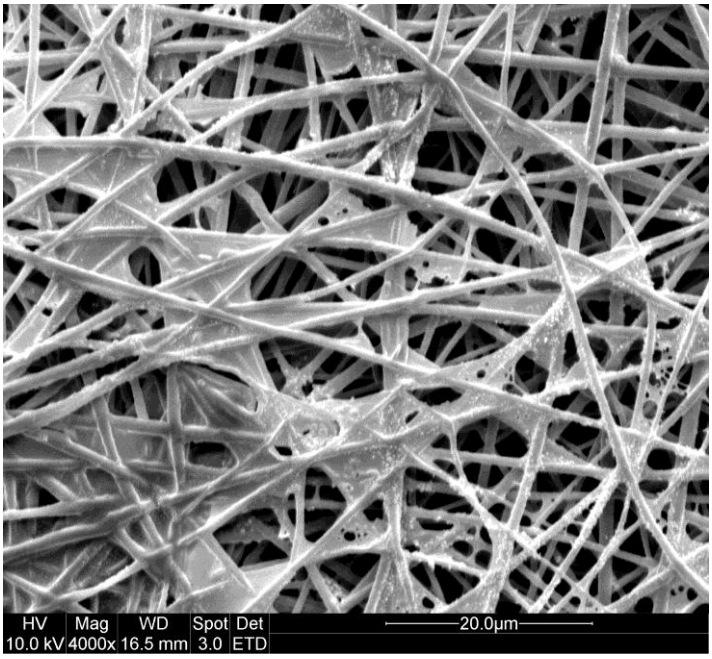

Figure 4.12. Top surface image of composite ENM-B prepared by approach B (i).

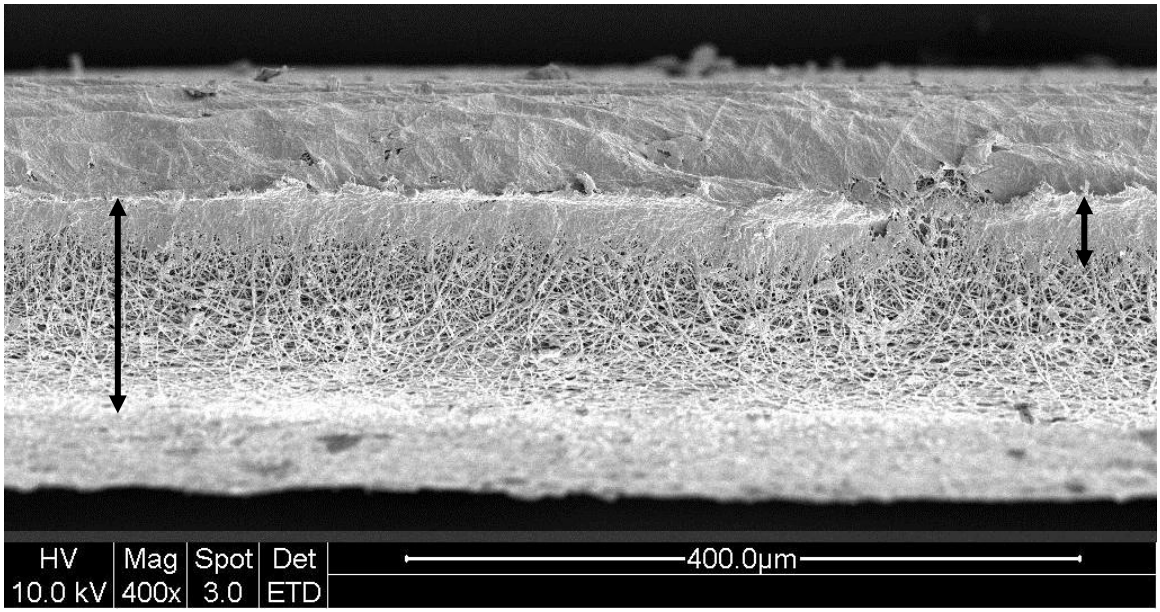

Figure 4.13. Cross-sectional image of composite ENM-B prepared by approach B (iv).

The surfaces of the PVDF ENM, composite-ENM B, PPD and TMC were characterized by ATR-FTIR (Figure 4.14). The chemical species present in the polyamide layer could be

differentiated from the non-modified PVDF ENM. The spectrum of the composite-ENM indicates that interfacial polymerization has occurred since the acid chloride band at 1760 cm^{-1} (present in TMC) was absent and an amide I band at 1650 cm^{-1} (amide I) was present which is characteristic -C=O- band of an amide group. In addition to this, other band characteristic of the polyamide layer, amide II, -C-N- stretch, was also seen at 1520 cm^{-1}.

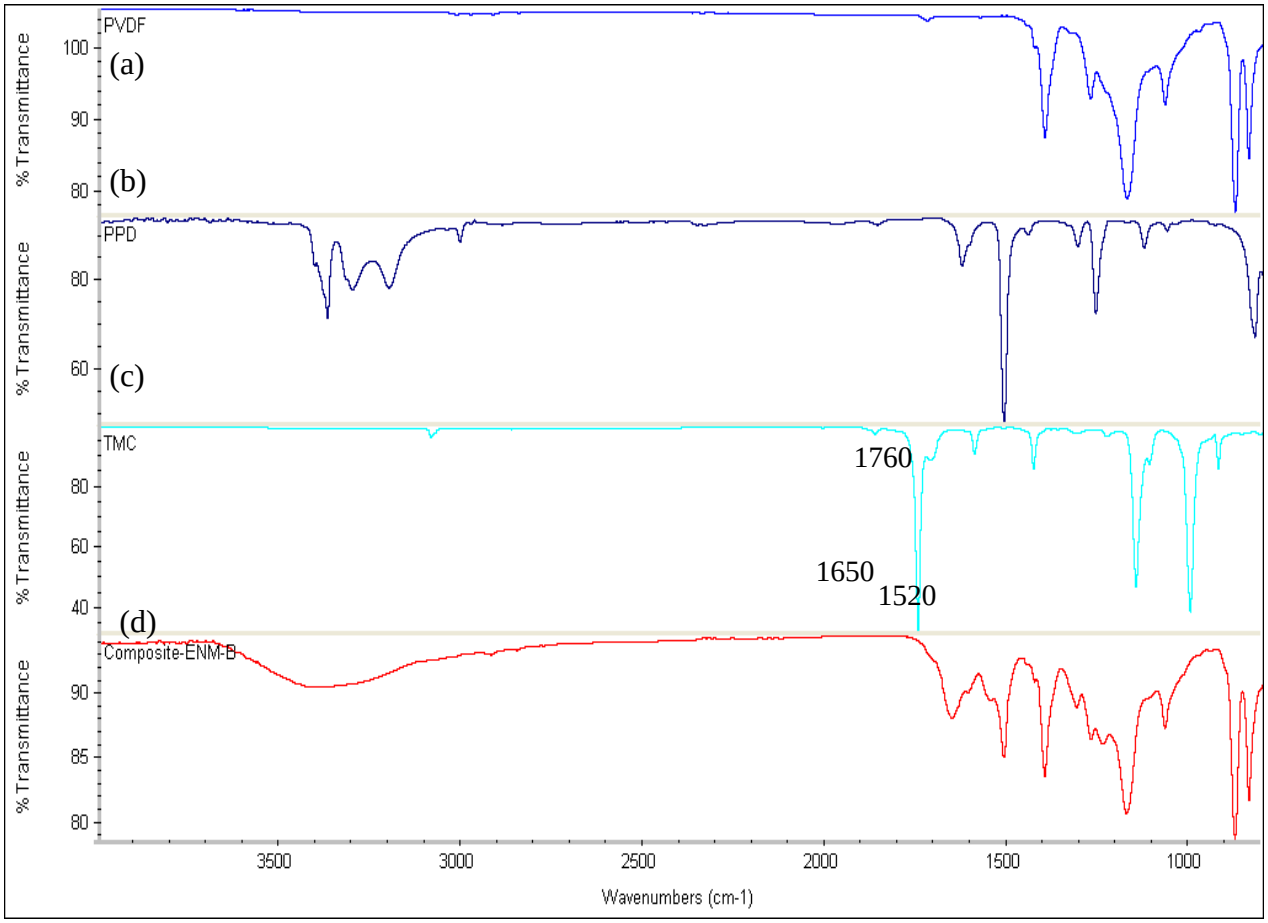

Figure 4.14. ATR-FTIR spectrum of (a) PVDF ENM (b) PPD, (c) TMC and (d) TFNC-B(iv).

4.3.7. Influence of soaking and contact time

The condition which gave the best salt rejection (TFNC-1) was further manipulated in terms of soaking time of TMC and contact time with PPD. The concentration of TMC and PPD were fixed at 0.25 wt% and 4 wt%. The times were manipulated to increase the flux. By

reducing the time, the thickness and cross-linking density of the film might be affected. The rejection results of 2000 ppm $MgSO_4$ and NaCl is shown in Table 4.5. With a decrease in soaking and contact time, the rejections decreased but with an increased flux. For TFNC-2, the rejection of $MgSO_4$ and NaCl dropped by 27% and 79% respectively while the fluxes increased by 59% and 742% respectively (in comparison to TFNC-1). On the other hand when the reverse was done where the soaking time of TMC was 30 s while the contact time with PPD was 1 min, the rejection of $MgSO_4$ and NaCl dropped by 17% and 41 % respectively while their fluxes increased by 449% and 128 % respectively (in comparison to TFNC-1). When TFNC-2 and TFNC-3 were compared, TFNC-3 had an improved rejection indicating that additional contact time with PPD is an influential parameter in improving the rejection but at the expense of flux.

4.3.8. Comparison with commercial membranes

The separation performance of TFNC-1 was compared with commercial Dow membrane- NF 270 and NF 90 and the results are tabulated in Table 4.6.

In addition commercial ultrafiltration (UF) membrane was used as a support instead and a polyamide barrier film of the same composition to that of TFNC-1 was formed at the surface of the UF membrane. This was done so as to compare the difference in separation performance by changing the support layer. It was observed that by changing the support layer and retaining the same barrier layer composition, different throughputs were attained. This was due to the different surface architecture of the support. A high pressure of 400-800 psig was required to separate salts across the NF-UF (1) membranes. The separation of these membranes could not be performed on the dead-end Amicon cell as no flux was obtained at

70 psig within one working day and instead separation of salts were performed on a reverse osmosis cross flow set up.

Table 4.5. Rejection of 2000 ppm $MgSO_4$ and NaCl on 0.25% (w/v) TMC and 4% (w/v) PPD with different soaking and contact time.

Membrane ID	Time of TMC (min)	Time of PPD (min)	$MgSO_4$		NaCl	
			R (%)	F (L/m^2h)	R (%)	F (L/m^2h)
TFNC-1	3	10	80.7	0.51	67	0.52
TFNC-2	1	1/2	59.3	1.1	13.8	4.38
TFNC-3	1/2	1	69.13	2.8	39.3	1.8

Table 4.6. Comparison of TFNC with commercial membranes and composite membrane based on the same barrier layer composition but different support.

Membrane Type	psig	NaCl R(%)	Flux (L/m^2h)	Flux/psig	$MgSO_4$ R(%)	Flux (L/m^2h)	Flux/psig
NF90	70	79.7	9.28	0.1326	97.5 *(>97%)	17.47 *(41.7)	0.2496 *(0.5957)
NF270	70	35.6	38.8	0.5543	94.36 *(>97%)	43.58 *(52.13)	0.6226 *(0.7446)
NF-UF (1)	400	83.2	11.83	0.0296	-	-	-
NF-UF (1)	800	86.1	13.5	0.0169	84.5	12.3	0.1456
TFNC (1)	70	67	0.5	0.0071	80.7	0.5	0.0062

*Source: Dow Filmtec

The preliminary results have shown that ENM can be used as a self- supporting nanofilter and is capable to support a polymeric barrier film despite its large pore-size and through proper and careful optimization, excellent performance can be realized.

4.4. Conclusion

Interfacial polymerization (IP) was carried out on the surface of PVDF ENM by two approaches. These two approaches led to different surface architectures and subsequently different salt rejection values. In the first approach (A), PVDF ENM was soaked in aqueous phase followed by organic phase. The polyamide film formed was non-uniform due to hydrophobic nature of PVDF ENM and thereby wettability was poor and hence rejection of salts was not successful. Attempts were made to overcome this hydrophobic nature by chemical and plasma methods. Although interesting architectures were obtained, but rejection of salts remained unsuccessful, which was due to the presence of several tiny holes. The approach (B) of soaking PVDF ENM in an organic phase first followed by aqueous phase led to the formation of a uniform polyamide film with wettable surface. This composite membrane was able to reject several salts.

With this approach, composite PVDF-ENM (ENM-A and ENM-B) with two different pore-sizes was prepared. A higher flux and higher salt rejection efficiency were obtained with a membrane of having larger bubble point and fine fiber diameter, whereas comparatively lower flux and lower rejection were obtained with a membrane having beaded fibers.

In addition, it has been observed that the difference in ratio of the monomers during IP played an important role in the overall membrane separation efficiency. When the difference

between the two monomers ratio was increased, rejection of the salts were also increased due to the requirement of more concentration of PPD for the polymerization. The best ip condition performed on the surface of the ENM resulted in the rejection of 80.7% of $MgSO_4$ and 60% of NaCl.

The feasibility of developing TFNC-ENM was explored and results obtained thus far are encouraging. Contrary to popular belief, IP could take place on ENM surface even though the top layer does possess 'pores' larger than 2µm.

The pore-size was not the bottle-neck but the surface energy of the ENM. Interestingly the traditional approach to carry out interfacial polymerization does not promote the formation of continuous, defect free film on a 'hydrophobic' ENM. When the ENM was saturated with the organic phase first, film formation was successful. The next strategy is to use a polymer which is hydrophilic and has been used in membrane separation and to carry out Approach A.

The preliminary results produced here highlight the potential of ENM as self-supporting nanofilters. With careful optimization of the surface film and selection of an appropriate polymer material for ENM, the rejection rate and flux may be greatly improved. With better optimization and understanding of their separation behavior, efficient nano-filters based on electrospun membranes can be designed and developed. Hence in the next chapter, the objective was to develop a systematic composite structure which will possess improved separation and rejection. This will be achieved by adopting a three-tier-composite structure with improved adhesion between the ENM layer and backing material.

CHAPTER 5

THREE TIER THIN FILM NANOFIBROUS COMPOSITE MEMBRANE BASED ON POLYACRYLONITRILE ENM

5.1. Introduction

In Chapter 4, the author has shown that interfacial polymerization (IP) could be successfully performed on the surface of the ENM by soaking in organic solution followed by aqueous solution.

This method is a reverse of what is conventionally practiced as the PVDF ENM is hydrophobic. Despite attempts to make it hydrophilic, it was difficult to have a uniform interfacial polymerized layer. In addition, by using the reverse method, a thicker layer was produced and manipulating the soaking and contact time did improve the flux but not in the comparison region to commercial membranes. Here the author proposes using a hydrophilic polymer, polyacrylonitrile (PAN), so that the typical way of introducing the interfacial polymerized can be achieved and compared with commercial membranes. PAN has been used as a polymer in NF membrane [Oh 2001]. It is also a common material used in UF and dialysis [Kroshcwitz 1990]. PAN is also used for aqueous systems by virtue of their resistance to solvents and chemicals.

As revealed in Chapter 4, separation of mono and divalent salts were successful however at low flux rate. It is the intention here to have the flux of the developed composite improved. The intention in Chapter 4 was to use a self-supporting membrane without any backing

material (BM). It was realized by the author that perhaps this might not be the most practical approach as the entire cross-section of the membrane was not utilized for separation but rather the top most layer and an increase in thickness of the membrane adds on to compaction.

The author would like to emphasize that it is not the intention of this thesis to create a membrane better than the commercial membrane but rather to understand its role in separation.

The author has taken the experiments to the next level where a three layer composite structure is developed. The first layer is a top ultra-thin selective barrier layer prepared by interfacial polymerization, the second layer comprises of the ENM and third layer is a non-woven fabric. The primary objective of this chapter was to study the influence of heat treatment and pressure on the ENM and how this treatment influences the membrane property as well as separation performance after interfacial polymerization (as TFNC membrane). At this stage, a cross flow unit was set-up in the lab.

5.2. Experimental section

Experiments in this chapter were conducted at the National University of Singapore.

5. 2.1. Materials

Non-woven polyester (Hollytex 3242 supplied by Ahlstrom Mount Holly Springs, USA), Polyacrylonitrile (PAN) average Mw 150,000 (Aldrich Product Number 181315), N,N-Dimethylformamide GR ACS (DMF) (Merck Ltd, Product code 1.03053), Piperazine

(Sigmaaldrich Product Number P-45907), Bipiperidine dihydrochloride (Sigmaaldrich Product Number 180742), Triethylamine (TEA, Sigmaaldrich Product Number T0886), Sodium hydroxide (Sigmaaldrich Product Number S8045), Water (Milli Q), 1,3,5-Benzenetricarbonyl trichloride (trimesoyl chloride abbreviated hereafter TMC) (Sigmaaldrich Product Number 147532), Hexane anhydrous (Sigmaaldrich Product Number 296090), Washing water for membrane (Milli Q), magnesium sulphate ($MgSO_4.7H_2O$ (Sino Chemicals Co. Pte Ltd)). DMF was treated with molecular sieves to remove moisture. All other chemicals and solvents were used as received.

5.2.2. Preparation of support membrane

Electrospinning was performed on a fully automated electrospinning machine (Nanon-01A electrospinning machine, manufactured and supplied by MECC CO, Ltd, Japan). The rotating metal drum was initially covered with an aluminium foil followed by a polyester backing material (BM). 8 wt% of PAN was dissolved in DMF at 60 ^{o}C for 2 days until it became a homogeneous solution. The PAN solution was then loaded into a syringe fitted to a pump. The positive terminal of a high voltage DC power supply was connected to the metallic needle (22 G, B. Braun Melsungen AG) of the syringe. A backing material (Hollytex 3242, BM), with dimensions: 66 cm (length) x 22 cm (width) x 0.014 cm (thickness) was used as the target to collect the electrospun membranes. The syringe pump was set to deliver the solution at a rate of 1.2 ml. h^{-1} and high voltage of 15 KV was applied. Electrospinning was carried out at room temperature and the rotational speed of collector was 150 rpm. Humidity was maintained at 50-60%. A summary of the electrospinning condition is shown in Table 5.1.

After electrospinning, the nanofibrous support and backing layer was exposed to mild convective air flow in fume hood for at least 3 hour to remove residual solvent associated

with the web. The nanofibrous support and backing layer was hot pressed in thermal transfer press (Hotronix, Carmichaels, PA 15320, USA) at 87^{o}C for 999 s and pressure of 0.14 MPa, 0.28 MPa and 0.41 MPa. The membrane which is not treated will be labelled as ENM-control

Table 5.1. Electrospinning conditions used for preparation of nanofibrous support layer.

Parameters	Conditions
Backing layer (substrate) used for supporting the nanofibrous layer	Hollytex 3242 (length x width x thickness: 66 cm x 22 cm x 0.014 cm)
Spinning solution and time	8.75 ml of PAN solution from the 10 ml plastic syringe (Syringe internal diameter 14.4 mm) was spun for 7.25 h.
Spinning needle (22G x $1^{1/2}$", 100 Sterican^{TM} Φ 0.7 x 40 mm make B. Braun Melsungen AG)	Needle tip was made circular by using a Buehler Ecomet polishing machine
Tip to collector distance	10 cm
Voltage applied	15kV
Flow rate of spinning solution	1.2 mL/h
Rotational speed of collector (ϕ19.90 cm, length 22 cm)	150 rpm
Spinneret speed	10 mm/s
Coating width (length of coating coverage on the collector)	150 mm
Tip cleaning frequency	59 min

and the membrane treated at 0.14 MPa, 0.28 MPa and 0.41 MPa will be referred to as ENM-1, ENM-2 and ENM-3.

The pore-size distribution of the heat treated and non-heat treated membrane was determined using a capillary flow porometer (CFP-1200-A, Porous Materials Inc., USA). A wetting liquid, Galwick^{TM} (Porous Materials Inc., USA) of surface tension 0.0159 N/m was applied to fill the pores spontaneously in the ENM and differential pressure of nitrogen gas was slowly increased on the sample to remove the liquid within the pores and permit gas flow.

5.2.3. Preparation of TFNC membranes

Besides changing the ENM polymer layer, the chemicals that make up the interfacial layer has also been changed. It has been shown that when piperazine (PIP) and its diamino derivatives were used, their water fluxes were 3 to 4 times higher compared to membranes made of metha-phenylenediamine (MPD) but at the expense of rejection. It is to be noted here that MPD has the same molecular weight as PPD (PPD was used in Chapter 4) and the difference between them is the position of the amino group [Tomaschke 1999]. A combination of PIP and bipiperidine dihydrochloride (BP) was used here so as to have an improved flux. Pre-cut nanofibrous support layer (15 cm x 15 cm) was placed on the flat metallic surface in the tray. Aqueous diamine solution containing BP (0.3 % w/v), PIP (0.7 % w/v), sodium hydroxide (1.5 equivalent to BP concentration) and triethylamine (TEA, 1% w/v) were prepared. Additives (TEA and NaOH) were added to increase the polarity of the hydrocarbon solvent or as catalysts to increase the polymerization rate while not interfering with interfacial polymerization of the reactants [Schafer 2007].

The nanofibrous support layer in the tray was wetted by aqueous diamine solution for 1 min. The excess amine solution was drained by keeping the tray in vertical position for 3 min. The wetted membrane was taken in separate dried tray and edges of the support membrane were sealed by the adhesive tape (3M, USA). The amine-impregnated nanofibrous support membrane was covered completely by TMC (0.1 % (w/v) in hexane) solution. The shorter this contact time is kept, the higher the flux will be attained. However too low a contact time results in incomplete formation of the thin film and hence there will not be any rejection of salt. A balance has to be maintained between the contact time, complete thin film formation and reasonable flux. A short experiment was conducted to decide the desirable contact time. Contact times of 1, 2 and 4 min were selected and separation of 2000 ppm was performed on a dead-end set up. After selecting the desired contact times, subsequent experiments were carried out on a cross-flow set up. The modified post membrane processing conditions were used for curing and drying of thin film. After draining TMC solution, membrane was air dried in fume hood for 15 min followed by drying in the hot air oven with convective air flow at temperature of 65 °C for 20 min. Then, the membrane was exposed to convective air flow at 25 ^{o}C in the fume hood for 3.5 h. Dried TFNC membrane was washed with water three times for 1/2 to 1 day. The composite membrane having the base as ENM-control, ENM-1 and ENM-2 will be referred to as TFNC-control, TFNC-1 and TFNC-2 respectively.

5.2.4. Characterization

SEM analysis is similar to section 4.2.4. Quantitative surface roughness analysis of polyamide films was performed using an atomic force microscope, (AFM, 3100 AFM, Veeco Instruments, Edina, MN) equipped with standard silicon cantilever (NanosensorsTM PPP-NCH, non-contact/tapping mode type probe, Nanosensors, Switzerland) by tapping mode.

Inspection of surfaces by AFM provides a statistical analysis of surface roughness features. In the AFM roughness analysis, a mean-plane of length X and width Y defines the surface. Morphological features are defined by x,y,z coordinates which indicate the relative height (z) of the cantilever tip at each x and y planar location. The following AFM "roughness analysis" parameters were selected as key descriptors of membrane surface morphology: root mean square (RMS) roughness, the mean roughness (Ra), the difference in height between the highest and lowest points on the surface relative to the mean plane (Rmax), and surface area difference (SAD).

RMS effectively describes the standard deviation of an entire distribution of z-values for a large sample size. Ra is the average deviation of the measured z-values from the mean plane. For the membrane surface, Ra may be thought of as half the average peak-to-valley depth. Rmax indicates the difference between the largest positive and negative z-values. This does not indicate that any peak-to-valley depth of this magnitude exists, but more accurately provides quantification of the spread of the distribution of measured asperity heights. SAD is the increase in surface area, due to roughness over a flat plane with the same X and Y dimensions. The SAD is a critical parameter that describes the accumulated surface area of all roughness features on a sample [Hoek 2003].

The mechanical testing of membranes was done using the Instron (UK make 3345 Single Column Testing Systems). Specimens of size 8 cm x 2 cm were used for tensile strength measurements. The thickness of the membranes was measured.

Pure water flux of the ENM layer was performed on a dead -end AMICON stirred cell (8010) unit which is attached to a reservoir (Figure 5.1). TFNC and commercial membranes were

fixed in a custom-built cross-flow filtration cell (active filtration area of 19.63 cm^2). Before starting the filtration experiment, each membrane was compacted at a trans-membrane pressure (TMP) of 70 psig with 2000 ppm $MgSO_4$ feed solution. Each filtration experiment was run for 1 h at various TMP (70, 100, 130, 160 and 190 psi) before permeate was collected. Conductivity and temperature of feed before starting the filtration experiment and after the filtration run was measured by a digital conductivity meter (Thermo Scientific Orion 3-star Plus). The temperature of the feed solution was between 30-32 ^oC. Conductivity and temperature of permeate was also measured. The temperature of the permeate collected was between 22-24 ^oC. The pHs of $MgSO_4$ at a temperature of 22 and 30 ^oC are 6.98 and 7.31, respectively. The volume of feed was 5 L and the volume of permeate collected was approximately 20 mL. The permeate flux was determined by direct measurement of the permeate flow in terms of liter per square meter per hour (L/m^2h). Rejection (R %) of $MgSO_4$ was calculated using the following equation (4):

$$R\ (\%) = [1- (\lambda_p/\lambda_f)] \times 100\% \qquad (4)$$

Where, λ_p is the conductivity of permeate (µS/cm) and λ_f is the conductivity of feed (µS/cm) after the filtration. Each membrane was fabricated three times for filtration testing and each permeation test (at different pressures) was done three times. All experimental values were averaged.

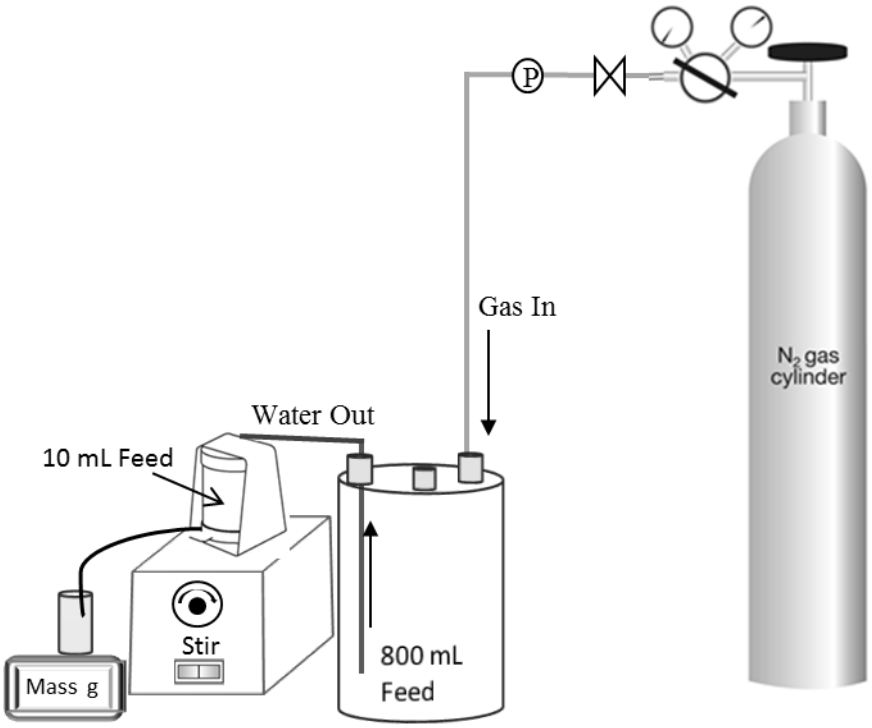

Figure 5.1. Schematic of dead-end pure water filtration unit.

The entire experimental design is clearly visualised in Figure 5.2.

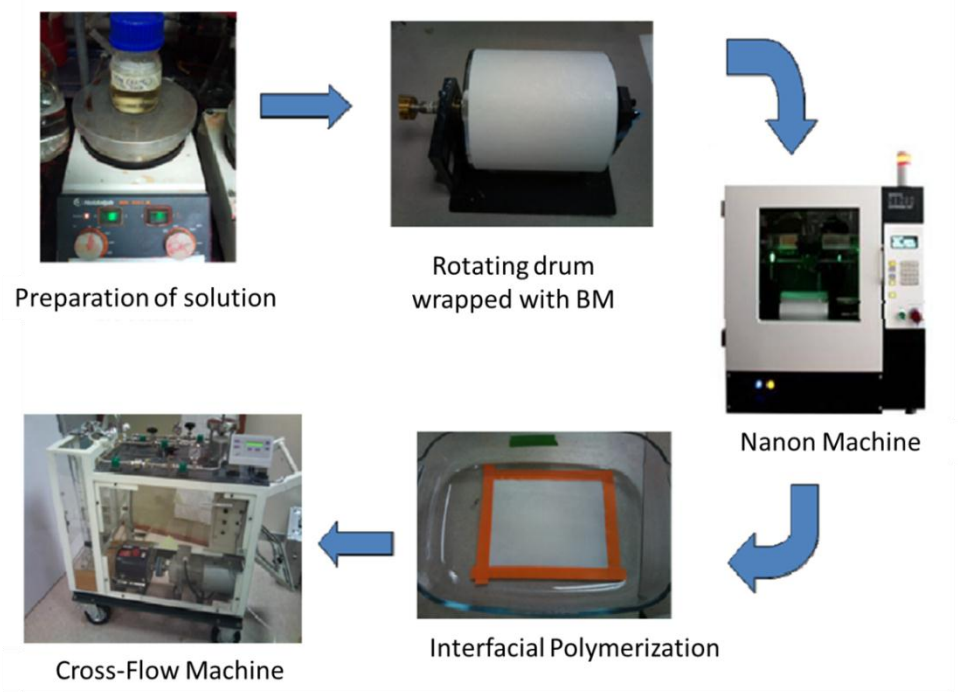

Figure 5.2. Pictorial view of experimental design.

5.3. Results and discussion

5.3.1. Surface morphology of ENMs

PAN solution was electrospun on a backing material (BM). The average fiber size of the BM was 32 µm which is several orders greater than the size of the electrospun fibers. In addition, the bubble-point was ~ 80 µm. The surface architecture and pore-size-distribution of this BM is reflected in Figures 5.3 and 5.4, respectively. The pore size range of the BM was between 5.02-80.78 µm. This range of pore-size is large and hence the BM is a suitable support as it will not interfere with the separation of the electrolytes. Also, since the electrospun fibers are extremely long [Hsiao 2008], they deposit easily on the BM and do not penetrate within the pores of the BM. The surface architecture of nanofibrous layer supported on the BM before and after hot-pressing at various pressures are shown in Figure 5.5. The non-heat treated membrane (control) had an average fiber size of 287±87 nm and when a pressure of 0.14 MPa was applied at 87^{o}C the average fiber size was determined as 275±100 nm. There was no significant change in the fiber size (as determined by the student t-test). When the pressure was increased to 0.28 MPa, the fiber size was found to be 344±112 nm and fusion of overlapping fibers was noticed (Figure 5.5(c)). When the pressure was increased further to 0.41 MPa, the fiber size was increased (434±172 nm) to 1.5 times larger than the control, which may be due to the fusion of two or more fibers (Figure 5.5d-e).

Figure 5.3. Surface architecture of BM.

5.3.2. Pore-size distribution and pure water flux

Pore-size distribution (Figure 5.6), thickness of the electrospun layer (Figures 5.7 and 5.8) as well as the pure water fluxes of each membrane (Figure 5.8) were measured and the relationship between these parameters is described here. The control had an average bubble-point of 5.60 µm and thickness of 74 µm. The variation of the bubble point (SD of ±1.45) between the non-treated samples was large in comparison to the treated membranes (see Figure 5.6), indicating that the ENM was not stable and the fibers could have shifted under the applied pressure. When a pressure of 0.14 MPa was applied, both the average bubble-point and thickness were reduced to 2.30 µm and 48 µm, respectively (see Figures 5.6 and 5.8).

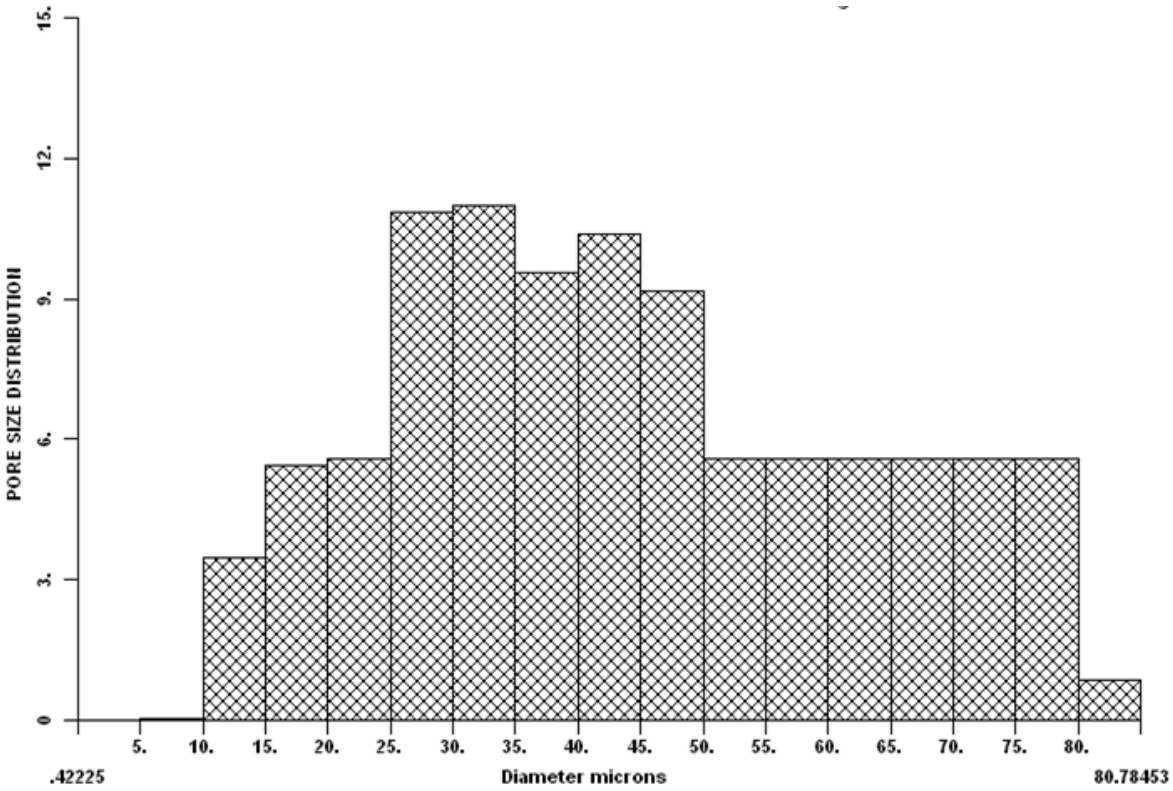

Figure 5.4. Pore-size distribution of BM.

When hot-pressing pressure was applied, both the average bubble-point and thickness were reduced, following the order of ENM-1>ENM-2>ENM-3. The bubble-points (Figure 5.6) for the ENM-control, ENM-1, ENM-2, and ENM-3 were found to be 5.6 µm, 2.3 µm, 1.1 µm, 0.8 µm, respectively. The mean pore-size and smallest pore-size also decreased in the above order. At the lower applied pressure, i.e. at 0.14 MPa, the adhesion between ENM and BM layer could have taken place. Hence the fibers were less likely to move, giving rise to a smaller variation (SD of ±0.45 µm), and were not as easy to be peeled off as the control. On the other hand, when the applied pressure was further increased, in addition to the adhesion between ENM and BM layer fusion between the fibers occurred at 0.28 MPa and over fusion at 0.41 MPa.

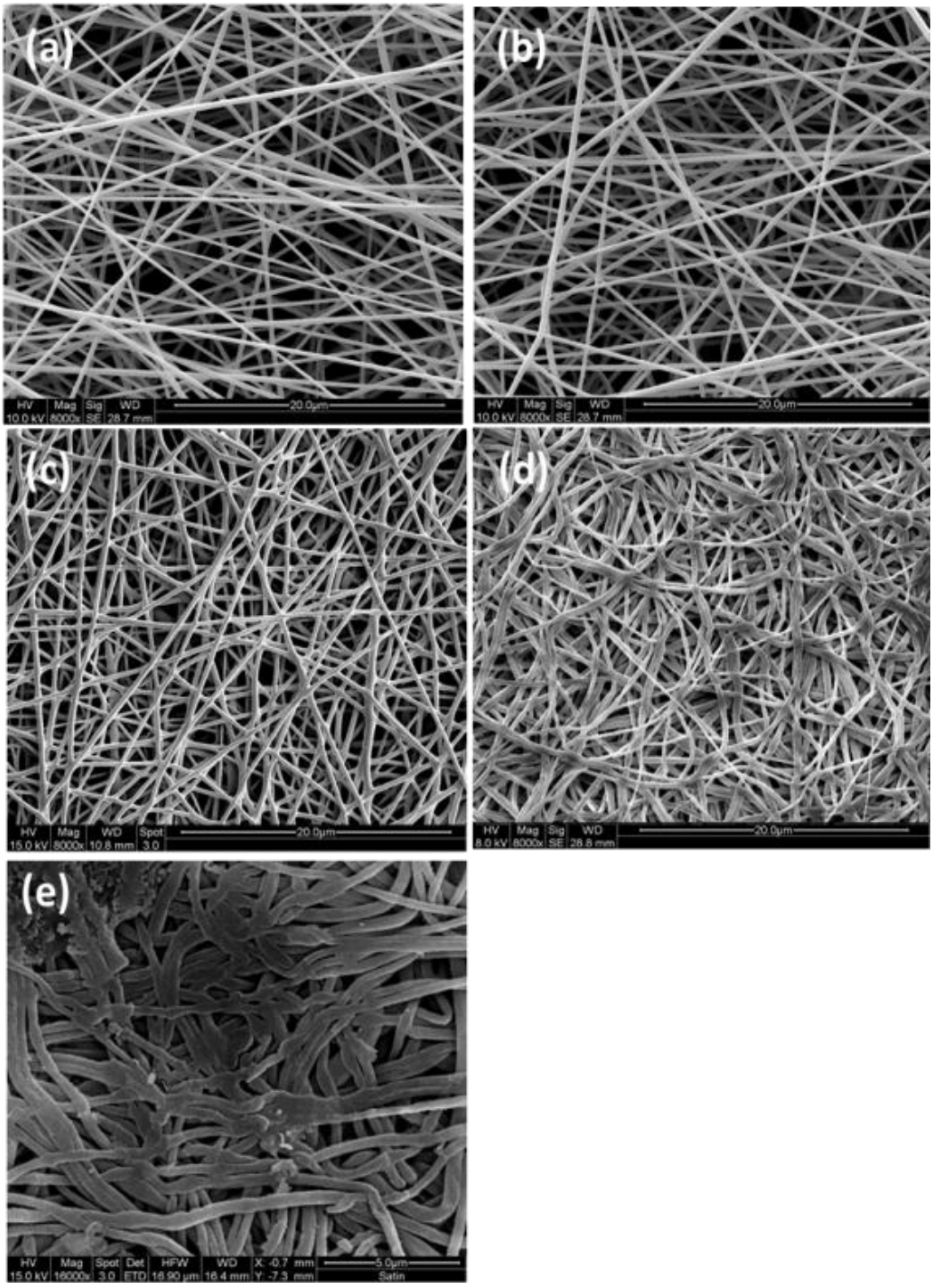

Figure 5.5. SEM pictures of (a) ENM-control, (b) ENM-1, (c) ENM-2, (d) ENM-3 and (e) higher magnification of 3(d).

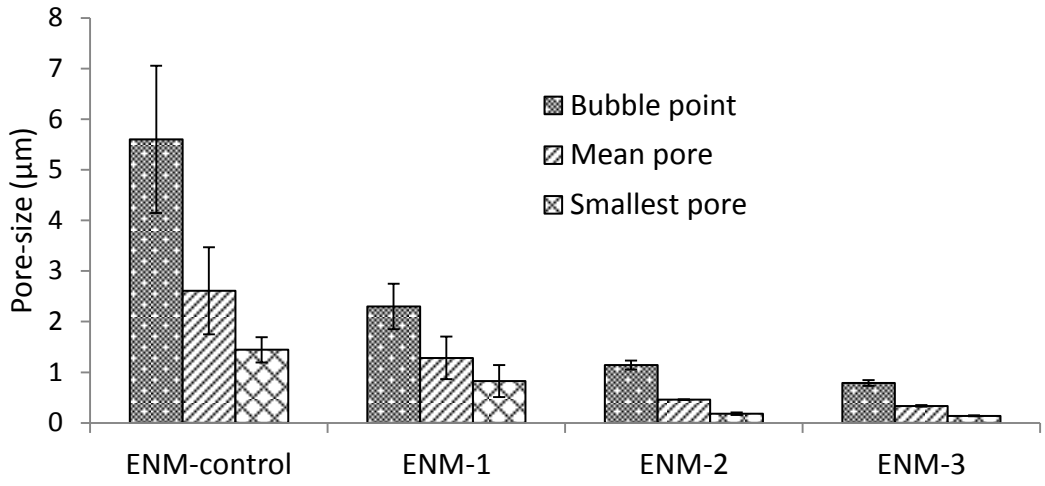

Figure 5.6. Bubble point of ENMs treated at different pressures at 87^{o}C.

Both ENM layer and BM were further compressed. Also the variation (SD ±0.09 µm) was much lesser for ENM-2 than the control, indicating that the membrane was stable. This compression was confirmed from the thickness of membranes hot pressed under different pressures. The thickness for the ENM-control, ENM-1, ENM-2, ENM-3 are found to be 74 µm, 48 µm, 21 µm, 18 µm, respectively. It was observed under SEM (Figure 5.5) that overlapping fibers fused at 0.28 MPa and over/excessive fusing occurred for ENM-3 hence accounting for the drastic decrease in bubble-point.

The cross-section of the various membranes is shown in Figure 5.7. From Figure 5.7(a) it was observed that the ENM-control had a loose fibrous form. At the right hand side of the picture, it can be seen that the membrane is easily compressible (see dotted arrow in Figure 5.7(a)). From Figure 5.7(c) and 5.7(d), it is apparent that the adhesion between the fibers and backing materials has been enhanced (see arrows). The base of the ENM follows the contours of the BM.

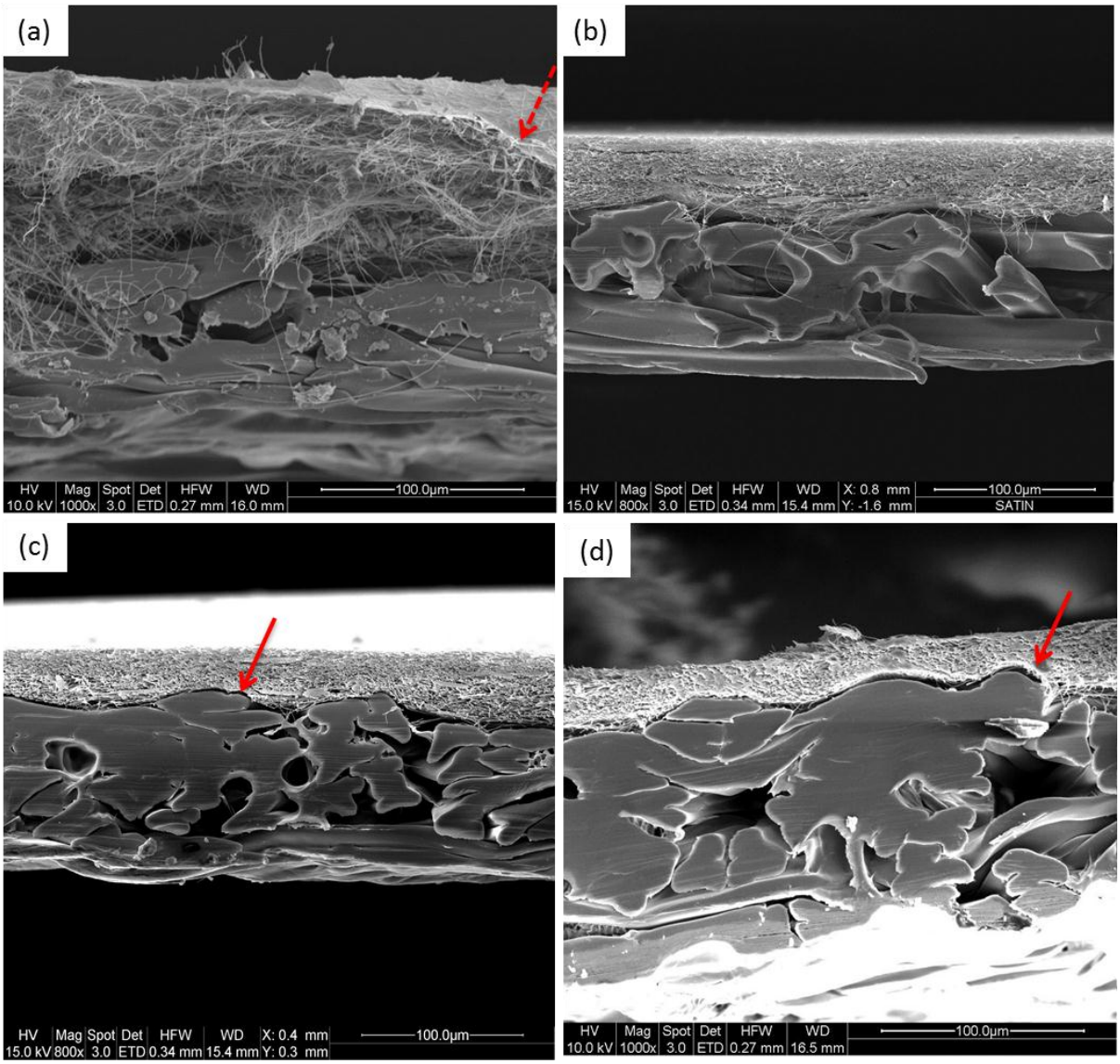

Figure 5.7. Thickness of (a) ENM-control, (b) ENM-1, (c) ENM-2 and (d) ENM-3.

The bubble-point has an important influence on the flux. As the bubble-point decreases, the flux also decreases, which follows in the order of ENM-control>ENM-1>ENM-2>ENM-3. Comparing the flux of ENM-control with hot-pressed membranes, the flux decline for ENM-1, ENM-2, ENM-3 were 6%, 19%, 51%, respectively. The flux profile is reflected in Figure 5.8.

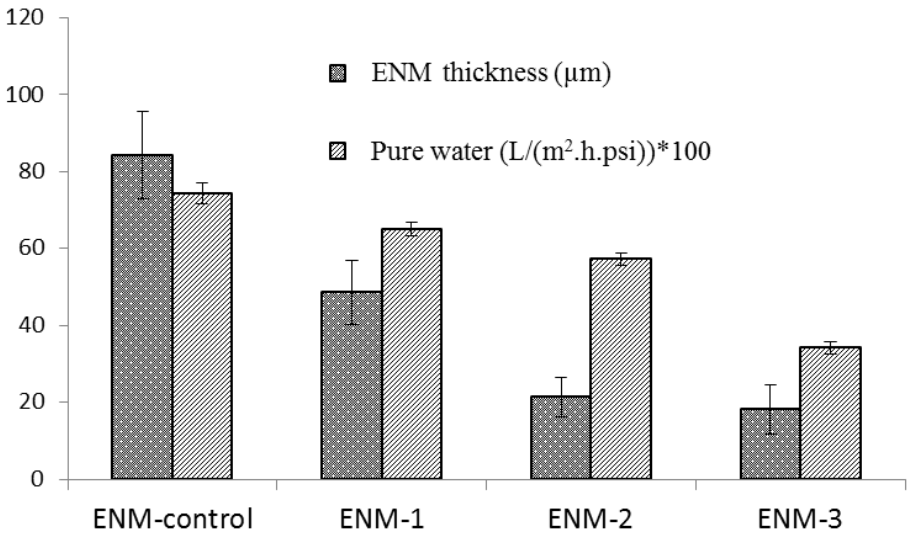

Figure 5.8. Cross-section thickness and pure water flux of the various treated ENMs.

5.3.3. Mechanical property

The mechanical strength of the different ENMs and BM was measured and the results shown in Figure 5.9 and Table 5.2. As mentioned previously, without heat treatment the adhesion between the BM and ENM layer was weak and hence the electrospun layer could be peeled off easily. The yield stress and tensile strength of the BM was 4.9 and 9.5 MPa, respectively. The control had a yield stress and tensile strength of 5.7 and 9.8 MPa, respectively. The yield stress improved by 16 % whereas the yield strength improved by only 3%. This additional improvement was attributed to the ENM layer. When a pressure of 0.14 MPa was applied, the yield stress and tensile strength were 6.2 and 13.93 MPa, respectively, corresponding to the increase by 9% and 42%, respectively. Interestingly, by applying a pressure of 0.28 MPa, the yield stress and tensile strength increased by 313% and 203%, respectively, when compared to the control. This increase in mechanical properties with an increase in the pressure is due to the increase in fiber diameter and pressure induced increase in crystallinity of the ENM and BM layer. Similar observation was reported in an earlier study on the diameter of PAN

nanofibers [Esrafilzadeh 2008]. However, when a pressure of 0.41 MPa was applied the per cent increase of the yield stress and tensile strength was by 206% and 144%, respectively. The yield stress was by 26% lower than 0.28 MPa and the yield strength was by19% lower than 0.28 MPa. The decrease in yield stress and yield strength of the membranes at 0.41 MPa from 0.28 MPa might have been because at this higher pressure, the PAN nanofibers were fused together and hence the stretching property decreased.

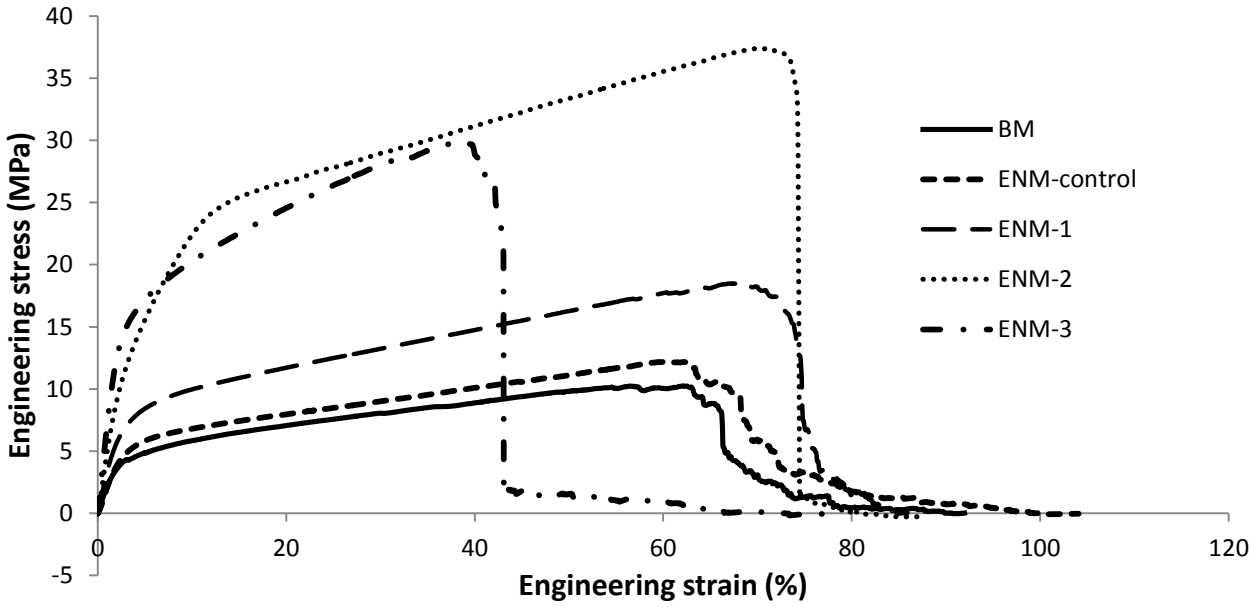

Figure 5.9. Mechanical properties of the various ENMs and BM.

5.3.4. Influence of contact time on rejection and separation

As mentioned in the experimental section, the contact time is an important parameter which influences the rejection and flux values. A quick experiment was performed on a dead-end separation unit to eventually select the desirable contact time. Three different contact times

(1, 2 and 4 min) of TMC were used on ENM-1 and separation was carried out on a 2000 ppm $MgSO_4$ at 65 psig. Table 5.3 reflects the rejection and flux values. It is apparent that an increase in contact time did not necessarily affect rejection but it significantly caused a decrease in flux. Hence for the subsequent experiments a 1 min contact time is selected and separations were performed on a cross-flow set-up.

Table 5.2. Mechanical properties of the various ENMs and BM.

Membranes	Yield stress (MPa)	Tensile strength (MPa)	Elongation at break (%)
BM	4.9	9.5	63.5
ENM-control	5.7	9.8	59.8
ENM-1	6.2	13.93	66.7
ENM-2	23.53	29.74	69.87
ENM-3	17.43	23.95	37.96

Table 5.3. Influence of contact time of TMC on rejection and flux properties.

Parameter studied	1 min	2 min	4 min
R(%)	82.9	81.5	83.6
Flux (L/m^2h)	88.7	75.3	70.1

5.3.5. Influence of hot-pressing on NF performance of TFNC membranes

Interfacial polymerization was performed only on selected ENMs (ENM-control, ENM-1 and ENM-2) and the resulting TFNC membranes are referred to as TFNC-control, TFNC-1 and

TFNC-2, respectively. The SEM image of the TFNC membrane surface is shown in Figure 5.10. It was observed that the polyamide layer was extremely thin such that imprints of the fibers were visible. The film is basically supported by the top nanofibrous layer.

Handling difficulties were experienced with the TFNC-control. Figure 5.11 gives a clear pictorial view of TFNC-control and TFNC-1 stability after separation. As shown in Figure 5.11, TFNC-control top structure creased after separation hence rendering it unstable. It was observed that the polyamide film and ENM layer easily dislodged from the BM, even before the filtration experiments. Despite this the TFNC-control was able to withstand the filtration pressure from 70 to 130 psig. The membrane was able to reject 86.5% $MgSO_4$ at a permeate flux of 102 L/m^2h at 70 psig. The membrane could not withstand the impact of high pressure particularly when the TMP was more than 130 psig. $MgSO_4$ rejection dropped from 88.78% to 53.60% and permeate flux was increased from 218.2 to 451.7 L/m^2h, when the TMP was increased from 130 psig to 160 psig (Figure 5.13(a)). It could be concluded that the membrane was unstable at higher pressures and hence the rejection was low. Concomitantly, TFNC-1 was able to withstand higher pressures and the membrane looked robust even after filtration experiments. This shows that hot-pressing had a strong influence on the membrane's separation performance. It is to be noted that the rejection of $MgSO_4$ was similar to the control from 70 to 130 psig (average of 87% with flux increase from 98.3 to 215 L/m^2h). Although the mechanical properties of the ENM-1 improved only slightly from the control, improvement in the supporting characteristics was more drastic at higher pressures. The average rejection of $MgSO_4$ increased from 86% and 88% when the feed pressure was increased from 130 psig to 190 psig. Concomitantly, the flux increased from 215 L/m^2h to 292 L/m^2h, as shown in Figure 5.12(b).

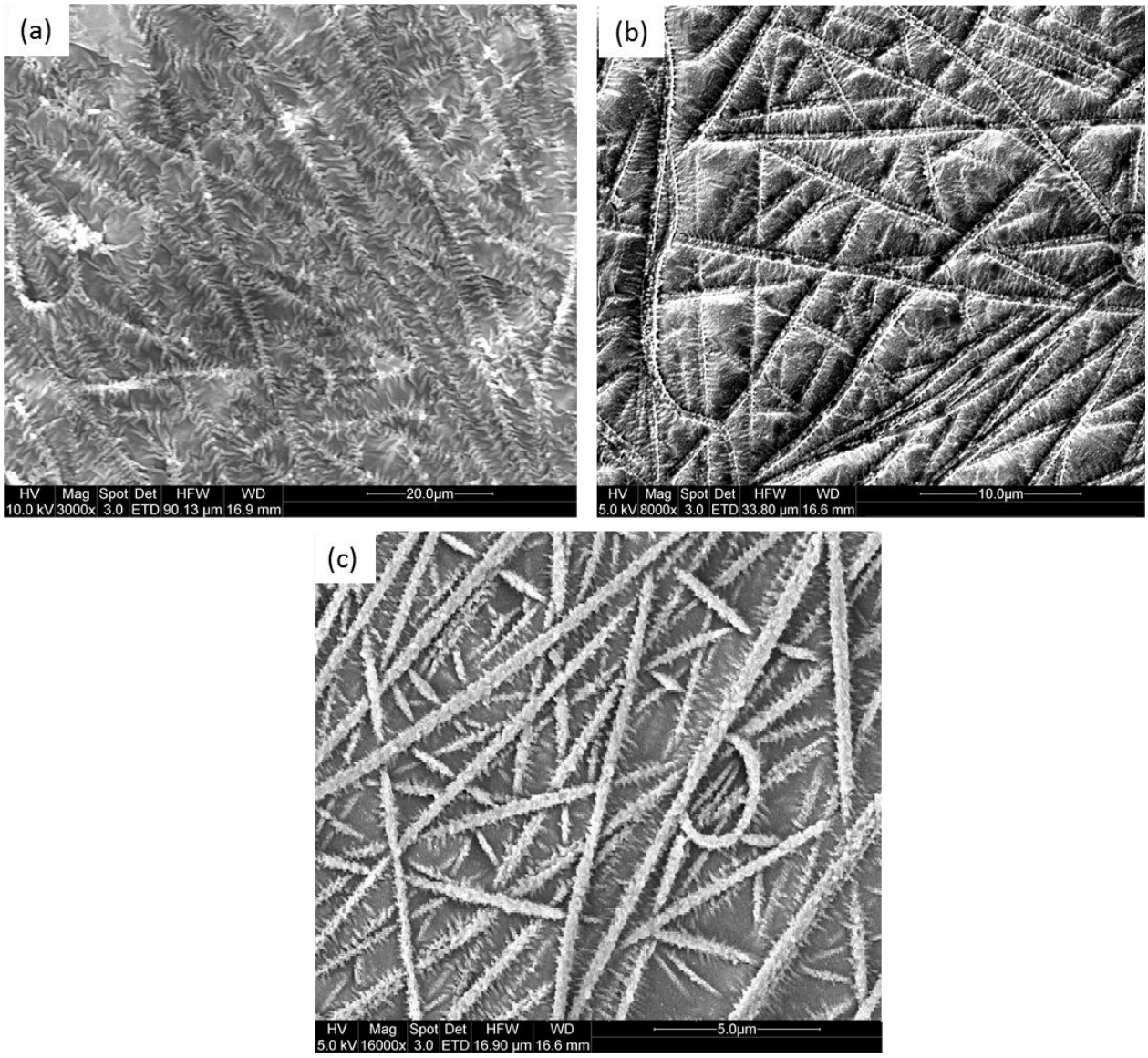

Figure 5.10. SEM surface architecture of (a) TFNC-control, (b) TFNC-1 and (c) TFNC-2.

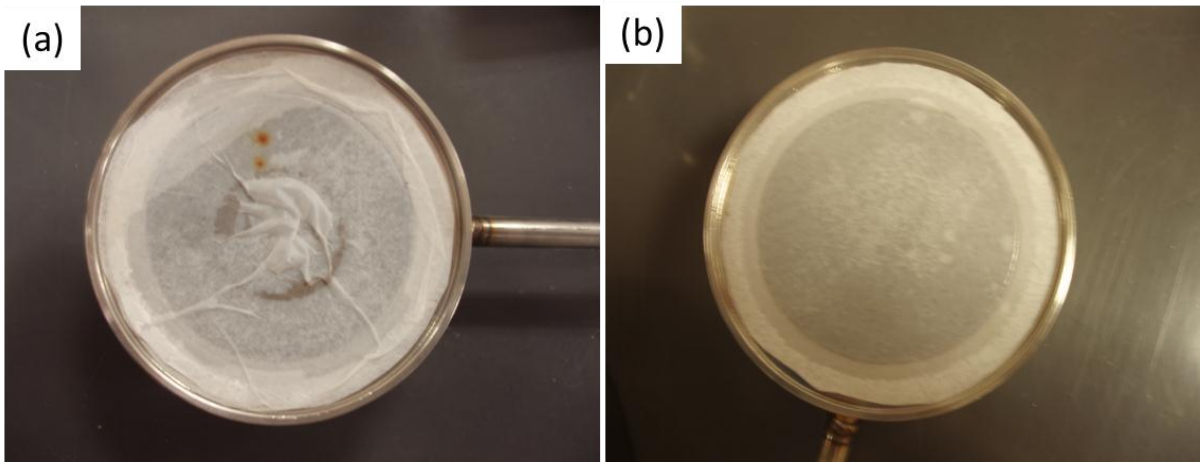

Figure 5.11. Pictures of (a) TFNC-control and (b) TFNC-1 after separation.

The separation of $MgSO_4$ for TFNC-2 started at 84.3% with a flux of 81 L/m^{2}h at 70 psig. These values were lower than the TFNC-control and TFNC-1. However, when TFNC-2 was subjected to higher pressures the rejection of $MgSO_4$ gradually increased and reached a rejection of 92% at 190 psig. The increase in solute separation from TFNC-1 to TFNC-2 is attributed to the smaller pore-sizes of the latter TFNC membrane (see Figure 5.6).

However, the highest flux achieved was 262 L/m^{2}h which was lower than the TFNC-1 by 30 L/m^{2}h. The decrease in flux could be explained from the pure water flux perspective where the pure water flux of ENM-1 was higher than ENM-2 by 785 L/m^{2}h.

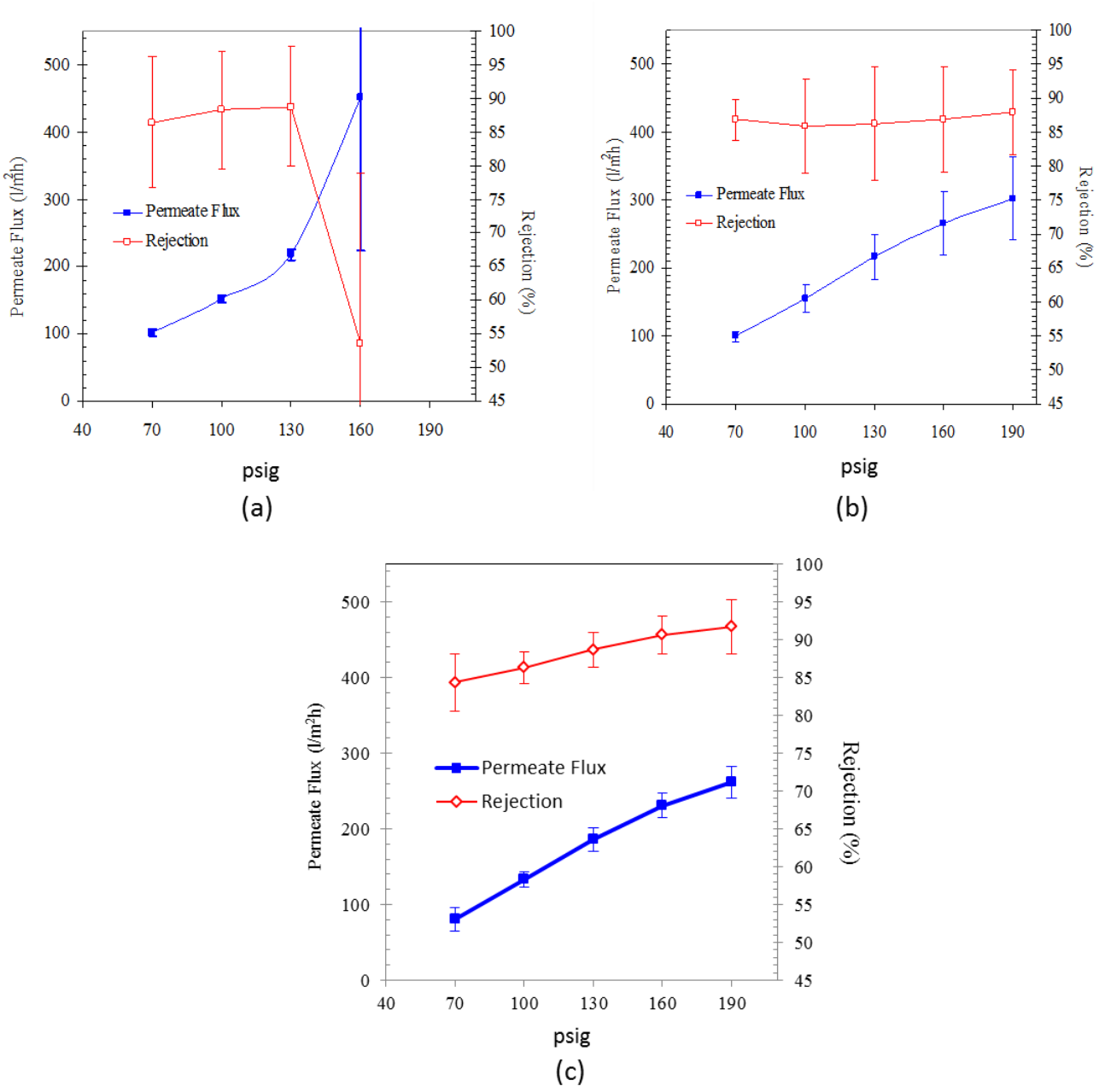

Figure 5.12. Separation and flux results of (a) TFNC-control, (b) TFNC-1 and (c) TFNC-2.

5.3.6. Comparison between separation efficiency of TFNC membranes with commercial membranes

As an important complementation of the SEM, AFM was also used to characterize surface morphology of the developed membranes and commercial nanofiltration membranes and images are shown in the Figure 5.13. The visible surface smoothness of NF membranes observed in the AFM pictures is in the following order: NF 270 >NF 90 >TFNC-2 >TFNC-1 > TFNC-control. This is confirmed with the reversed order in RMS values; i.e. NF 270 (11 nm) < NF 90 (73 nm) < TFNC-2 (107 nm) < TFNC-1 (136 nm) < TFNC-control (348 nm) (see Table 5.4). It is clear from the AFM images, that the surface of TFNC-1 and TFNC-2 is relatively smooth when compared to TFNC-control. The RMS values increase in the same order as Ra and are larger in magnitude than the Ra. A similar trend and relationship between RMS and Ra has been reported elsewhere [Hoek 2003]. SAD (%) of TFNC-control was the largest while that of NF270 was the lowest. TFNC-1 and TFNC-2 exhibited 2.8 and 2.5 times lesser SAD (%) than TFNC-control respectively. TFNC-1 and TFNC-2 SAD(%) values are close to that of NF 90. Rmax of TFNC-control was the largest and as revealed earlier, it has the highest flux. Earlier findings on other supports have shown that the rougher the surface the higher the initial flux and reason offered for this phenomenon was that the rougher and larger surface area of the membrane made it possible to have contact with more water molecules in the given projected area [Li 2008]. The rougher surface and surface area of TFNC-control are due to the large pore-size of the ENM-control and as observed earlier, large pore-size leads to higher flux. However possessing a high surface roughness is disadvantages as it has effect on fouling. The link of surface roughness to fouling has been pointed out by several researches. Effects of surface roughness on the interaction force between particles and membrane surface resulted in enhanced attachment of particles onto the

membrane surface and hence more severe fouling [Elimelech 1997]. TFNC-1 and TFNC-2 exhibited Rmax values close to that of NF 90. Since the surface roughness values of TFNC-1 and TFNC-2 have been extremely reduced after hot-pressing and with some of the AFM properties similar to NF 90, the fouling tendency is also expected to be reduced and perhaps comparable to the commercial membrane. This shows that hot-pressing is an effective method to reduce the surface roughness and subsequently fouling tendency.

Table 5.4. AFM properties of the various NF membranes.

Membrane	RMS (nm)	Ra (nm)	Rmax (nm)	SAD (%)
NF 90	73	54	749	19.25
NF 270	11	9	94	2.14
TFNC-control	348	291	1733	53.73
TFNC-1	136	108	892	19.1
TFNC-2	107	80	671	21.4

The salt rejection and permeate water flux of the commercial membranes (NF 90 and NF 270) with varying TMP are shown in the Figure 5.14. Figure 5.16 represents the top and cross-sectional SEM images of NF 90 and NF 270. The commercial membranes were subjected to 2000 ppm $MgSO_4$ separation at various TMPs. Both the membranes had >99% rejection. NF 270 had a flux of 239 L/m^2h while NF 90 had a flux of 82 L/m^2h at 190 psig. Although the developed TFNC-1 and TFNC-2 had approximately 8-12% lower rejections than the commercial membranes but their fluxes were greater. TFNC-1 had 22% greater flux than NF 270 and 256% greater flux than NF 90. TFNC-2 had 9.6% greater flux than NF 270 and 220% greater flux than NF 90. Hence the fluxes were more than tripled especially when

compared to NF 90. High fluxes were achieved by the developed TFNC membranes perhaps due to relatively thin polyamide layer, interconnected fibrous architecture of the ENM substrate membranes with high porosity, which may have facilitated the mass transfer of water.

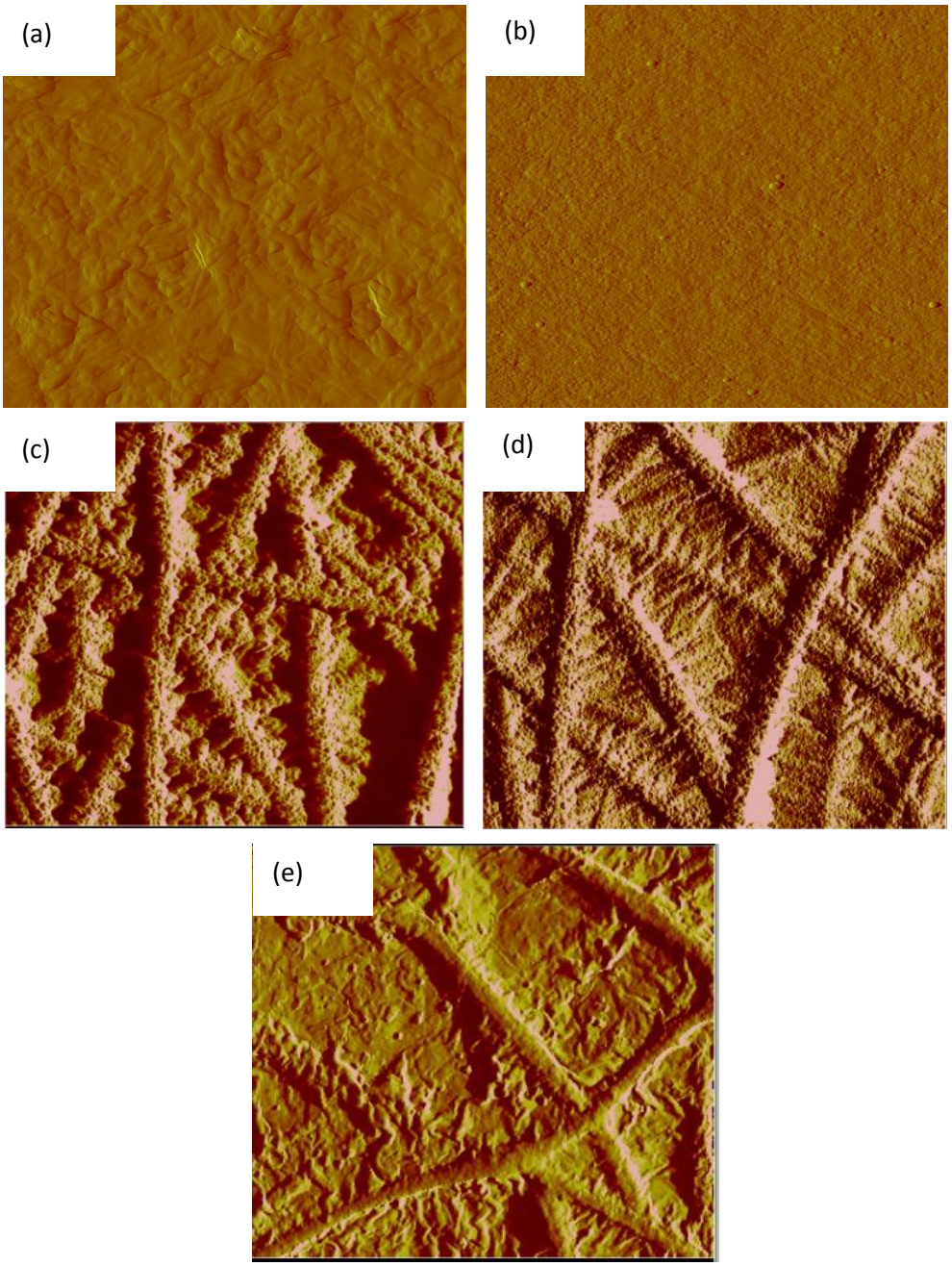

Figure 5.13. AFM images of (a) NF 90, (b) NF 270, (c) TFNC-control, (d) TFNC-1 and (e) TFNC-2.

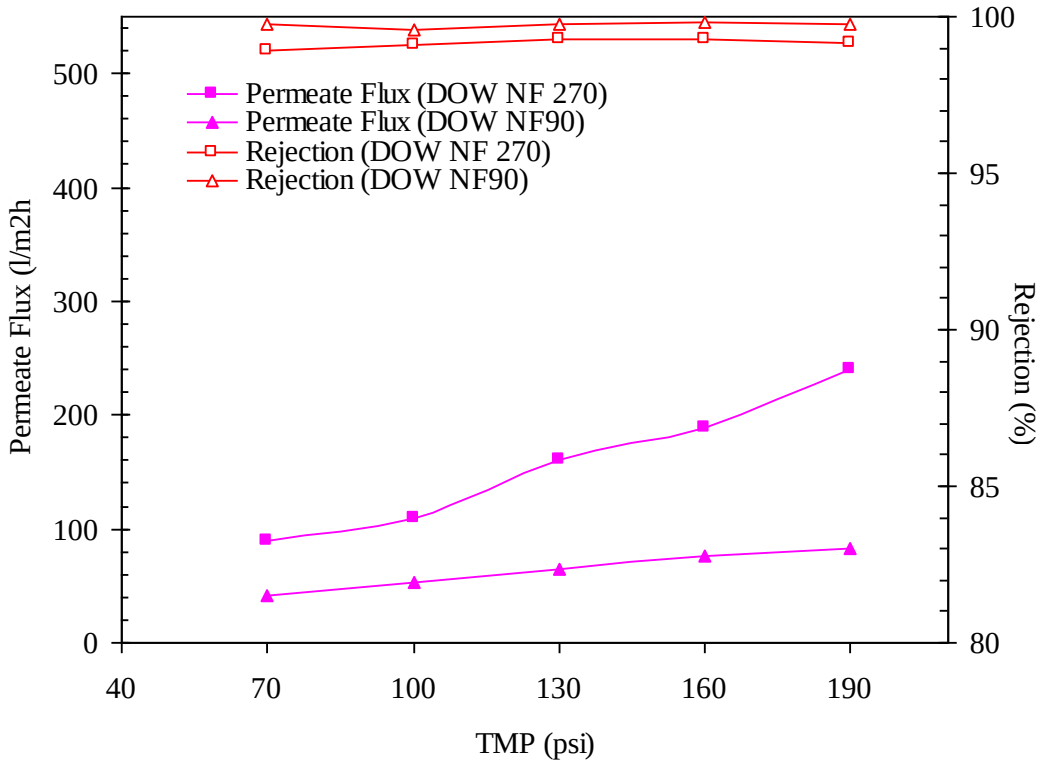

Figure 5.14. Separation performance of NF90 and NF270.

Figure 5.16 reflects the mechanical properties of NF90, NF270, TFNC without BM, TFNC with BM. TFNC prepared on ENM with BM (TFNC-2) has its mechanical properties in between NF270 and NF90. An additional experiment of producing a thin film on the surface of PAN ENM without BM was performed just for this mechanical test. This provides a glimpse of the mechanical strength of ENM without BM. Without any BM support, the ENM membrane with a thin film layer exhibited the lowest strength. However when the ENM is spun on BM (and with hot-pressing) followed by introducing a thin film layer, the yield stress and tensile strength values jumped instantly. This highlights that electrospinning ENM on BM is important especially if strength is a critical parameter during separation.

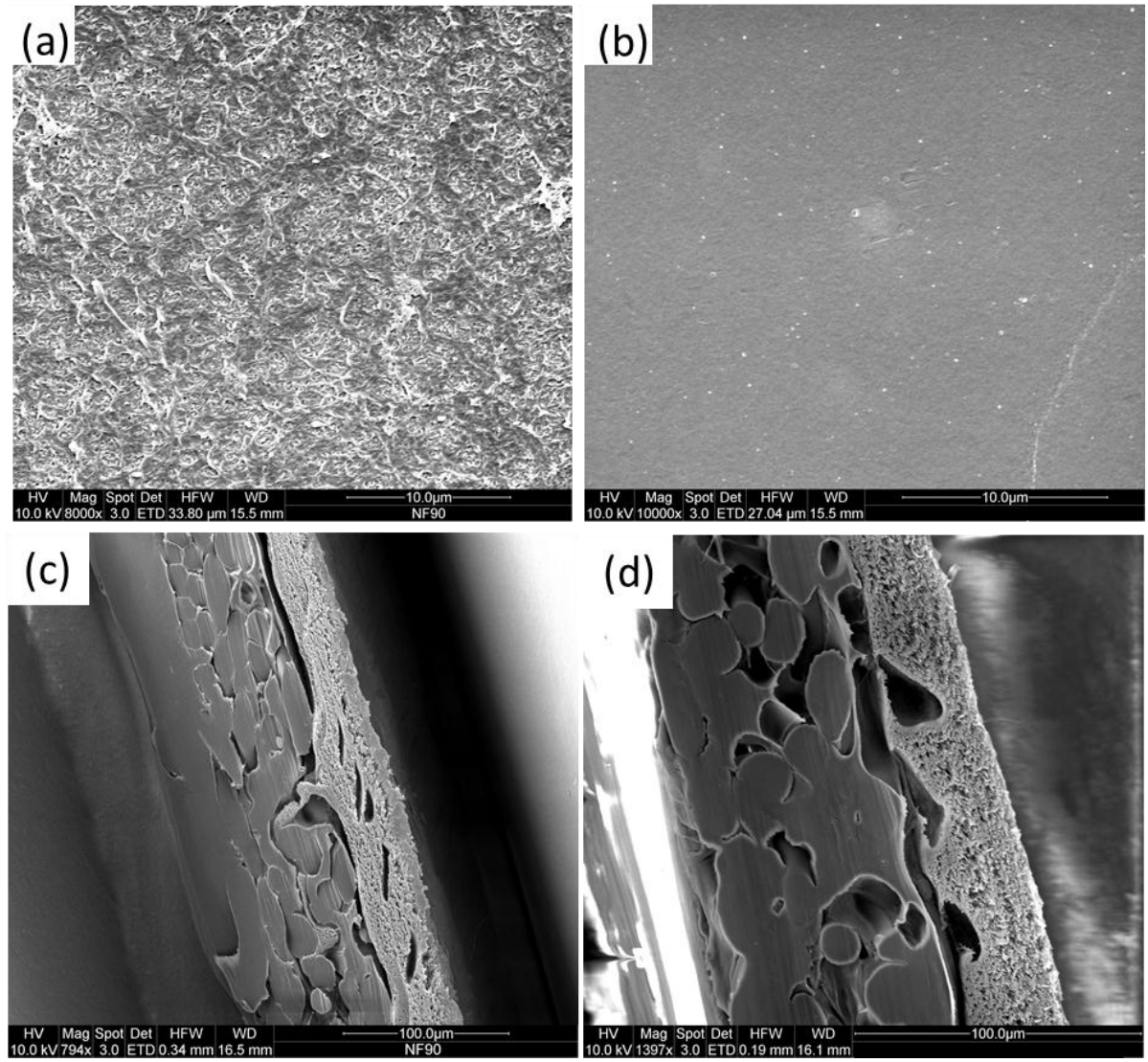

Figure 5.15. SEM images of (a) top view of NF90, (b) top view of NF270, (c) cross-section of NF90 and (d) cross-section of NF270.

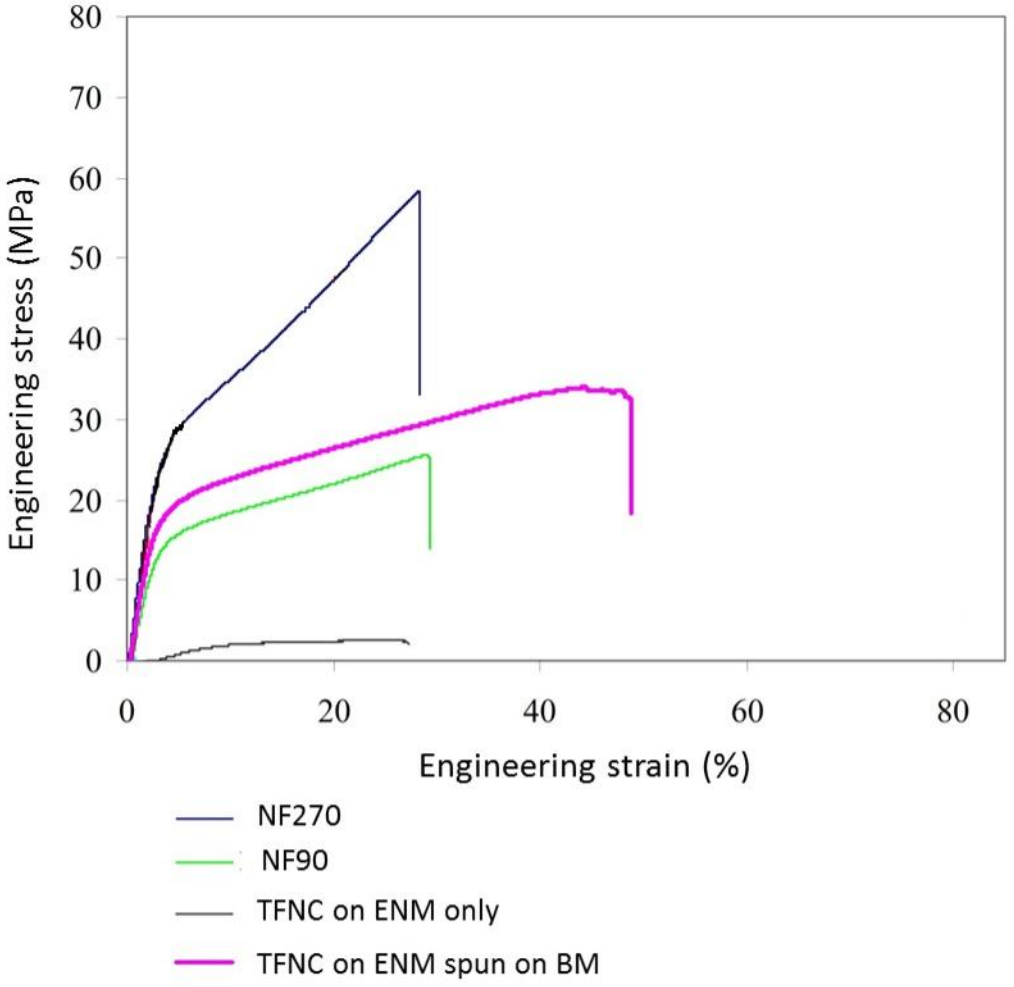

Figure 5.16. Mechanical properties of commercial membranes, TFNC without BM, TFNC with BM.

5.4. Conclusion

TFNC membranes based on ENM supports subjected to hot-pressing were fabricated. The hot-pressing of the nanofibrous support layer and backing material had a significant influence on the flux of the membranes and their mechanical and structural integrity. This subsequently influenced the separation performance, pressure tolerance and handling ease of the developed TFNC membranes. Without hot-pressing, ENM-control had a large pore-size (5.6 µm) as compared to ENM-1 (2.3 µm), ENM-2 (1.1 µm) and ENM-3 (0.8 µm) when measured by the bubble point method. ENM-control's large pore-size could be due to its 'loose' fibrous

architecture. This highlights the importance of hot-pressing as it influences the pore-size distribution of the substrate membranes and subsequently their pure water flux. The pure water flux was observed in the following order: ENM-control > ENM-1 >ENM-2 >ENM-3. By applying pressure, the thickness of the ENM layer decreased following the order ENM-control>ENM-1>ENM-2>ENM-3. This is because the fibers were compressed and, as the increase in mechanical properties with an increase in hot-pressing pressure indicates, adhesion between the ENM and BM was improved. Nanofiltration experiments were carried out with a feed solution of 2000 ppm $MgSO_4$ on TFNC-Control, TFNC-1 and TFNC-2. In the case of TFNC-control, it was not stable at higher fluxes. On the other hand, TFNC-1 and TFNC-2 were able to withstand TMP of 190 psig with rejections of 88% and 92%, respectively. This reflects the importance of hot-pressing. The fluxes of developed TFNC-1 and TFNC-2 were higher when compared to commercial NF270 and NF90 membranes, but they had approximately 8-12% lower rejection than the commercial membranes, which is attributed to the highly porous fibrous architecture of ENM.

CHAPTER 6

INFLUENCE OF ELECTROSPUN FIBER SIZE ON THE SEPARATION EFFICIENCY OF THIN FILM NANOFILTRATION COMPOSITE MEMBRANE

6.1. Introduction

As mentioned earlier, much research has been focused in improving the performance of TFC membranes in terms of selectivity (solute rejection) without any appreciable change in membrane productivity (flux) by altering the thin film layer. Not much attention has been given to the second layer ever since asymmetric membrane has been utilised in membranes. To recall, the second layer provides porous support to build the composite structure and should be biologically, chemically, mechanically and thermally stable. In addition, the morphology and chemistry of this layer may influence the formation of the ultrathin polyamide layer. It is the interest of this study to investigate the influence of the second layer on the separation of electrolytes. It is hypothesized here that the fiber size of the electrospun membrane will play an important role in the separation efficiency of salt solution. This is based on the fact that separation efficiency is dependent on the membrane pores, which can be altered by varying the nanofiber diameter. A detailed study of developing different fiber size electrospun membranes as the second layer and on which thin film of barrier layer was subsequently introduced through IP was performed. The composite membranes were characterized by measuring rejections and flux of salt solutions. In addition, an electrospun membrane supplied by ELMARCO has been modified where the thickness of the immediate fibrous layer which is in contact with the thin film is greatly reduced. This was to understand whether the thickness of the fibrous layer would have an impact on the flux as well as selectivity. This study shed new insight on the role of electrospun membranes as a support

membrane structure and overall performance of the composite membranes, which may contribute significantly towards the development of better NF membranes.

As observed in chapter 5, high fluxes were attained when the second layer was made of ENM. The important attributes discovered in chapter 5 was (a) ENM layer has to be hydrophilic and (b) the ENM layer and the BM has to be hot-pressed before interfacial polymerization can be carried out so as to 'lock' the fibers. Based on these findings, PAN was used and the membranes were hot-pressed before interfacial polymerization was carried out. Since this chapter involves the fabrication of different fiber sizes, the flow rate (electrospinning variable) of PAN solution was reduced. By reducing the flow rate, sufficient time was given for the polymer solution to stretch as much as possible.

6.2. Experimental

6.2.1. Materials

Polyacrylonitrile (PAN, with average molecular weight 150, 000 Dalton), piperazine (PIP), *p*-phenylene diamine (PPD), trimesoyl chloride (TMC), hexane, magnesium chloride ($MgCl_2$), sodium sulphate (Na_2SO_4), triethylamine (TEA), polyethylene glycol of MW 300, 600, and 3400 were purchased from Sigma-Aldrich. Non-woven poly(ethylene terepthalate) (Hollytex 3242) was supplied by Ahlstrom Mount Holly Springs, USA. Dimethylformamide (DMF) was purchased from Merck and was stored over molecular sieves (to remove moisture) before use. Magnesium sulphate ($MgSO_4.7H_2O$) was purchased from Sino chemicals. Sodium chloride (NaCl) was purchased from Merck. Commercial membrane NF270 has been

supplied by the FilmTec Corporation (Edina, MN, USA) and ELMARCO PA6 was a gift from ELMARCO s.r.o, Czech Republic.

6.2.2. Preparation of PAN electrospun membrane

Electrospinning was conducted in an automated electrospinning machine (Nanon-01A, MECC Co. Ltd. Japan) Nanon. A rotating drum covered with the Hollytex backing material (BM) of dimensions 66 x 22 x 0.014 cm was used as the collector. The rotating speed was fixed at 150 rpm. The spinneret speed was fixed at 10 mm/s and size of the spinneret was 21 G1/2 (0.88 mm dia). The spinneret to collector distance was set at 15 cm. 20 ml of 8% or 10% (w/w) PAN solution was directly electrospun onto the entire backing material (BM) at 30 kV (hereafter referred to as ENM-8 and ENM-10, respectively. Ten mL of 4% or 6% (w/w) solution was also electrospun on top of the nanofiber layer that was formed by electrospinning 10ml of 8% (w/w) PAN solution on the BM. The latter membranes are hereafter referred to as ENM-4 and ENM-6. The flow rate of all PAN solution was kept at 0.5 mL/h. The humidity was 70% at 22.5 ^{o}C. Figure 6.1 illustrates the four membranes developed. After electrospinning, the developed membrane was exposed to mild convective air flow in the fume hood overnight to remove any residual solvent. The membrane was cut into 15x15 cm pieces and was hot pressed in a thermal transfer press (Hotronix, Carmichaels, PA 15320, USA) at 80^{o}C for 999s at a pressure of 4 Pa.

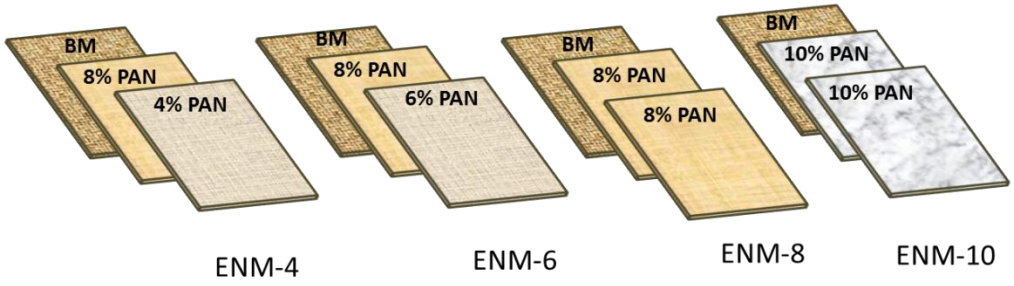

Figure 6.1. The four different ENMs developed.

6.2.3. Interfacial polymerization on PAN backing layer

IP was carried out on the electrospun PAN surface to develop thin film nanofibrous composite (TFNC) membranes. An ENM with an area of 15 x 15 cm was pasted on a clean dry glass container with an adhesive tape (3M, USA). The procedure for interfacial polymerization was as follows. The total amine concentration in the aqueous phase was kept at 2% (w/v); i.e.0.75% (w/v) PIP, 0.25% (w/v) PPD and 1% (w/v) TEA. The ENM was left immersed in the aqueous phase for 3 min. The solution was blotted from the ENM surface and the ENM was kept in a vertical position for 13 min, before being pasted on a clean dry glass container. Interfacial polymerization was completed by making a ENM surface in contact with 0.1% (w/v) TMC solution in hexane for 1 min. The resulting polyamide TFC membrane was subsequently heat cured at 80 ^{o}C for 10 min and finally washed thoroughly with de-ionised water before conducting separation test. The membranes were stamped out into circular coupons with diameter of 6.5 cm. The thin film that is produced on ENM-4, ENM-6, ENM-8 and ENM-10 will be labelled as TFNC-4, TFNC-6, TFNC-8 and TFNC-10, respectively. ELMARCO PA6 nanofiber membrane was also surface modified in the same way as above and it will be labelled as TFNC-E.

6.2.4. Characterization of PAN and polyamide films

Surface morphology of the PAN ENMs and polyamide layers was observed by scanning electron microscopy, SEM (quanta 200F, FEI). The average fiber diameter of PAN ENM was determined from the FE-SEM image using the Image J software (http://rsb.info.nih.gov/ij/). All data were expressed as mean ± standard deviation (SD).

The bubble point (largest pore-size), mean pore-size and smallest pore of the Hollytex backing material (BM), and the PAN layer electrospun on the BM were determined using a capillary flow porometer (Porous Materials Inc, USA). The membranes were completely wetted with Galwick^{TM} (Porous Materials Inc, USA) liquid for at least 5 min and then placed in the test cell with an effective diameter of 1 cm.

Quantitative surface roughness analysis of the membranes is the same as section 5.2.4.

6.2.5. Separation test

Pure water flux of the ENM layer was measured on a dead-end AMICON stirred cell (8010) unit having a capacity of 10 mL and it was attached to an 800 mL reservoir (RC800) as shown in Figure 6.2. Membranes with an effective filtration area of 4.1 cm^2 (25 mm in diameter) were placed in the stirred cell.

On the other hand, TFNC membranes were placed in a custom-built continuous cross-flow filtration cell (active filtration area of 19.63 cm^2). Before starting the filtration experiment, each membrane was compacted for 1 h at a transmembrane pressure (TMP) of 70 psig with

2000 ppm salt ($MgSO_4$, $MgCl_2$, Na_2SO_4, NaCl) feed solution. Each filtration experiment was run for 1 h at various TMP (70, 100, 130, 160 and 190 psig) before permeate was collected. Conductivity of the feed solution before starting the filtration experiment and after the filtration run was measured by a digital conductivity meter (Thermo Scientific Orion 3-star Plus). The temperature of the feed solution was between 30-32 ^oC. Conductivity and temperature of the permeate were also measured. The temperature of permeate collected was between 22-24 ^oC.

The total volume of the feed solution was 5 L and the volume of permeate collected was approximately 20 mL. The permeate flux was determined by direct measurement of the permeate flow in terms of liter per square meter per hour (L/m^2h). The solute rejection (R %) was calculated using the following equation (4):

$$R\ (\%) = [1- (\lambda_p/\lambda_f)] \times 100\% \text{ ------(4)}$$

Where, λ_p is the conductivity of permeate (µS/cm) and λ_f is the conductivity of feed (µS/cm) after the filtration. Each membrane was fabricated three times for filtration testing and each permeation test (at different pressures) was done three times. All experimental values were averaged.

Separation experiments of 2000 ppm PEG 300, PEG 600 and PEG 3400 were also carried out at 70 psig on the AMICON dead-end cell. The membranes were compacted with water for the first 1 h before separation of PEG was carried out. The stirring was kept at 500 rpm using a stir plate to minimise concentration polarization. The first 3 mL of permeate was discarded and the next 10 mL of permeate was collected in a 10 mL capacity vial. The PEG

concentration of the feed in the reservoir before and after the filtration experiment, in the stirred cell and in the permeate was determined by a total organic carbon (TOC) analyser. Solute rejection was calculated using equation (1). However two different concentrations were considered for C_f , one for the concentration in the stirred cell (10 mL) and the other in the reservoir taken before the filtration experiment (800 mL).

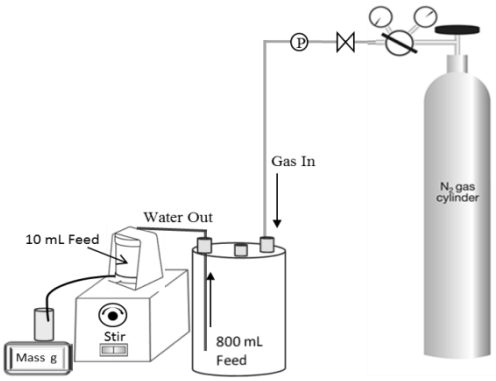

Figure 6.2. Schematic diagram of the dead-end test cell.

6.3. Results and discussion

6.3.1. Effect of polymer solution concentration on fiber size

Before attempting the electrospinning of 8 wt% PAN solution on the backing material, we have first electrospun 4 wt% or 6 wt% PAN solution directly on the BM and the resulting ENMs, called ENM-4 and ENM-6, respectively, were subsequently hot pressed. However, the electrospun layer peeled easily when it was disturbed. This could be due to the extremely fine fiber size and weak adhesion between the electrospun PAN layer and the backing material despite hot-pressing. This problem was solved when 8% PAN was electrospun. The surfaces of the ENMs are shown in Figure 6.3.

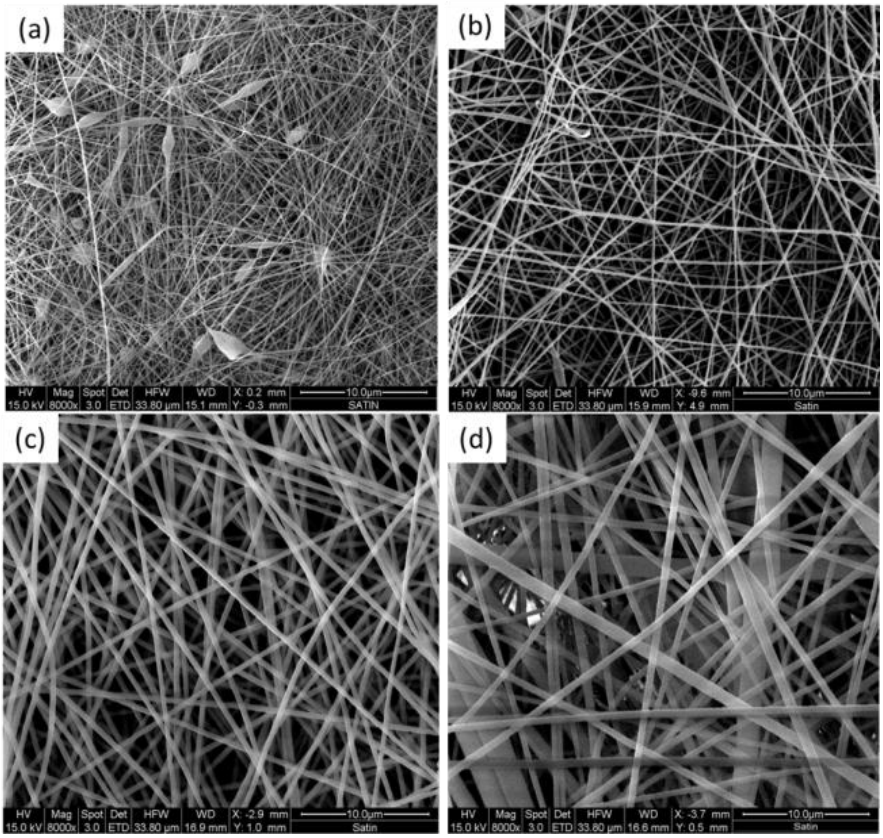

Figure 6.3. Surface architecture of (a) ENM-4, (b) ENM-6, (c) ENM-8 and (d) ENM-10.

The fiber sizes of ENM-4, ENM-6, ENM-8 and ENM-10 are 67±27, 158±39, 337±60, and 573±335nm, respectively. It is well known that increasing the polymer concentration increases the diameter of the electrospun fiber. ENM-10 (prepared from 10 wt% PAN solution) had the largest fiber size and the largest standard deviation. As observed from the SEM micrograph (Figure 6.3a), there were two distinct fiber sizes namely in the 400 and 700 nm region and this accounts for the large variation in the fiber diameter. Comparing the fiber size of ENM-10 with the other membranes, the fiber size for ENM-8, ENM-6 and ENM-4 was reduced to 41%, 72% and 88% respectively. Besides the reduced fiber diameter, the fiber diameter variation (in standard deviation) became smaller with a decrease in polymer solution concentration. However, lowering the PAN concentration to 4 wt% leads to the formation of beads. These observations are similar to several experiments performed with other polymeric

material [Fong 1999, Mit-uppatham 2004]. It has already been reported that higher polymer concentration increases the viscosity of the solution and hence favours thicker fibers, whereas the intermediate concentration produces thinner nanofibers with beads [Huang 2006]. Concomitantly, in the present study, ENM-10 and ENM-4 falls in the higher concentration and intermediate concentration, respectively.

6.3.2. Influence of fiber size on pore-size distribution and pure water flux

The ENMs can be classified as a "tortuous-pore" MF membrane due to a network of interconnecting tortuous flow paths. The pore openings do not correspond to the limiting pore-size within the depth of membranes [Porter 1990], and hence pore-size characterization using the SEM is not suitable. With the use of capillary flow porometer, the pore-size distributions of the several ENM membranes were determined. The average of the bubble-point pore-sizes was 0.54, 0.61, 0.89 and 7.75 μm, respectively, for ENM-4, ENM-6, ENM-8 and ENM-10. The pore-size distribution of the membranes is reflected in Figure 6.4. There is a close relationship between the fiber size and the pore-size and also the fiber size and the pore-size distribution. As the fiber diameter decreases, the maximum pore-size obtained by the bubble point measurement also decreases. In addition, the pore-size distribution (i.e. the distribution from the largest pore to the smallest pore) becomes narrower. We believe that a narrow pore-size distribution may be better to achieve good filtration efficiency. Overall, the pore-size distribution is the widest in ENM10, highlighting the unevenness generated by the variation in fiber sizes.

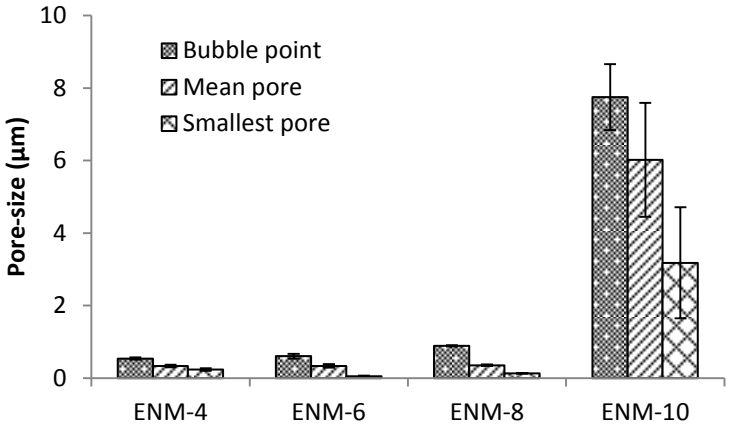

Figure 6.4. Pore-size distribution of the different ENMs.

Consequently, the pore-size distribution has affected the flux performance. The average pure water fluxes of ENM-4, ENM-6, ENM-8 and ENM-10 were determined as 1840, 3032, 5509 and 6993 L/(m^2h psig), respectively (Figure 6.5). When compared to ENM-10, the observed reduction in fluxes for ENM-8, ENM-6, ENM-4 were 17%, 57% and 74% respectively. It is to be noted here (from SEM images in Figure 6.3) that the number of fibers in a given area follows the order of ENM-4 >ENM-6 >ENM-8 >ENM-10. Hence it is expected that the pores for ENM-4 will be smaller than ENM-10, as more fibers could have provided an obstacle to the flow of water and hence leading to lower fluxes.

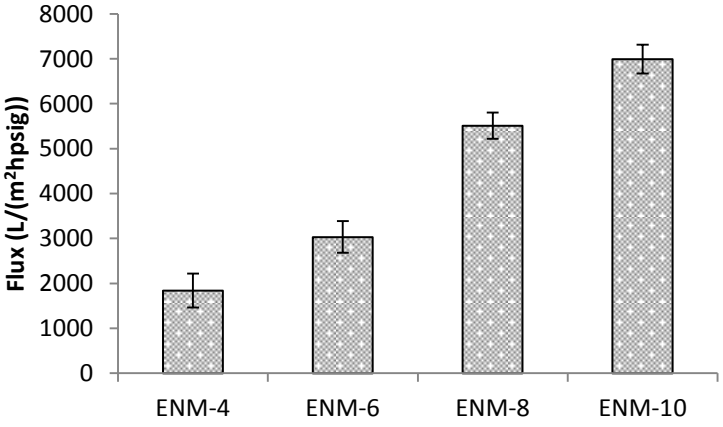

Figure 6.5. Flux profile of the various ENMs.

6.3.3. Influence of fiber size on TFNC formation

In order to determine the differences in the morphologies of the TFNC layers on the different ENMs, SEM images were recorded. Figure 6.6 gives an overview of the surface topography of the various TFNCs. It was observed that there was a difference in topography of the TFNCs fabricated from the various ENMs. In the case of larger fiber diameter membranes, the imprints of the fibers became clearer and the texture seemed more smooth and transparent. On the other hand, when the fiber size of the ENM was smaller (in the case of TFNC-4 and TFNC-6), the surface morphology appeared to be so called ridge- and valley structure, which is similar to the previously published results [Kwak 1999]. This is because the pores are efficiently covered by the reactants in the membrane of lower fiber diameter and thereby favors efficient film formation.

Figure 6.7 shows the surface architecture of the various layers present in the composite structure (TFNC-4 was used as example) while Figure 6.8 provides the cross-sectional image. From Figure 6.8, it was observed that the interfacial film was formed fully on the first layer of the fibers, and thickness was less than 500 nm and thin film formation has not penetrated within the pores of the ENM. Overall, it can be concluded that the surface morphology of the TFNC layer is influenced by the fiber size.

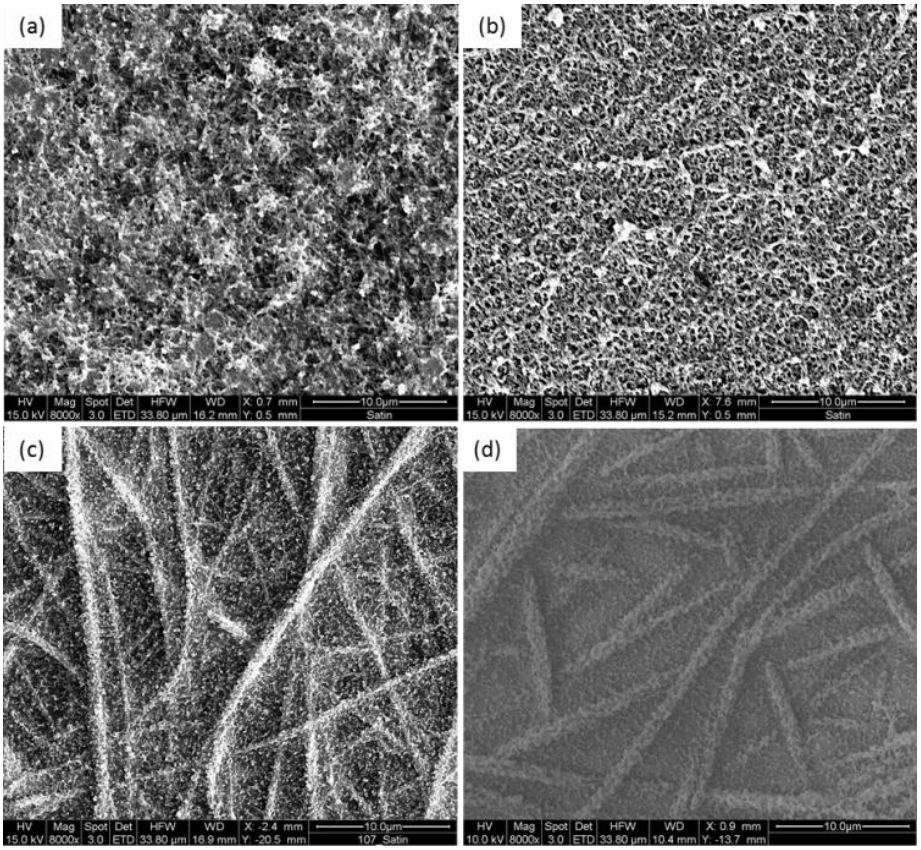

Figure 6.6. Surface architecture of (a) TFNC-4, (b) TFNC-6, (c) TFNC-8 and (d) TFNC-10.

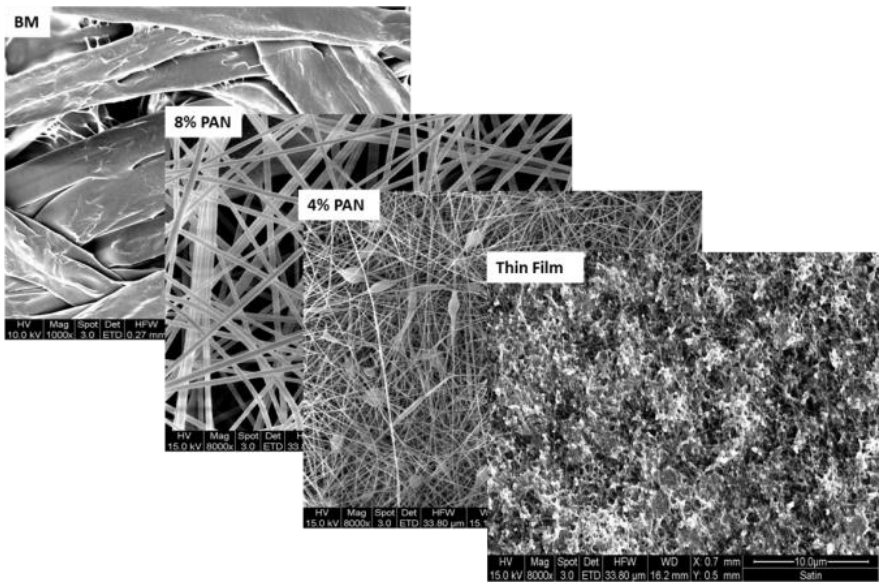

Figure 6.7. Illustration of the layers present in TFNC-4.

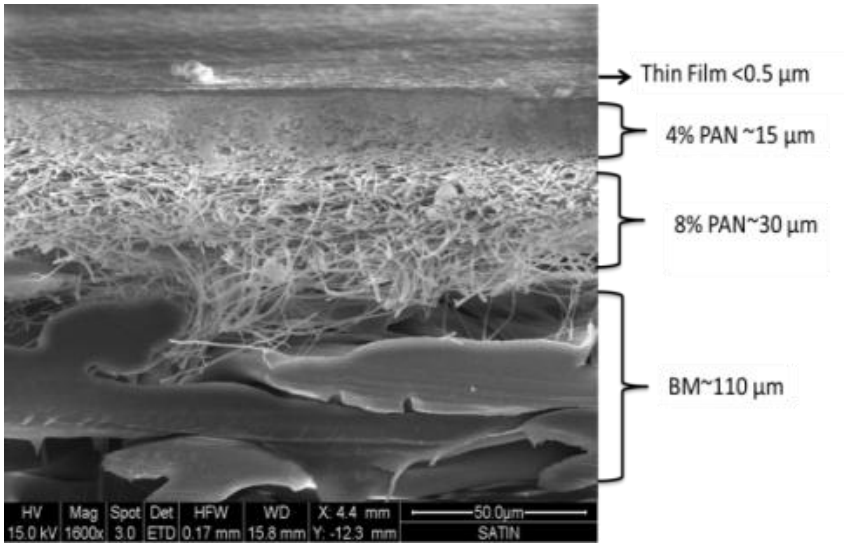

Figure 6.8. Cross-sectional view of TFNC-4.

6.3.4. Influence of fiber size on the separation performance of TFNC membranes

Separation of $MgSO_4$ from the solution of 2000 ppm was evaluated for TFNC-4, TFNC-6, TFNC-8 and TFNC-10 membranes. In the case of TFNC-4, TFNC-6 and TFNC-8, they successfully separated $MgSO_4$, while the rejection of TFNC-10 decreased with an increase in pressure. The rejection and flux profiles of TFNC-10 are shown in Figure 6.9. At 50 psig, the rejection was 68.7% with a flux of 115 L/m^2h and the rejection dropped slightly to 65.4% at 70 psig while the flux increased to 142 L/m^2h. Subsequently at higher pressures, the rejection dwindled with a non-linear increase in flux. This shows that the ENM-10 layer was not able to support the TFNC layer at higher pressures, probably due to its larger pore-size. This indicates that there is a restriction on the fiber size and pore-size to support the interfacial layer.

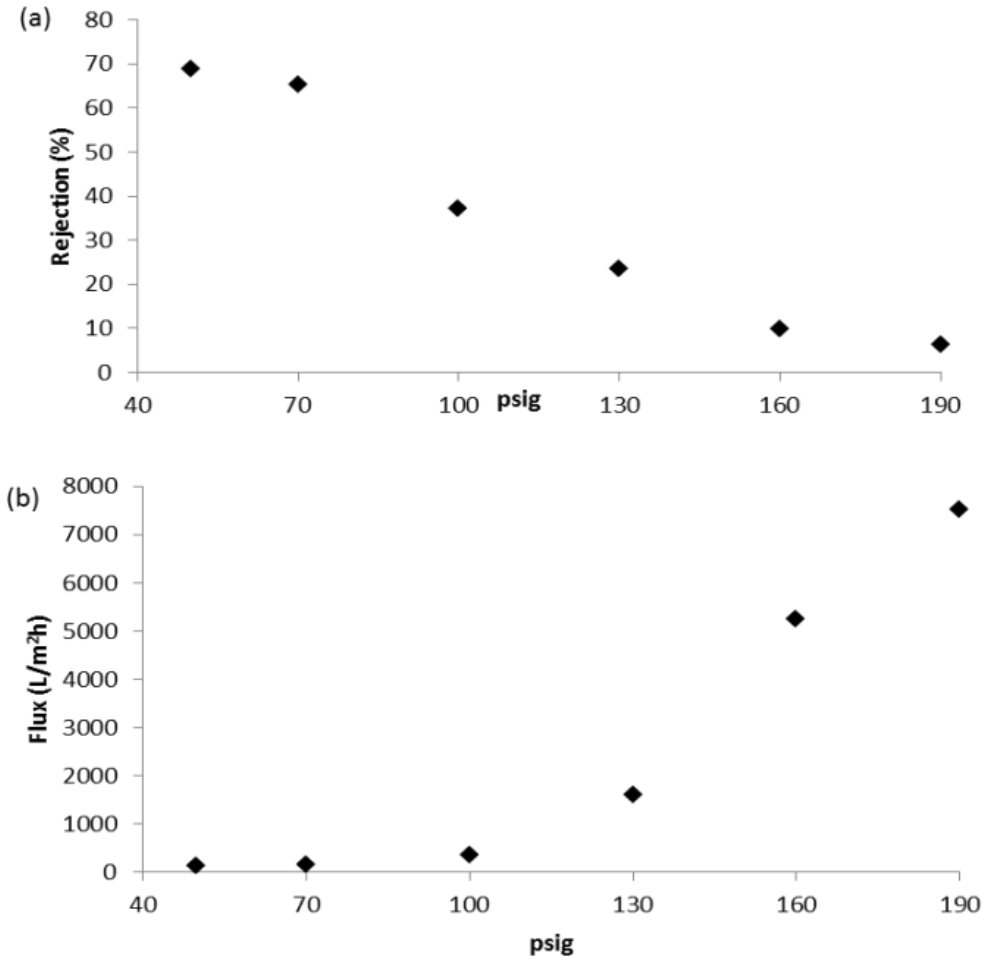

Figure 6.9. Effect of operating pressure on(a) salt rejection and (b) permeate flux. (Feed, 2000 ppm aqueous $MgSO_4$ solution; membrane, TFNC-10)

The separation and flux profile of TFNC-4, TFNC-6 and TFNC-8 are shown in Figure 6.10.

TFNC-4 and TFNC-6 showed a slight increase of ~1.5 % rejection of $MgSO_4$ whilst the rejection of TFNC-8 increased by 4% in this pressure range. The increase in rejection of TFNC-4 and TFNC-6 with respect to TFNC-8 was determined as 6 % and 3 %, respectively at 190 psig. This small increase in rejection is greatly valued in the field of water treatment**.** When the pressure increased from 70 to 190 psig, the flux increased for TFNC-4 and TFNC-6 was more gradual when compared to TFNC-8, and the increase in fluxes in the above

pressure range were 147 %, 157 % and 274 %, respectively, for TFNC-4, TFNC-6 and TFNC-8. This difference in flux and rejection among TFNCs are attributed to the difference in fiber size of the ENMs. As the fiber size decreases, the packing density of the fibers increases which leads to a decrease in the pore-size and pore-size distribution, hence further leading to a decrease in flux. This favours the uniform formation of the thin film, which may adopt a more cross-linked and packed (chain stiffness) structure with decreased chain mobility, thereby contributing to an improved rejection but a decrease in the permeate flux. Similar observation on other type of support membrane has been reported in the literature [Li 2007].

Solute rejection usually increases with pressure (up to an asymptotic value) since water flux through the membrane increases while solute flux is essentially unchanged when pressure is increased [Bhattacharyya 1992]. The same trend was observed in the present study, with the flux and salt rejection depending on the fiber size. Hence, both rejection and flux can be controlled by altering the fiber size.

AFM was employed for morphological characterization of the TFNC membrane surface and Table 6.1 gives the roughness properties of the ENM layer and TFNC layer. The mean roughness (Ra), root mean square (RMS) value and Rm values for ENM layer are in the following order ENM-8 > ENM-4 > ENM-6 and for TFNC layer TFNC-8 ≈ TFNC-4 > TFNC-6. Among ENMs, it is expected that ENM-4 should have the lowest roughness value as its fiber size is the smallest. As well, the variation in the fiber size and the space between each fiber is the least. However the surface roughness of ENM-4 is not necessarily the least, perhaps due to its beaded morphology.

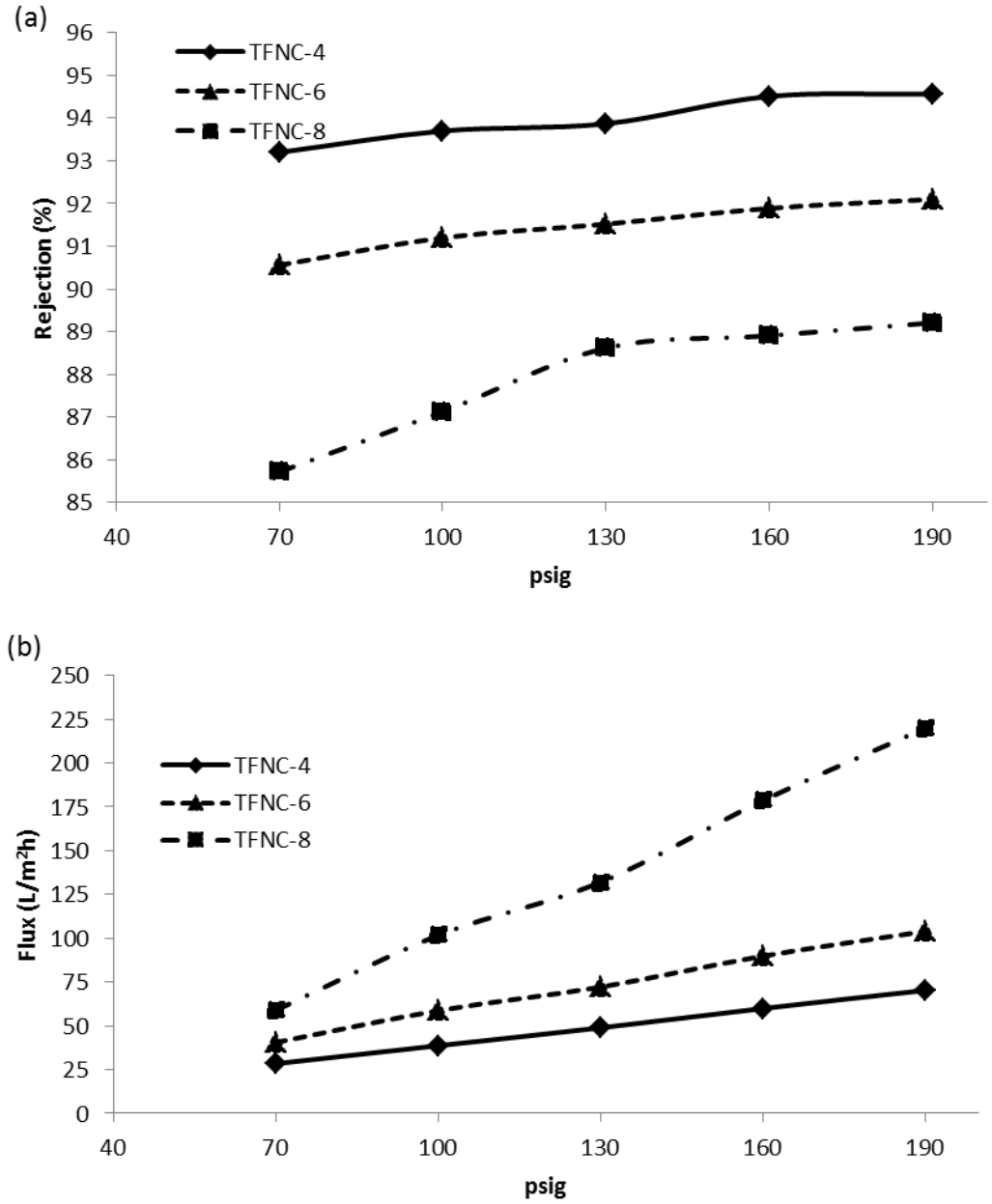

Figure 6.10. Effect of pressure on (a) salt rejection and (b) permeate flux for different TFNCs. (Feed, 2000 ppm aqueous $MgSO_4$ solution)

When a thin film was formed on ENM-4 and ENM-6 surfaces to produce TFNC-4 and TFNC-6, the roughness values slightly decreased. On the other hand, the surface roughness of TFNC-8 was drastically reduced when compared to ENM-4 and ENM-6. As a result, the

roughness values of TFNC-8 and TFNC-4 became almost the same. The observed variation in surface roughness properties of these TFNC membranes may be related to the difference in surface architecture formed on the ENM layer, which is caused by the difference in diffusion rates of the diamine monomer (and then polymer formation) when in contact with different fiber sizes of the ENM. Further, the influence of architecture on the surface roughness was evidenced by comparing the ENM-4 (beaded fiber) with ENM-6.

Table 6.1. AFM properties of ENM and TFNC membranes.

Membrane ID	Ra (nm)	RMS (nm)	Rm (μm)	SAD(%)	SA (μm^2)
ENM-4	205.99±10.14	258.67±24.05	2.16±0.80	136.02±7.62	236.02±7.62
ENM-6	123.16±6.49	160.93±11.77	1.49±0.23	33.84±0.82	133.84±0.82
ENM-8	388.78±7.66	478.44±13.29	2.75±0.31	92.02±3.96	192.02±3.97
TFNC-4	193.96±19.48	236.75±21.71	1.34±0.08	29.24±0.35	129.24±0.24
TFNC-6	111.01±27.29	140.12±35.27	0.92±0.22	23.77±3.27	123.77±3.27
TFNC-8	190.15±32.77	234.52±40.62	1.413±0.19	28.12±2.22	128.12±2.21

A more thorough study of separation of other salts, namely Na_2SO_4, $MgCl_2$, NaCl besides $MgSO_4$ was performed on TFNC-4. The rejection of the various salts was in the following order Na_2SO_4 >$MgSO_4$ > $MgCl_2$ >NaCl (Figure 6.11). The flux profile was observed in the following order $MgSO_4$ > Na_2SO_4 > $MgCl_2$ >NaCl and difference in flux readings does not deviate largely between each salt. The order in the separation of various electrolytes suggests that the mechanism involved in the separation is not necessarily the electric charge

interaction. If the latter would be the case, the order in the separation would become Na_2SO_4 >$MgSO_4$ > NaCl > $MgCl_2$, as observed often for other NF membranes, due to the presence of negative charge coming from the unreacted carboxyl group of TMC.

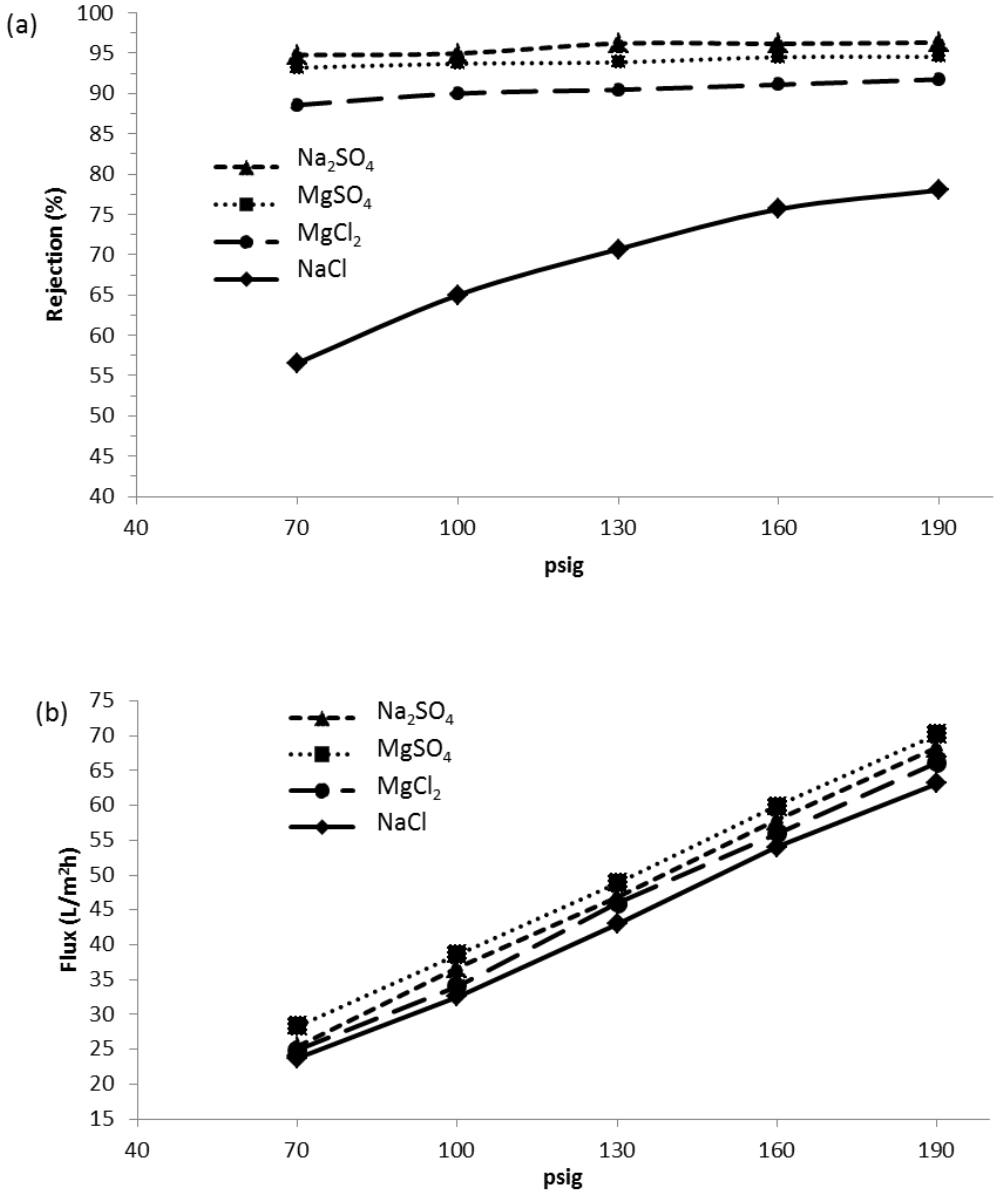

Figure 6.11. (a) Separation and (b) flux of TFNC-4 membrane for different electrolytes in the feed solution.

If the dielectric effect governs the rejection, the ionic valence will play an important role. The divalent ions are repelled more strongly from the membrane surface than the monovalent counterpart, regardless of the nature of the charge (either positive or negative). Then, the order in the electrolyte separation is expected to be $MgSO_4$ > Na_2SO_4≈ $MgCl_2$>NaCl. The experimentally observed order is similar to the electric charge effect in the first half and similar to the dielectric force in the latter half. Hence, it can be concluded that the electrolyte separation is governed both by the charge and the dielectric repulsion effect.

Table 6.2. Separation of PEG 300, 600 and 3400 by TFNC-4 at 70 psig.

Feed	R(%)- 800 mL	SD	R(%)-10 mL	SD
PEG300	93.20	1.93	97.17	0.95
PEG600	93.23	1.08	96.87	0.87
PEG3500	93.57	0.65	97.20	0.53

Separation of PEG 300, 600 and 3400 was carried out on a dead-end set-up on TFNC-4 to evaluate the separation mechanism of the membrane. The results of the separation are shown in Table 6.2. As mentioned in the experimental section, two different concentrations were considered for the feed, concentration in the 10 mL stirred cell and in the 800 mL reservoir. The separations based on the stirred cell concentration are higher than those based on the reservoir concentration as the former are higher than the latter. This is only natural because stirring is limited in the stirred cell and the solutions in the cell and in the reservoir are not well mixed. Interestingly, the separation does not depend on the PEG molecular weight. This is because the higher separation of PEG3500 is compensated by the more severe concentration polarization.

6.3.5. Influence of ENM thickness and fiber size -separation of 2000 ppm NaCl on TFNC and commercial membranes.

It has been observed that by decreasing the fiber size, the rejection of salt increased. Hence it is hypothesized that a further decrease in fiber size together with a decrease in the thickness layer of the top most fiber layer, will not only increase the rejection, but will also increase the flux of the membrane as the tortuous depth/path is reduced for the flow of water. The commercial ELMARCO nanofibrous polyamide membrane satisfies such requirement with its fiber diameter of 42 ± 26% nm and bubble point pore-size of 0.174 ± 2% µm. To recall, the smallest fiber size and bubble point pore-size of the laboratory made membranes were 67 nm and 0.54 µm, respectively. SEM images of this membrane are shown in Figure 6.12. Interfacial polymerization was carried out on this ELMARCO nanofibrous membrane and the resulting TFNC membrane is called TFNC-E. It was observed that the thickness of the top most nanofiber layer, which is in contact with the TFNC layer, is approximately 1 µm. This is much smaller than the thickness of the top nanofiber layer (~ 15 µm) of the laboratory made TFNC-4. The surface morphology of TFNC-E (Figure 6.12 d) is similar to that of TFNC-4 and TFNC-6 (Figure 6.6 a and b). The NaCl rejection and flux at different operating pressures are shown in Figure 6.13 for all laboratory made TFNCs together with those of the commercial NF 270 membrane. The rejection of NaCl appears in the following order TFNC-E >TFNC-4 >TFNC-6> NF 270> TFNC-8. The rejection of TFNC-E membrane was better when compared to TFNC-4, TFNC-6, TFNC-8 and NF 270 by 6.6%, 13.5%, 35.3% and 30.5%, respectively at 190 psig. This shows that the fiber size (due to lesser interconnecting pore-size) has an essential influence not only in the way the thin film is formed, but also the quality of the thin film formed (more cross-linked and stiffer film) and thereby preventing the passage of salt. Interestingly, TFNC-E flux was not the lowest. The permeate flux was

determined as TFNC-8 > NF 270 >TFNC-E >TFNC-6 >TFNC-4. Earlier we concluded that a decrease in fiber size resulted in a decrease in flux. Adhering to this principle, the flux of TFNC-E should be lower than TFNC-4 as its fiber size and bubble-point pore-size are smaller than those of TFNC-4. However, TFNC-E flux was 38% higher (at 190 psig) than that of TFNC-4. This is because there is another important feature that plays a role in influencing the flux and that is the cross-sectional thickness of the nanofiber. The thickness of the nanofibrous layer (~<1 μm) in TFNC-E was ~15 times smaller than that of TFNC-4 (~ 15 μm) top most layer. By decreasing the thickness of the nanofibrous layer in contact with the interfacial layer, the overall hydraulic resistance drops, hence enhancing water transport (high flux). It is believed that by optimizing the chemistry of the polyamide layer of the TFNC-E membrane, the flux and rejection could be further improved.

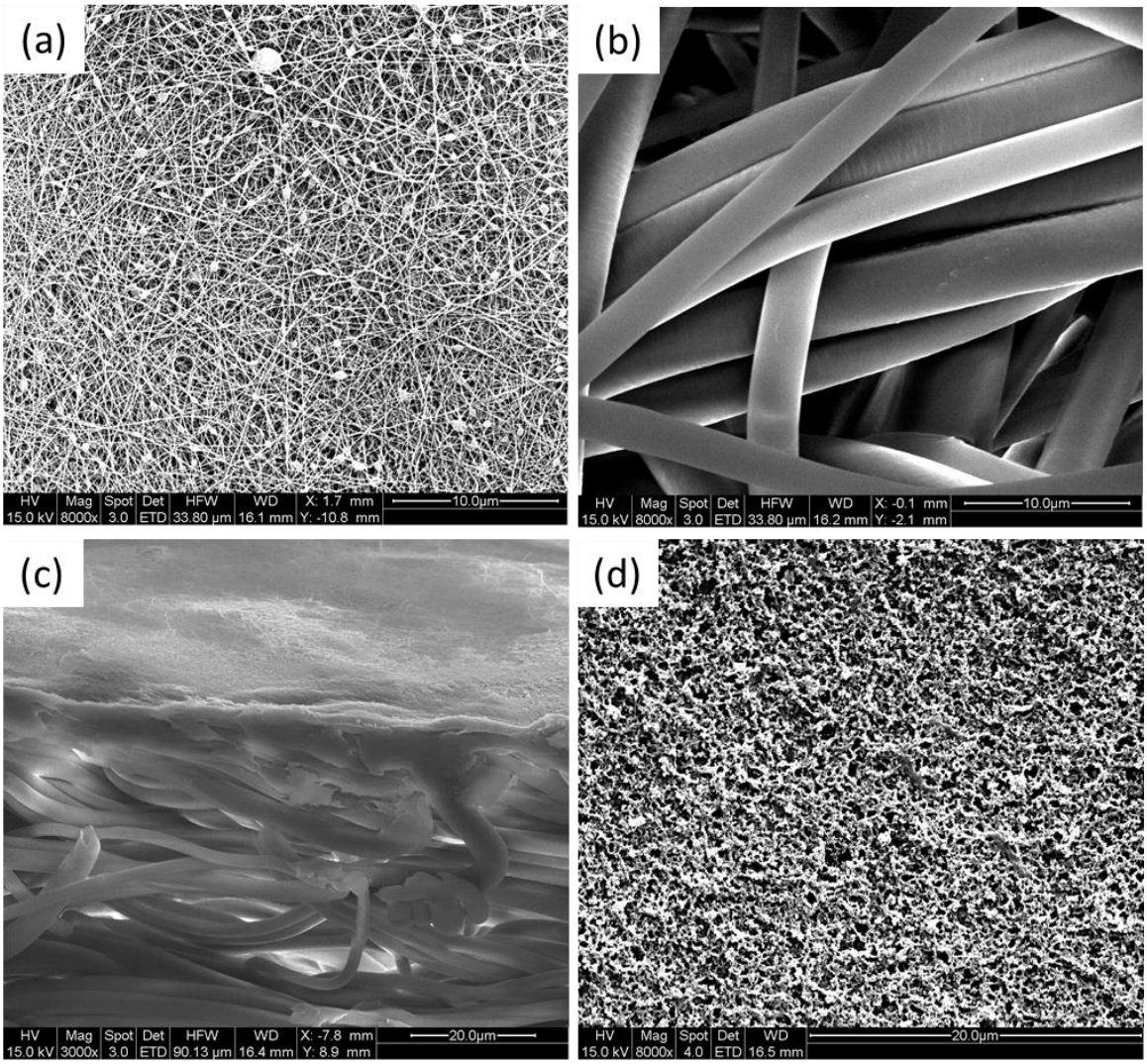

Figure 6.12. SEM images of (a) top polyamide nanofiber layer of ELMARCO membrane, (b) polyamide spunbond support of ELMACRO membrane, (c) cross-section of section (a) and (b) combined, (d) TFNC-E surface layer produced on the top nanofiber layer of ELMACRO membrane.

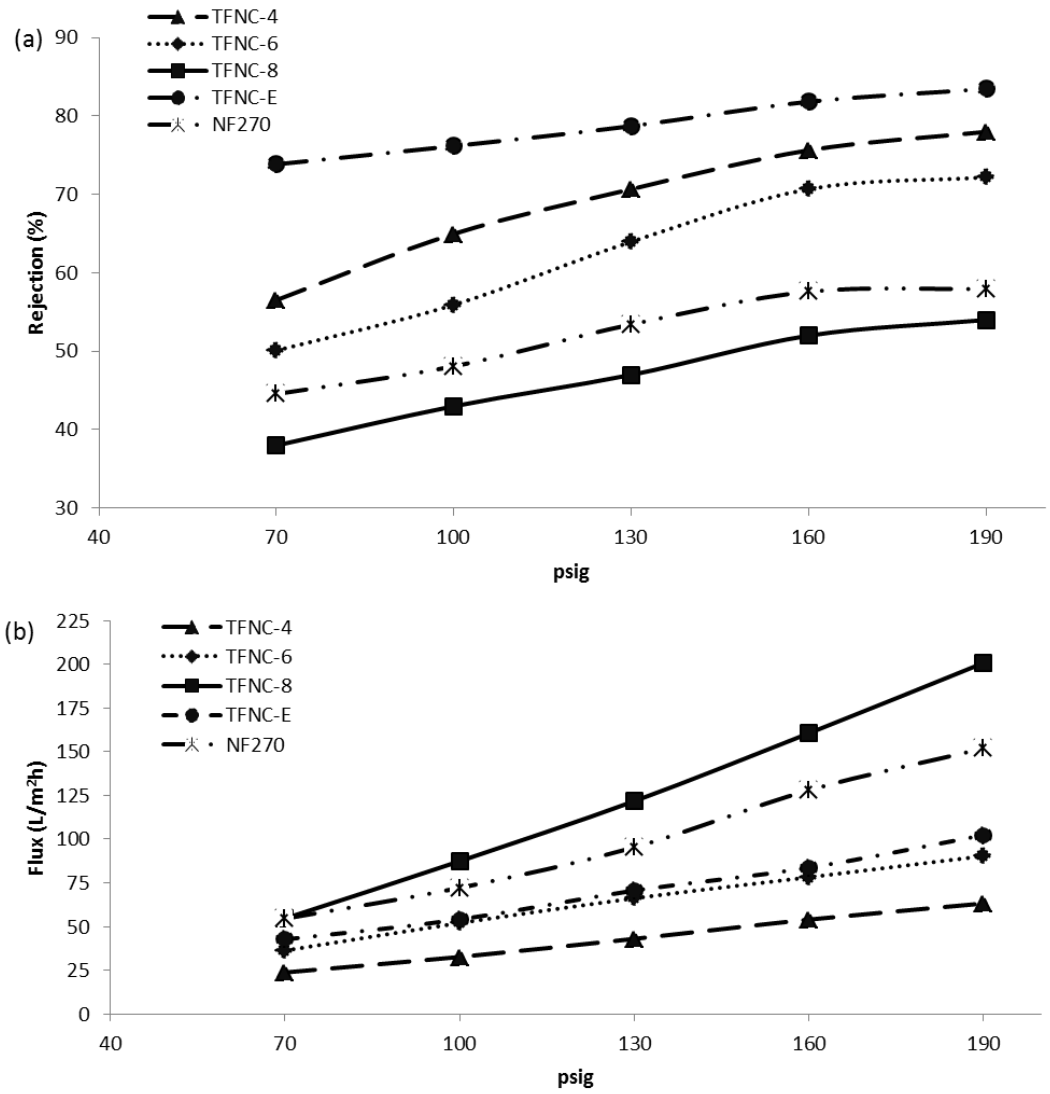

Figure 6.13. (a) NaCl rejection and (b) flux as a function of pressure. (Feed NaCl concentration, 2000ppm)

6.4. Conclusions

TFNC membranes based on electrospun nanofibrous membrane (ENM) support were investigated as suitable nanomaterials for water treatment by evaluating their rejection and flux performances in filtration of aqueous electrolyte solutions involving divalent and monovalent ions. Interfacial polymerization of a mixture of piperazine and *p*-phenylene

diamine with trimesoyl chloride was carried out on the surface of different fiber sizes of PAN ENM. The developed TFNC membranes exhibited typical nanofiltration properties. It is realised from this research that by changing the fiber size, salt rejection and permeate flux can be altered. By increasing the fiber size, the flux of the membrane becomes higher due to the presence of large pores. However, there was an upper limit to the fiber size and the pore-size, since, if the sizes are too large, ENM can no longer support the thin interfacially polymerized layer. The optimum concentration of PAN polymer used to prepare ENM layer to support interfacial layer was 8 wt%. At 8 wt% of PAN (ENM-8), the TFNC-8 membrane was able to separate both $MgSO_4$ and NaCl at 89% with a flux of 220 L/m^2h and 54% at a flux of 200 L/m^2h respectively. Although decreasing the concentration further to 6 wt% and 4 wt% improved the rejection of $MgSO_4$ and NaCl, this has resulted in decreased flux. When the cross-sectional thickness of the nanofiber in contact with the interfacial layer (in the case of TFNC-E) reduced, the flux improved, which was due to a decrease in the hydraulic resistance of the nanofibrous support with the interfacial layer. The capability of altering the fiber size and thickness of the electrospun layer so as to manipulate the rejection and flux as desired is highly advantageous for the water treatment applications.

CHAPTER 7

PREPARATION AND CHARACTERIZATION OF SURFACE MODIFIED ELECTROSPUN MEMBRANES FOR HIGHER FILTRATION FLUX

7.1. Introduction

As seen from Chapter 3 when popular polymeric membrane materials such as poly(vinylidene fluoride) (PVDF) is electrospun, they exhibit high contact. As evinced from Chapter 4, it was difficult to wet the membrane with aqueous solution and despite several attempts to make the membrane hydrophilic, interfacial polymerization was unsuccessful. When a material is rendered hydrophobic it is highly undesirable for pressure driven membrane processes. For water based filtration applications the membrane material generally preferred is hydrophilic as a hydrophilic surface is a key property for fouling resistance [Ghosh 2008]. Fouling is a major obstacle to the widespread use of membrane technology since it is a major cause for flux decline [Rana 2010]. This makes electrospun PVDF unattractive in the area of liquid filtration whether as a microfilter or nanofitler.

Hence, the present chapter deviates away from TFNC and focuses on the ENM layer to make it more hydrophilic. Among the various methodologies adopted in the literature (such as blending, radiation or chemical grafting, coating, chemical vapor deposition etc) [Gopal 2006b] blending is one of the easiest and convenient ways [Suk 2002]. Hence, blending of a hydrophilic surface modifying macromolecule (SMM) to the PVDF polymeric solution before electrospinning was carried out in this study. Surface modifying macromolecules

(SMMs) based on polyurethane prepolymers were prepared from the synthesis of bis(p-phenyl isocyanate) (MDI) with poly(ethylene glycol)s, PEGs, of number average molecular weights (400, 600, and 1000 Da) and poly(propylene glycol)s, PPGs, of number average molecular weights (425 and 3500 Da). Different molecular weights of PPG were selected to investigate the influence of the spacer length in polyurethane on the surface properties and hydrophilicity.

In comparison, membranes were also prepared by the phase inversion technique using SMM blended PVDF solutions as casting dopes. The comparison allows us to gain an insight into the influence of the two adopted techniques (electrospinning and phase inversion) on the surface properties. During phase inversion, the SMMs are supposed to migrate to the membrane surface [Rana 2010], which will have three benefits: (1) an asymmetric structure of the membrane is achieved; (2) a more hydrophilic surface is achieved; (3) less fouling and higher flux are achieved. Hitherto, no reports are available regarding the effects of SMMs on the surface properties of electrospun membranes. It is to be taken note that for this chapter, the electrospun membranes will be abbreviated as EM rather than ENM because some of the membranes had fiber sizes in the micron range.

7.2. Experimental section

7.2.1. Materials

Acetone (Chromasolv grade for HPLC, >99.9% purity, Sigma-Aldrich Company, St. Louis, MO, USA), N,N-Dimethylacetamide (DMAc, anhydrous, 99.8% purity, Aldrich Chemical Company, Inc., Milwaukee, WI, USA), Tetrahydrofuran (THF, Chromasolv grade for HPLC,

>99.9%, Sigma-Aldrich Company, St. Louis, MO, USA), 4,4′-Methylene bis(phenyl isocyanate) (MDI, 98% purity, Sigma-Aldrich, Inc., St. Louis, MO, USA), Poly(ethylene glycol) (PEG, typical M_n 400, 600, and 1000 Da, Sigma Chemical Company, St. Louis, MO, USA), Poly(propylene glycol) (PPG, typical M_n 425, and 3500 Da, Sigma Chemical Company, St. Louis, MO, USA) were purchased and used as received. Poly(vinylidene fluoride) (PVDF, average molecular weight $4.41x10^5$) was purchased from Arkema Singapore, Singapore.

7.2.2. Preparation of surface modifying macromolecules

The SMMs were synthesized by a two-step solution polymerization method. To eliminate the effects of moisture, all glass-wares were dried overnight at 120 ^oC. The first polymerization step was conducted with a predetermined composition to form polyurethane prepolymer. To a solution of vacuum distilled methylene bis(p-phenyl isocyanate) (MDI, 0.03 mol) in 50 mL of degassed N,N- dimethyl acetamide (DMAc) was added 0.02 mol of degassed PPG ($M_{n,}$ either 425 or 3500 Da) in 100 mL of degassed DMAc. The mixture was stirred for 3 h at 48-50 ^oC. To this solution, 0.02 mol of PEG (either $M_{n,}$ 400, 600 or 1000 Da) dissolved in 50 mL of degassed DMAc was further added drop-wise and the solution was stirred for 24 h at 48-50 ^oC. The solution was then added dropwise into a 4 L beaker filled with distilled water in 24 h under vigorous stirring to precipitate the SMM. Depending on the molecular weight of PEG, the SMMs so prepared were called, respectively, SMM 400, SMM 600 and SMM 1000. It should be noted that PPG of M_n 425 Da was used to synthesize SMM 400 and SMM 600 while PPG of M_n 3500 was used to synthesize SMM 1000 (see Table 7.1). The SMM 1000 was gel like, while SMM 400 and SMM 600 were elastomeric. All SMMs were cut into smaller pieces and dried in an air circulation oven at 50 ^oC until the weight became constant.

The molar ratio of monomers used in the SMMs synthesis was constant at MDI:PPG:PEG = 3:2:2. Table 7.1 summarizes the number of moles and weights of the reactants employed to synthesize the various SMMs. All SMMs have a common name which is poly(4,4′-diphenylenemethylene propylene-urethane)-co-poly(4,4′-diphenylenemethylene ethylene-urethane) with both ends capped by PEG. The chemical structure of the SMM is reflected in Figure 7.1.

Table 7.1. Preparation composition of the SMMs.

SMM	MDI, g, in 50 mL DMAc	PPG, g, in 100 mL DMAc	PEG, g, in 50 mL DMAc
SMM-1000 (MDI-PPG3500-PEG1000)	7.5 (0.03 mol)	70 (0.02 mol)	20 (0.02 mol)
SMM-600 (MDI-PPG425-PEG600)	7.5 (0.03 mol)	8.5 (0.02 mol)	12 (0.02 mol)
SMM-400 (MDI-PPG425-PEG400)	7.5 (0.03 mol)	8.5 (0.02 mol)	8 (0.02 mol)

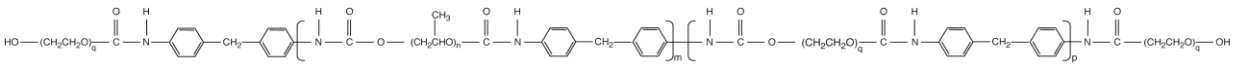

Figure 7.1. Chemical structure of SMM.

7.2.3. SMM characterization

The glass transition and melting temperature of the various SMM additives were characterized by using differential scanning calorimeter (DSC equipped with a universal analysis 2000 program DSC Q1000, TA Instruments, New Castle, DE). The SMM sample was annealed at 260 ^{o}C for 10 min and then quenched to -50 ^{o}C, and scanned at a heating rate of 10 ^{o}C /min. The molecular weight, number average molecular weight (M_n) and weight average molecular weight (M_w), of the synthesized SMMs were measured by gel permeation chromatography (GPC) using a Waters model 410 (Milford, MA) equipped with Waters 410 refractive index detector. Three ultra-styragel columns (10^3, 10^4, and 10^6 Å) were used at room temperature with tetrahydrofuran (THF) as the mobile phase. The SMM molecular weight was calculated using the universal calibration curve provided with the Millenium 32 software for data acquisition.

7.2.4. Preparation of electrospun membranes (EMs)

PVDF solution of 20 % (w/v) concentration was prepared in a mixture of DMAc and acetone at a ratio of 2:3. A syringe pump (74900 series, Cole-Parmer Instrument Company, Vernon Hills, IL) was utilized to supply the polymer solution at a constant flow rate of 4 mL/h during electrospinning. A voltage of 15 kV was applied by a transformer (DW-P503-1C, Beijing Shining Technical & Commercial Centre, Xisanqu, Tiantongyuan, Changping District, Beijing, PR China) to draw fibers from the prepared solution. The fibers were collected on a grounded 100 cm^2 aluminum plate. The relative humidity was controlled between 15 to 18 % and the temperature at 15 ^{o}C. After the electrospun membranes (EMs) were formed, they were heated at 60 ^{o}C for 1 h. Subsequently, the membranes were heated up to 157 ^{o}C to

improve the structural integrity of the membrane. The fiber diameters were determined from the SEM image using the ImageJ software (http://rsb.info.nih.gov/ij/). The SMM blended EMs were prepared by adding SMM (8 wt% of PVDF) to the 20 % (w/v) PVDF solution. The control EM without SMM blending will be hereafter referred to as EM-PVDF. The EMs blended with SMM-400, SMM-600 and SMM-1000 will be hereafter referred to as EM-400, EM-600 and EM-1000, respectively.

7.2.5. Preparation of asymmetric membranes (AMs) by the phase inversion technique

The asymmetric membranes (AMs) were prepared from 20 %(w/v) polyvinylidene fluoride (PVDF) solution dissolved in a mixture of N,N-dimethyl acetamide (DMAc) and acetone at a ratio of 2:3. A thin strip of solution was poured almost at the edge of a clean glass plate and immediately spread by a blade across the glass plate. The glass plate together with the cast polymer solution film was then placed in a cold water bath. After several minutes the membrane was removed from the cold water bath and stored in de-ionized water. To prepare the casting dope for the SMM incorporated membrane, a polymer solution containing 15 %(w/v) of PVDF was first prepared and then SMM (8 wt% of PVDF) was added to the PVDF solution. The control asymmetric PVDF membrane without SMM blending is hereafter referred to as AM-PVDF. The asymmetric membranes blended with SMM-400, SMM-600 and SMM-1000 are referred to as AM-400, AM-600 and AM-1000.

7.2.6. Membrane Characterization

Elemental analysis of the surface of the EMs was performed by X-ray photoelectron spectroscopy (XPS) using Kratos Axis HIS Mono-Al X-ray photoelectron spectrometer

(Manchester, UK). The X-ray source was operated at 15 kV, 10 mA, 150 W, the take-off angle was 90° (vertical to sample surface) and the detection depth was not more than 10 nm. EMs were also characterized by Differential Scanning Calorimeter (DSC, TA instrument SDT Q600 equipped with TA instrument's universal analysis 2000 software version 3.9a).

Field Emission Scanning Electron Microcopy (FE-SEM, FEI-QUANTA 200F, The Netherlands) was used to observe the surface morphology of EMs and AMs. The membranes were sputtered with a thin layer of gold before being placed in the SEM chamber. Coated samples were examined at an accelerating voltage of 15 kV. Scanning Electron Microcopy - Energy Dispersive Spectrometer (SEM-EDX, model Tescan Vega-II XMU VPSEM, Tescan USA Inc., Cranberry Twp., PA) was used to provide the atomic percentage at the surface of the EMs and AMs.

Static contact angle (SCA) measurements were performed on the EMs and AMs using an Advanced Surface Technologies, Inc., video contact angle (VCA) Optima Surface Analysis System, Billerica, MA. A water drop of 0.5 µL was dispersed on the membrane surface and the SCA determined using the system software. The asymmetric membranes were dried at 50 ^{o}C overnight before SCA was measured.

The pore-size distribution, bubble point and mean flow pore of EMs were determined using a capillary flow porometer (Porous Materials Inc, USA) which was able to detect pore-size from 0.013 to 500 µm. The membranes were completely wetted with wetting liquid Galwick^{TM} (Porous Materials Inc, USA) and pressure was applied on one side.

Circular EMs of 25 mm in diameter with an effective area of 4.1 cm^2 were stamped out and subsequently used for flux studies. All tests were conducted on an Amicon stirred cell model 8010, which was able to withstand a maximum operating pressure of 75 psig, with a feed capacity of 10 mL. The permeation cell was connected to an 800 mL water bath, as schematically shown in Figure 5.1. The nitrogen gas was used to supply pressure to the feed water. The pressure was slowly increased from 0 to 20 psig and the corresponding water flux was measured by weighing water collected during a predetermined period. The pressure of gas was detected using a digital gauge (Meriam instrument, Merigauge). Constant stirring was applied during the collection of pure water.

7.3. Results and discussion

7.3.1. Surface Modifying Macromolecules (SMMs)

The structure of the SMMs in terms of the number of repeating units (m, n, p, and q (see Figure 7.1)) was obtained as follows. The values of the n and q were calculated from the average molecular weight of PPG and PEG, respectively. The values of m and p were calculated (assuming that all of the added MDI and PPG were consumed) using the number average molecular weight M_n of the SMM obtained from GPC experiments. The results are listed in Table 7.2 together with number average (M_n) and weight average (M_w) molecular weight.

The glass transition temperatures (T_g) at the onset and the mid- point of the thermograph were determined by DSC. The results are also depicted in the Table 7.2. According to the

table, as the molecular weight of PPG increases (from 425 to 3500 Da, or n = 7.02 to 60.03 in Table2), the M_n of SMM also increases.

Table 7.2. Characteristics of different SMMs.

Polymer	m	n	p	q	M_n, kD	M_w, kD	Tg, °C onset	Tg, °C midpoint
SMM-400	9.59	7.02	4.79	8.68	10.9	36.1	19.74	29.06
SMM-600	10.07	7.02	5.03	13.23	15.7	47.9	8.97	18.28
SMM-1000	3.96	60.03	1.98	22.32	19.7	38.4	22.85	29.59

7.3.2. Influence of different SMMs on fiber size

Table 7.2 summarizes the fiber diameters of the different EMs (the last column). The fiber diameter of EM-1000 was by 0.15 μm larger than EM-PVDF. Interestingly, fiber diameters of the EM-400 and EM-600 were much smaller than EM-PVDF and EM-1000, i.e. the fiber size of EM-1000 was larger by ~3.7 times and ~4.3 times than EM-400 and EM-600, respectively. Figure 7.2 shows the surface architecture of the different EMs observed by SEM. There is a direct relationship between the fiber size and the size of the largest pore measured by the bubble point method (Table 7.2, the first column). For example, when the fiber diameter increased by 3.7 times from EM-400 to EM-1000, the bubble point increased by ~1.5 times. Similarly, as the fiber diameter increased by ~ 4.3 times from EM-600 to EM-1000, the largest pore-size increased by ~2.0 times. Other pore-sizes are also included in Table 7.3 to show the degree of pore-size distribution. The above observation indicates that, when the

fiber diameter decreases, the number of fibers per unit area increases and the larger pores are split into smaller pores.

Table 7.3. Pore-size distributions and fiber diameters of the different EMs.

EMs	Largest pore (bubble point) diameter, µm	Mean flow pore diameter, µm	Smallest pore, µm	Fiber size, µm
EM-PVDF	4.77	2.09	1.47	1.00 ± 0.52
EM-400	3.14	0.96	0.47	0.31 ± 0.10
EM-600	2.32	0.68	0.44	0.27 ± 0.09
EM-1000	4.74	2.33	1.02	1.15 ± 0.55

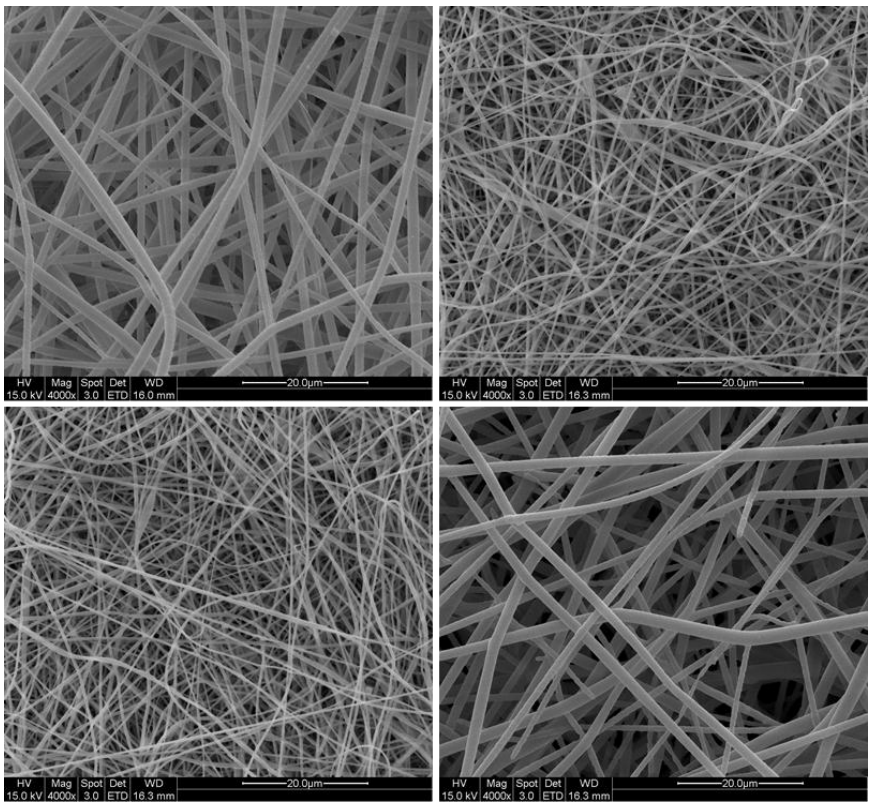

Figure 7.2. Surface architecture of (a) EM-PVDF, (b) EM-400, (c) EM-600, and (d) EM-1000.

7.3.3. Influence of SMM on hydrophilicity.

The three SMMs synthesized had different effects on the surface hydrophilicity of the EMs. As the static contact angle (SCA) data summarized in Table 7.4 show the contact angles of EM-400 and EM-600 (~140° for both) and EM-PVDF (~131°) are much higher than a heat pressed PVDF film (~87^{o}). Significantly higher SCAs of EMs are often recorded for various polymers and the increase in SCAs is attributed to its inherent roughness and trapped air pockets [Wenzel 1936, Cassie 1944, Singh 2005]. On the contrary, EM-1000 had a contact angle of 0^{o}. To understand the observed remarkable differences in SCAs, particularly between EM-1000 and other EMs, XPS analysis was conducted. As the results of the XPS analysis, the atomic concentrations of fluorine (F), oxygen (O), nitrogen (N) and carbon (C) are also listed in Table 7.4. According to Table 7.4, the F content that represents the hydrophobic PVDF decreases from EM-PVDF to SMM blended EMs (EM-400, EM-600 and EM-1000) due to the absence of F in SMM. However, the F content of EM-1000 is not necessarily the lowest. Thus, the atomic compositions obtained by XPS cannot explain the extremely high hydrophilic nature of EM-1000.

Table 7.4. Static contact angle (SCA) and surface atomic composition by XPS of the various blended EMs

Membrane ID	SCA, ^{o}	XPS results, Atomic conc. wt%			
		F (1s)	O (1s)	N (1s)	C (1s)
EM-PVDF	131.54 ± 4.47	51.11	0.56	0	48.34
EM-400	139.79 ± 4.70	44.02	3.04	0.74	52.20
EM-600	140.00 ± 3.10	40.19	4.55	0.98	54.28
EM-1000	0	42.10	4.84	0.06	53.00

In the case of PVDF, it has only three elements (H, C and F) and its N composition was obviously zero as expected. On the other hand, SMMs have additional elemental groups such as N and O. Hence it would be expected that all the three blended membranes would have a high N and O peak under the XPS spectrum. However, the N content was almost negligible for EM-1000 when compared to the other two blended membranes, but the O content for the latter membrane was marginally higher than the other two blended membranes. The content of O increases from SMM-1000 > SMM-600 > SMM-400. This was expected which can be explained as follows. The higher molecular weight PEG and PPG were used to synthesize SMM-1000 when compared to SMM-400 and SMM-600 and hence former has more content of oxygen. But, the N content for EM-400 and EM-600 was 0.74 and 0.98 respectively, which indicates that the N-H group for these two membranes was majorly at the surface and hence the amide group (-NH-C=O) may contribute to a higher contact angle compared to EM-PVDF. The contact angle and XPS analysis suggests that the orientation of the three SMMs within the PVDF blended fiber was different.

SEM-EDX analysis summarized in Table 7.5, on the other hand, provided the results remarkably different from the XPS analysis. Atomic compositions were also calculated based on the assumption that the SMM was uniformly distributed in the EMs using the molecular structures of the SMMs listed in Table 7.3 and the SMMs' content in the EMs. The results are also listed in Table 7.5 in the brackets. It is to be noted that the content of F, the marker for PVDF, measured by EDX is significantly lower than the calculated F value, while the contents for O and N, the markers for the SMM, measured by EDX are significantly higher than the calculated values, indicating the surface migration of the SMM in the EMs. In particular, EM-1000 showed exceptionally low F content and high O content, indicating a

high degree of surface coverage by SMM-1000. The N content was not as high as expected from the remarkable increase of O, about which discussions will be made later in detail.

Table 7.5. EDX results for the various EMs and theoretical atomic compositions (in the bracket) when SMMs are uniformly distributed in EMs

Membrane ID	EDX results, Atomic conc. wt%			
	F	O	N	C
EM-PVDF	-	-	-	-
	(61.3)	(0)	(0)	(38.7)
EM-400	50	4	6	42
	(56.40)	(2.26)	(0.35)	(40.99)
EM-600	54	3	3	40
	(56.40)	(2.36)	(0.31)	(40.93)
EM-1000	2	30	4	62
	(56.40)	(2.56)	(0.09)	(41.00)

The degree of the surface coverage by SMM can be calculated using the atomic composition at the surface. The evaluation of the surface coverage by three SMM components; i.e. PVDF repeat unit, polyurethane repeat units (those including polyethylene glycol and polypropylene glycol soft segments combined) and end-capping groups, was done by using the F and C content of EM-1000. The results were: PVDF repeat unit: 58.1 %, Polyurethane repeat unit: 3.6 % and End-capping group: 38.3 %, indicating that a substantial part of the membrane surface is covered by polyethylene glycol end-capping group. Classifying the type of SMM configuration at the EM surface into 4 modes depicted by Figure 7.3, the above results show

that the configuration of SMM-1000 at the EM surface belongs to type 4 (exposed). On the other hand, SMM-400 and SMM-600 did not migrate to the surface as much as SMM-1000 and many SMM molecules belong to type 1 (embedded).

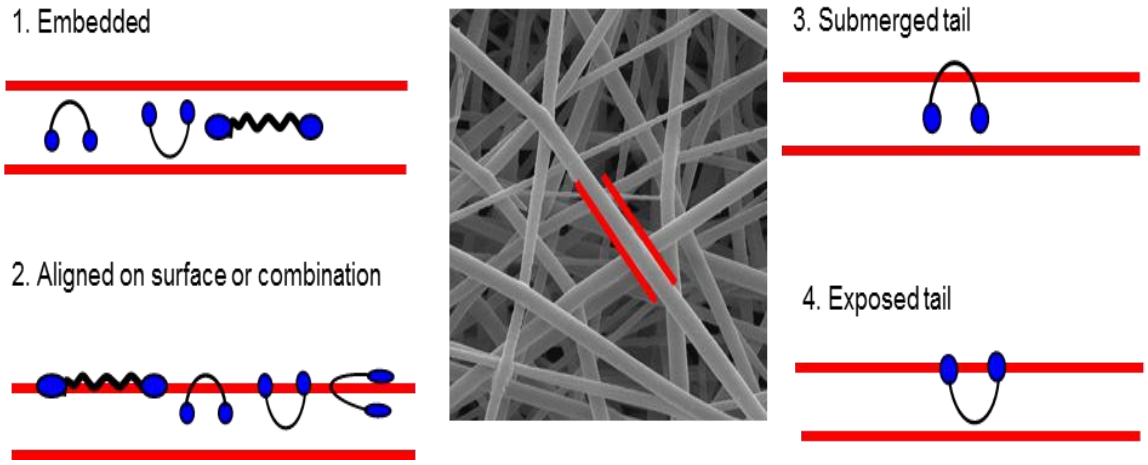

Figure 7.3. Schematic illustration of the SMM configuration on a single fiber.

EDX further allows us to obtain atomic compositions at different parts of the EM. Thus, EDX analysis of EM-1000 was conducted at 53 spots as shown in Figure 7.4. It was revealed that the results are grouped into two categories; one with high N contents of average 10 wt% and the other low N contents of nearly equal to 0 wt%. Since N belongs only to the middle polyurethane section of SMM, the high N content suggests that the surface configuration of SMM-1000 is type 3 (submerged). Thus, SMM-1000 was either in the 3rd or 4th configuration, enhancing, in either case, the surface hydrophilicity as compared to PVDF.

7.3.4. Influence of SMM-1000 on filtration flux

The pure water flux of EM-PVDF and EM-1000 is given in Figure 7.5 and it was observed that the pure water flux of EM-1000 is 20% higher than EM-PVDF. Since both EMs structures are similar (see Figure 7.2 and Table 7.3) the observed increase in water flux was probably due to the increase in hydrophilicity from EM-PVDF to EM-1000. Also, it is to be noted that EM-PVDF looked opaque while EM-1000 appeared transparent after the permeation test.

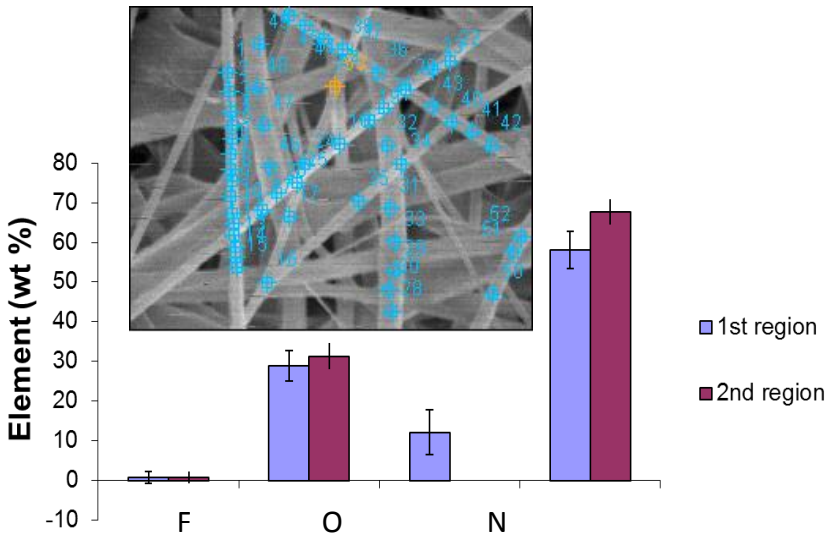

Figure 7.4. Elemental analysis on several fibers of EM-1000.

7.3.5. Influence of SMM on thermal behaviour

The EMs were further characterized by their thermal behaviour. Table 7.6 shows the enthalpy of fusion and the melting point of the EMs. DSC thermograms are given in Figure 7.6. The melting point of the SMM blended membranes changed slightly, either upwards or downwards, from the EM-PVDF. The deviation of melting point from the semi-crystalline

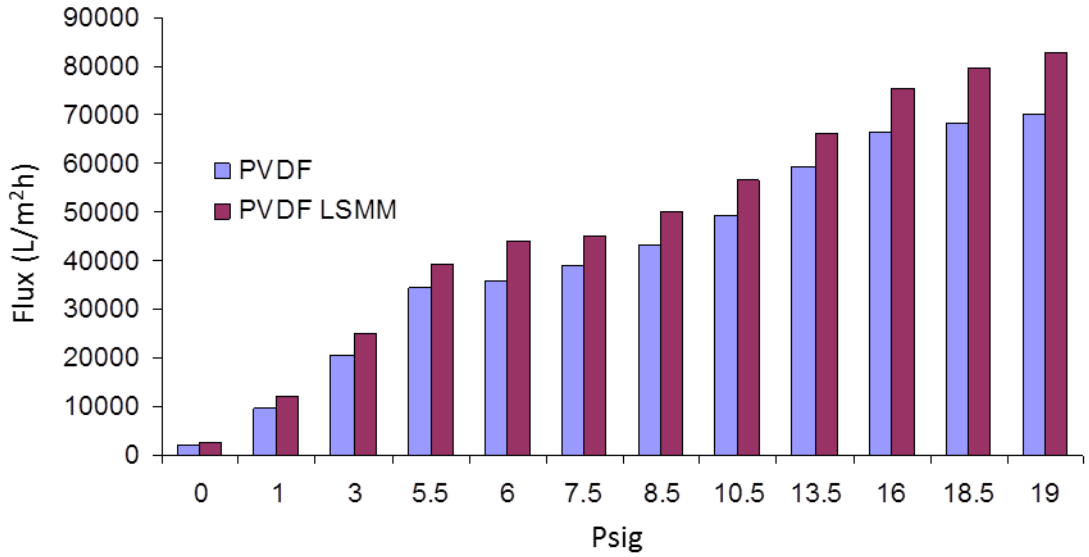

Figure 7.5. Water permeation flux of non-blended EM-PVDF and EM-1000.

PVDF membrane can be explained using polymer-diluent crystallization concept. The pure PVDF is associated mostly with α crystalline phase. When PVDF lamellae are blended, at least partially, by amorphous SMM, the blended system becomes associated more with β crystalline structure due to the presence of SMM. Similar observation, appearance of double melting peaks, has been noticed [Dang 2010]. On the other hand, in the case of enthalpy of fusion, decrease in enthalpy of fusion was noticed from EM-PVDF to EM-400. The blending of EM-400 decreases the crystalline nature of PVDF and thereby increases amorphous structure in the blend. It has been reported in literature that increasing the concentration of PEG-b-PMMA (high molecular weight) in PVDF blend resulted in an increase in the amorphous content [Xiao 2009]. As the length of the PEG increased from PEG-400 to PEG-600 (EM-400 to EM-600) the enthalpy of fusion increased This could be due to the increase in crystalline nature with an increase in PEG length thereby allowing higher amount of packing during crystal growth and hence more energy is required to melt the polymer chains. This indicates that length of PEG and/or PPG chains greatly influence the crystallization of

the PVDF chain segments. It is already reported in literature that PEG 200 is amorphous in nature, whereas PEG 400 and PEG 600 are crystalline in nature [Park 2005]. It is to be noted here that in the case of EM-1000 additional exothermic crystallization peak at higher temperature was observed. In general, the endothermic melting peak is observed at higher temperature than the exothermic crystallization peak. It is suggested that the formation of the strong hydrogen bonding between fluorine (PVDF) and hydrogen (SMM) in the liquid crystalline structure takes place. Notably, the additional peak has been observed for the particular SMM (SMM-1000) due to the higher molecular weight of PPG and PEG in comparison to the other SMMs (SMM-400, and SMM-600).

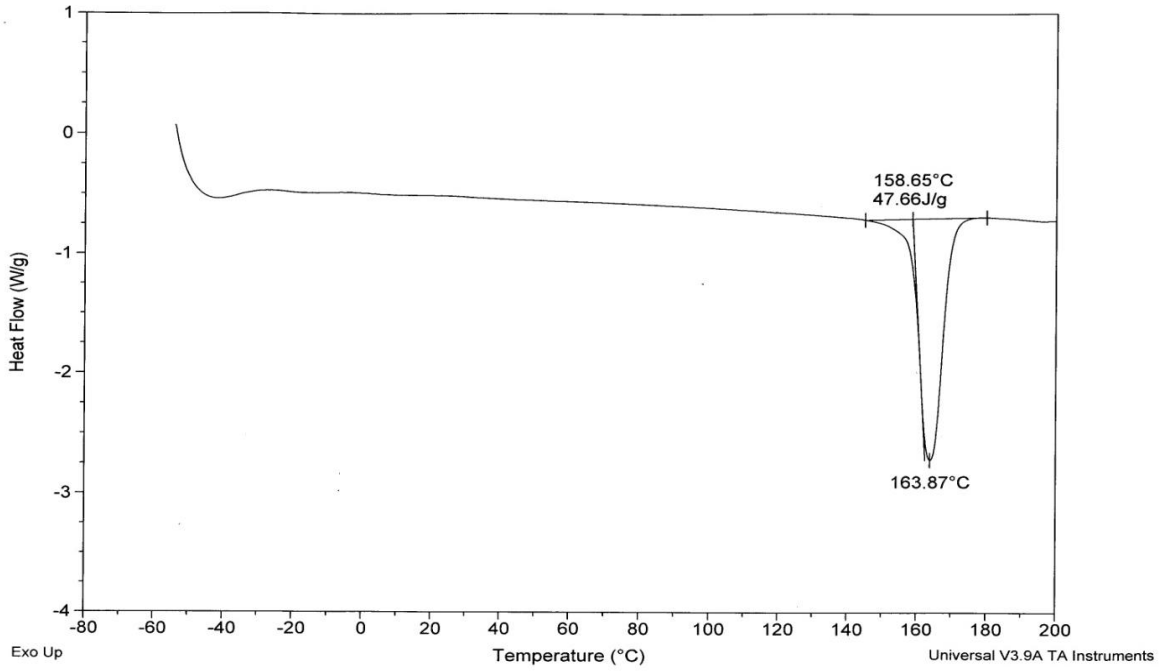

(a) EM-PVDF

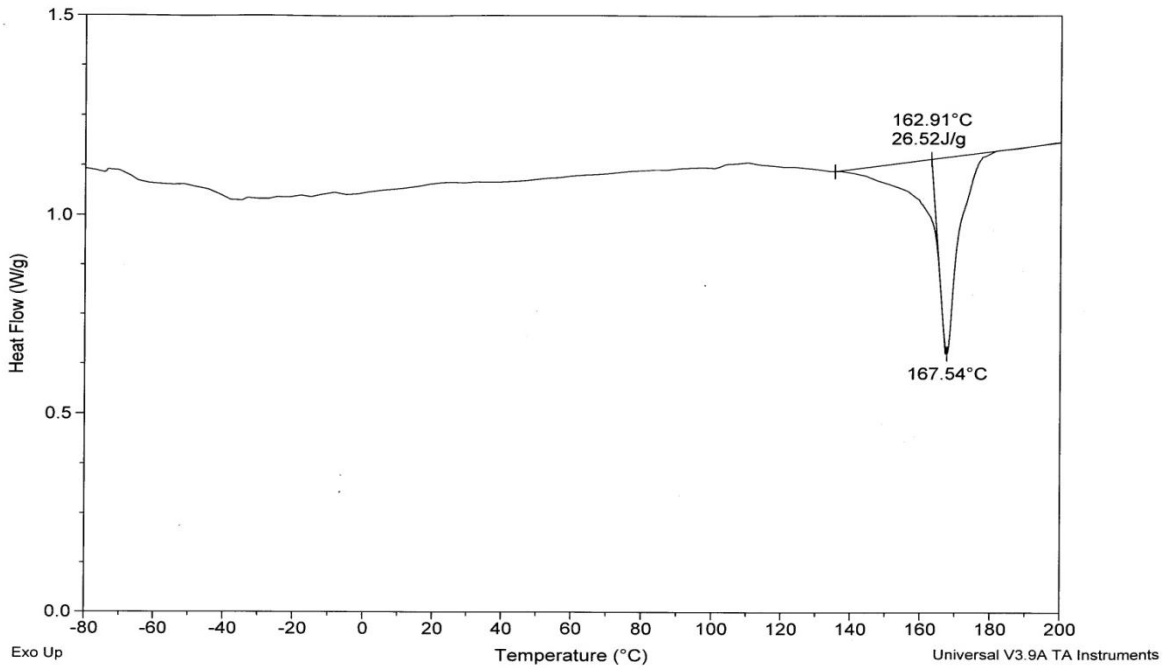

(b) EM-400

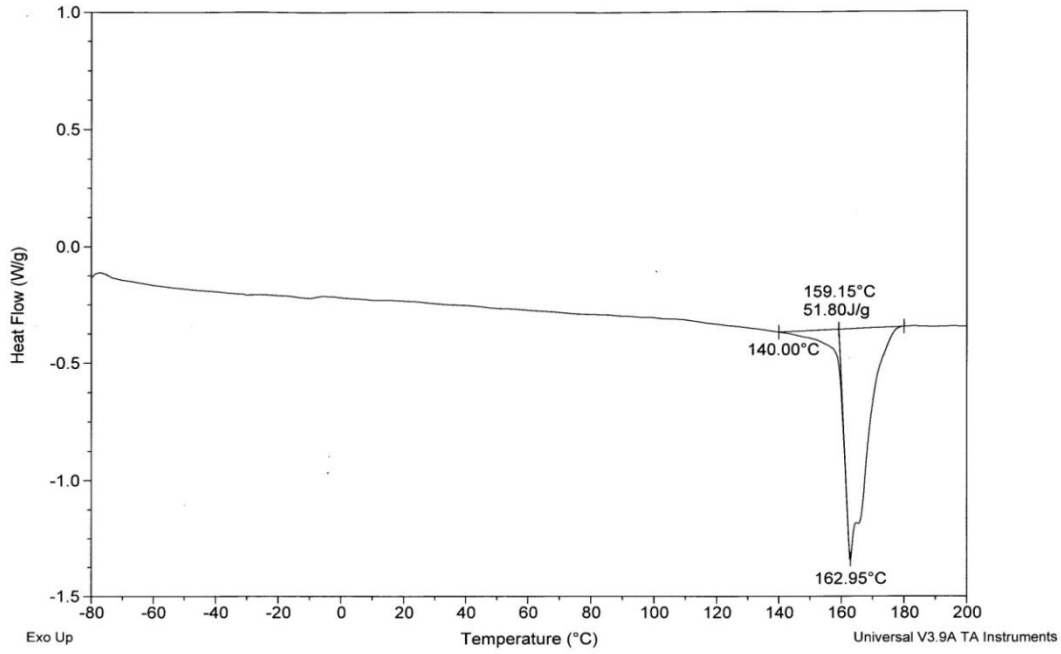

(c) EM-600

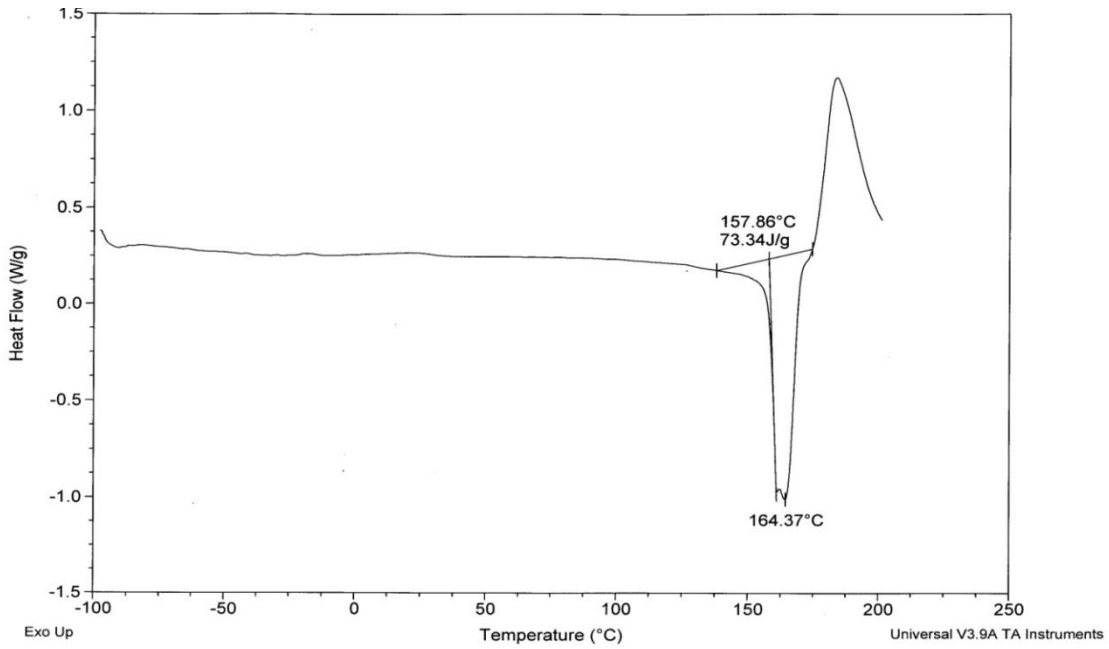

(d) EM-1000

Figure 7.6. DSC response for (a) EM-PVDF, (b) EM-400, (c) EM-600, (d) EM-1000.

Table 7.6. Thermal properties of electrospun membranes (EMs).

EMs	$\Delta H^o_{f,}$ J/g	Melting point (M_p), ^{o}C
EM-PVDF	47.66	163.9
EM-400	26.5	167.5
EM-600	51.8	162.9
EM-1000	73.3	164.3

7.3.6. Influence of SMM in the asymmetric membranes prepared by the phase inversion method

The SCAs of asymmetric membranes (AMs) are summarized in Table 7.7 The SCA of AM-PVDF is very close to the SCA of PVDF film (~87^o). Small changes are noticed from AM-

PVDF to AM-400 and AM-600 but they are within the error range. On the other hand, a significant change is noticed from AM-PVDF to AM-1000 (by 36^{o}).

Interestingly, comparison of Table 7.4 and Table 7.7 reveals large differences between the SCAs of EMs and AMs. First, SCAs of EM-PVDF, EM-400 and EM-600 are much larger than those of AM-PVDF, AM-400 and AM-600, which is ascribed to the presence of a large quantity of air in EMs. From SEM images of EMs (Figure 7.2) and AMs (Figure 7.7) it is obvious that the porosity of EMs is larger than AMs. Therefore, EMs contain a larger amount of air, which increases the SCA. Conversely, the SCA of EM-1000 (nearly 0^{o}) is much smaller than AM-1000 (53.9^{o}). This can be attributed to a much greater coverage of the EM surface, in exposed configuration (see Figure 7.3), by SMM-1000 than the AM surface. This was confirmed by SEM-EDX analysis of AMs, the results of which are summarized in Table 7.8.

Table 7.7. Surface contact angle (SCA) values of the various AMs.

AMs	SCA , ^{o}
AM-PVDF	90.10 ± 9.31
AM-400	102.15 ± 4.56
AM-600	85.89 ± 2.86
AM-1000	53.90 ± 9.70

Comparing among AMs, the F content (marker of PVDF) of AM-1000 was the lowest while its O content (marker of SMM) was the highest. It indicates the highest degree of SMM-1000 migration to the surface and hence the surface becomes the most hydrophilic. This coincides

with the lowest SCA of AM-1000 among all AMs. Comparing Table 7.5 (atomic compositions of EMs) with Table 7.8 (atomic composition of AMs), those of EM-400 and EM-600 are almost the same as AM-400 and AM-600. Therefore, much higher SCAs of EM-400 and EM-600 than those of AM counter parts are due not to higher hydrophobicity of the material, but to the higher porosity of EMs. Comparing EM-1000 and AM-1000, F content of the former is much lower and O content much higher than the latter. This explains the much lower contact angle of EM-1000 than AM-1000.

Table 7.8. EDX results of AMs (wt% given in brackets are theoretical values, see Table 7. 5)

AMs	EDX results, Atomic conc. wt%			
	F	O	N	C
AM-PVDF		-	-	-
	(61.3)	(0)	(0)	(38.7)
AM-400	48.15±4.28	3.60±0.66	4.22±1.46	44.04±4.08
	(56.40)	(2.26)	(0.35)	(40.99)
AM-600	50.14±4.31	4.49±2.25	7.25±1.97	38.13±3.60
	(56.40)	(2.36)	(0.31)	(40.93)
AM-1000	46.66±7.69	7.02±1.93	4.87±2.50	41.45±5.05
	(56.40)	(2.56)	(0.09)	(41.00)

A question arises why the surface of EM-1000 could be highly covered by SMM-1000, while the degree of SMM coverage on the AM-1000 surface was not as high as EM-1000. This may be either due to the much smaller dimension of EM-1000 (fiber diameter was 1.15 μm) as compared to AM-1000 (membrane thickness was ~115 μm) or due to the disruption of the highly packed macromolecules in the surface layer, which prevents protrusion of highly

hydrophilic SMM end-capping groups to the surface, by the high voltage applied during electrospinning process.

Figure 7.7 shows the SEM images of AMs. The figure reveals the gradual increase of pore-size from AM-PVDF to AM-1000. This was probably caused by the increase in the rate of water influx in the solvent/non-solvent exchange process as the surface hydrophilicity increases by the enhanced SMM migration from SMM-400 to SMM-1000.

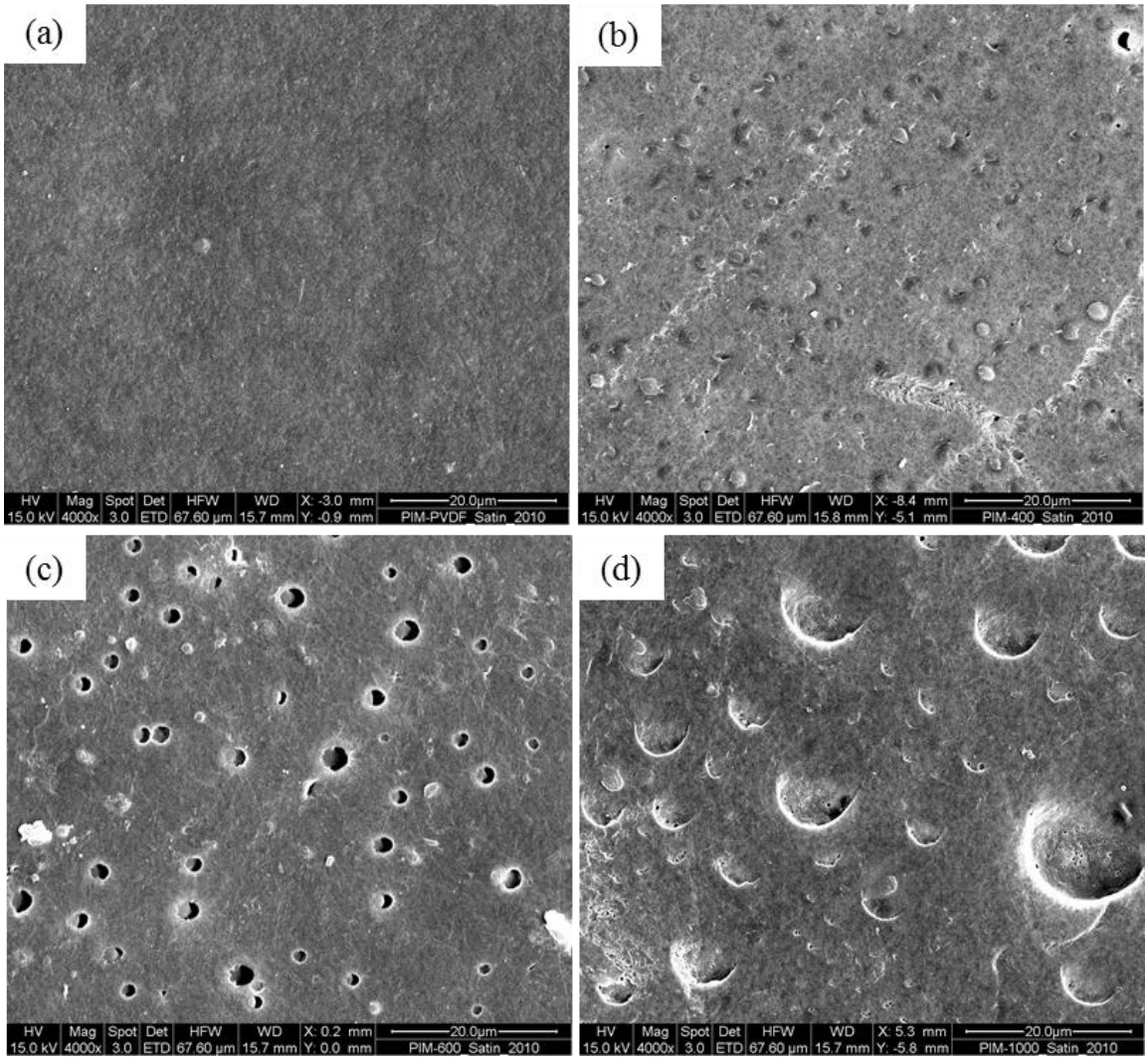

Figure 7.7. SEM of 20 %(v/w) phase inverted membranes: (a) without SMM, (b) with SMM-400, (c) with SMM-600, and (d) with SMM-1000.

7.4. Conclusion

The following conclusions were drawn from the experimental data.

1. Both the fiber diameter and pore-size depended on the SMM used.
2. SMM-1000 played a significant role in increasing the hydrophilicity of the blended electrospun membrane, which has 0^{o} contact angle when compared to SMM-400 and SMM-600 of slightly increased hydrophobicity. This was due to the orientation the SMMs adopted during electropinning in which hydrophobic part of SMM-400 and SMM-600 was majorly at the surface as compared to SMM-1000 wherein the hydrophobic moiety was encapsulated by PVDF polymer.
3. The EM-PVDF showed a higher SCA (~132°) when compared to that of AM-PVDF (~90°), which was due to the large surface pockets and rough topography in the former.
4. When we compare the AM-1000 with EM-1000 membrane, the contact angle did not reach 0° but reduced to ~54° instead. This shows that besides surface modification agents, the nature of membrane formation also plays an important role in influencing the hydrophilicity of the membrane. We believe that during electrospinning process, the SMMs and PVDF chains are phase separated and there is a greater possibility of the SMMs to be at the surface while during phase inversion process the SMMs slowly migrate to the surface and the amount of SMMs on the surface may be smaller.
5. The pure water flux of EM-1000 was 20% higher than that of non-blended EM-PVDF. This indicates that the hydrophilicity of a highly porous membrane does contribute significantly to the water flux.

CHAPTER 8

CONCLUSIONS

8.1. Introduction

The overall purpose of the work in this thesis was to investigate and relate the material-structure-property of ENM in nanofiltration application. The major contributions of this work are reviewed and any recommendations of materials and methods as well as future work are discussed.

8.2. Summary and contributions

Electrospinning is an advantageous technique as it can be used to manipulate both fiber size and cross-sectional thickness of the ENM. The diameter of the fiber can be reduced by decreasing the concentration of the polymer solution and the cross-sectional thickness of the ENM can be adjusted by either increasing or decreasing the collection time of the fibers. This is a very convenient method to adjust the fiber size. Also, by decreasing the concentration of the polymer solution cost of material is reduced. By manipulating these two parameters, the rejection and flux of salt solution can be adjusted as desired. It is concluded from this thesis that for the best rejection and flux data of electrolytes, it is desirable to have the ENM fiber size as small as possible (~40 nm) and thickness layer as thin as possible (<1um). It is to be noted that having this combination without any structural support, the membrane would be considered to be too weak for filtration at high pressures. Hence it is advised that if extremely thin fibers and thin ENM layer is to be considered to support the interfacial layer, these fibers should be deposited on a backing material (BM) as used in the

thesis, any other robust material or fibrous layer possessing thicker fibers, large bubble point (so that it doesn't affect resistance to flow) and last but not least good mechanical strength. The advantages of using a base support layer as discussed above are that it would easily absorb any compression force and ease handling situations.

To ensure that the ENM layer properly adheres to the BM, it is advised that hot pressing should be applied. Without hot pressing, handling difficulties were faced and the ENM layer tended to dislodge from the BM when higher pressures were applied and hence separation became unstable at higher pressure. The pressure, temperature and time of hot pressing should be considered wisely. The criterion of temperature setting is that it should be set either about the polymer's melting point (T_m) or glass transition temperature (T_g) of polymers. In the present study, the T_m and T_g of PAN were found to be 317 ^oC and 85 ^oC, respectively. Hence, in this investigation, the temperature was set at 80 ^oC for low fiber diameter membranes and at 87 ^oC for higher fiber diameter samples. The pressure was adjusted between 0.28 to 0.41 MPa and time of exposure was fixed at 999 s. The surface and cross-sectional morphologies was checked by SEM in order to ensure that fibers are not overfused and the cross-section shows a uniform non-fluffy layer.

To successfully support an interfacial layer at higher pressures such as 190 psig, the ENM has to possess fiber size of less than <400 nm. When a fiber size greater than 400 nm was used i.e. ~570 nm, it was not able to support an interfacial layer when separation was performed at higher pressures. It is to be noted here that when the fiber size was smaller, the bubble point was also smaller, which lead to the higher rejection. An average PAN fiber size of ~ 340 nm (TFNC-8) led to the best flux of 200 L/m^2h of NaCl at a rejection of 54 % while an average PAN fiber size of 67 nm (TFNC-4) with a cross-sectional thickness of 0.54 µm led to the best

NaCl rejection of 78% at a flux of 63.22 L/m^{2}h. When an ENM of fiber size 42 nm (TFNC-E) with cross-sectional thickness of ~<1 µm was used for separation, the rejection of NaCl increased to 83.47% at a flux of 102.34 L/m^{2}h. This study suggested that in-order to obtain a membrane with high rejection and flux, it is essential to use fiber size and cross-section thickness of the membrane to be at its minimum. In the economic point of view, having such parameters are fantastic as less material is required and thereby cost of manufacturing is reduced! If moderate rejections with extremely high fluxes are required, then larger fiber sizes (~400nm) as well as thin cross-sectional ENM layer would be preferred. As such electrospinning is a fantastic technique in manipulating fiber size and overall thickness of the ENM layer.

Another important parameter to be considered is that a hydrophilic ENM layer has to be used so as to successfully facilitate the formation of interfacial layer as well as to increase the flux. This study also suggests that an alternative method to use of hydrophilic polymer is that a hydrophobic membrane can be transformed into a hydrophilic membrane by blending with surface modifying macromolecules prior to electrospinning.

8.3. Recommendations for future work

There are several interesting directions for future work in the areas of research presented in this thesis. The findings contained within this thesis point to ENMs having a role in separation technology. The use of electrospinning provides a membrane scientist with a potential tool to manipulate the architecture at the nano-scale and have those features manifest into interesting properties.

The candidate feels there is so much more to study and evaluate the effectiveness of ENM in NF and has offered her suggestions of other possible parameters that have not been studied and may affect/influence the separation performance as well as possible applications:

(i) It is important to identify if it is the fiber size or the pore size that plays an important role in supporting the interfacial layer. For example if smaller fiber size was used but its pore size was manipulated by depositing the fibers either densely or loosely will it be able to support the interfacial layer and subsequently separate the electrolytes?

(ii) Decreasing the fiber size <10nm and studying its influence on separation,

(iii) Further optimization of the cross-sectional thickness of the ENM layer has to be studied. Will there still be optimal separation if the thickness was reduced to 500 nm or even 100 nm? How much the flux would be increased?

(iv) Compression study with respect to pressure and any structural changes should be looked into. Also, compression study with respect to fiber size and cross-sectional thickness should be studied as well.

(v) Electrospinning aligned fibers that are structurally layered over one another at a certain angles. This is to investigate if alignment of fibers would play an important role in supporting the film and subsequently affect the separation.

(vi) Studying the stability and separation performance of the TFNC membrane over a period of few months and investigating any structural change subjected to the membrane.

(vii) A greater variety of polymer needs to be studied as this will provide a greater understanding of material influence,

(viii) Varying the type of aqueous and organic phases employed for flux enhancement,

(ix) Creating ordered structures where fibers are aligned extremely close to one another and hence reducing the bubble-point and hence subsequently improving the separation

(x) Widening the application of ENM in artificial kidneys, controlled drug delivery systems, electrodialysis, recovery of hydrogen from off-gases, membrane chromatography, forward osmosis (since it is less energy intensive than RO) and (last but not least and not limiting to) in membrane distillation since certain polymeric material such as PVDF are hydrophobic

(xi) Exploring the stretching capability and extent of the thin film on the surface of the ENM and relating it to its selectivity.

References

ArtuÄŸ G, Roosmasari I, Richau K, Hapke J

A comprehensive characterization of commercial nanofiltration membrane

Sep.Sci.Technol. 2007, 42, p. 2947

Aussawasathien D, Teerawattananon C, Vongachariya A

Separation of micron to sub-micron particles from water: Electrospun nylon-6 nanofibrous membranes as pre-filters

J. Membr. Sci., 2008, 315, p. 11

Ayutsede J, Gandhi M, Sukigara S, Micklus M, Chen HE and Ko F

Regeneration of Bombyx mori silk by electrospinning. Part 3: characterization of electrospun non-woven mat

Polymer 2005,46, p. 1625

Baker RW

Membrane Technology and Applications

John Wiley & Sons, Ltd.: Chichester, 2004

Bhattacharyya D. Williams M.

Theory - Reverse Osmosis, in: W.S.W. Ho, K.K. Sirkar (Eds.)

Membrane Handbook, Van Nostrand Reinhold, New York, NY, 1992, p. 269

Bitz K

Non-woven in filtrations

The Non-woven industry, Nov 2001

Bognitzki M, Czado W, Frese T, Schaper A, Hellwig M, Steinhart M, Greiner A and Wendorf J H

Nanostructured Fibers via Electrospinning

Adv. Mater. 2001, 13,p. 70

Bose GM

Recherches sur la cause et sur la véritable théorie de l électricité.

Wittennberg, 1745

Bruggena BV, M¨antt¨ ari M , Nystr¨omb M

Drawbacks of applying nanofiltration and how to avoid them: A review

Sep. and Pur. Tech. 2008,63,p.251

Buchko CJ, Chen LC, Shen Y and Martin DC

Processing and microstructural characterization of porous biocompatible protein polymer thin films

Polymer 1999,40, p. 7397

Casper CL, Stephens JS, Tassi NG, Chase DB and Rabolt JF

Controlling Surface Morphology of Electrospun Polystyrene Fibers: Effect of Humidity and Molecular Weight in the Electrospinning Process

Macromolecules 2004, 37,p.573

Cassie ABD, Baxter S

Wettability of porous surfaces

Trans. Faraday Soc. 1944, 40, p.546

Choi H, Zhang K, Dionysiou DD, Oerther DB, Sorial GA

Effect of permeate flux and tangential flow on membrane fouling for wastewater treatment

Separation and Purification Technology, 2005, 45, p. 68

Chu B and Hsiao B S.

The Role of Polymers in Breakthrough Technologies for Water Purification

J. Polym.Sci., Part B: Polym. Phys. 2009, 47, p. 2431

Cooley JF

Apparatus for electrically dispersing fluids

1902, U.S. Patent no.: 692631

David F, Vokhmin V, Ionova G

Water characteristics depend on the ionic environment. Thermodynamics and modelisation of the aquo ions

J. Mol. Liquids 2001, 90, p. 45

Deitzel J M, Kleinmeyer J, Harris D and Tan N C B

The effect of processing variables on the morphology of electrospun nanofibers and textiles

Polymer, 2001, 42, p. 261

Demir M M, Gulgun Yilgor I, Yilgor E and Erman B

Electrospinning of polyurethane fibers

Polymer, 2002, 43, p. 3303

Dickenson C

Filters and Filtration Handbook

Elsevier Advanced Technology Oxford, UK, 1992, 3rd ed.

Dang HT, Amelot C, Rana D, Narbaitz RM, Matsuura T

Performance of a newly developed hydrophilic additive blended with different ultrafiltration base polymers,

J. Appl. Polym. Sci. 2010,116, p. 2205

Elimelech M, Zhu X, Childress AE, Hong S

Role of membrane surface morphology in colloidal fouling of cellulose acetate and composite aromatic polyamide reverse osmosis membranes

J. Membr.Sci., 1997, 127, p. 101

Esrafilzadeh D, Jalili R, Morshed M

Crystalline order and mechanical properties of as-electrospun and post treated bundles of uniaxially aligned polyacrylonitrile nanofiber

J. appl. Polym.Sci.,2008, 110, p. 3014

Fong H, Chun J, Reneker DH

Beaded nanofibers formed during electrospinning

Polymer, 1999, 40, p. 4585

Formhals A

Process and apparatus for preparing artificial threads

U.S. Patent, 1,975,504, 2,077,373, 2,109,333, 2,187,306, 2,323,035 and 2,349,950.

Frank KK

Chapter 8: Nanofiber Technology

Nanotubes and nanofibers, edited by YuryG, Boca Raton, Fl: Taylor and Francis, 2006.

Furukawa DH and Burton FL

Membrane technologies for water and waste water treatment

Tech Commentary, 1997, p.1

Gilbert W

De Magnete

English translation, 1893 ed. Dover books, 1600

Gopal R, Kaur S, Ma Z, Ramakrishna S, Matsuura T

Electrospun nanofibrous filtration membrane

J. Mem. Sci., 2006, 281, p. 581

Gopal R, Kaur S, Ma Z, Ramakrishna S

Surface Modification and Application of Functionalized Polymer Nanofibers

In Molecular Building Blocks for Nanotechnology: From Diamondoids to Nanoscale Materials&Applications; Manssori, A. G., George, T. F., Zhang, G., Assoufid, L., Eds.; Springer: New York, 2006 b; p. 72

Gopal R, Feng CY, Chan C, Ramakrishna S. Matsuura T
Proceedings of the 2007, AWWA Membrane technology conference
March 18-21, 2007 (a)

Gopal R, Kaur S, Feng C, Chan C, Ramakrishna S, Tabe S and Matsuura T
Electrospun nanofibrous polysulfone membranes as pre-filters: particulate removal
J. Membr. Sci., 2007 (b), 289, p. 210

Gosh AK, Jeong BH, Huang X, Hoek EMV
Impacts of reaction and curing conditions on polyamide composite reverse osmosis membrane properties
J. Membr. Sci., 2008, 311, p. 34

Grafe T, Graham K
Polymeric Nanofibers in Air Filtration Applications
Rev. INJ Spring, 51, 2003

Groitzsch D, Fahrbach E
Microporous multilayer non-woven material for medical applications
US patent 4,618,524, 1986

Hinds WC
Aerosol Technology
John Wiley & Sons, New York, 1982.

Ho JY, Matsuura T, Santerre JP
The effect of fluorinated surface modifying macromolecules on the surface morphology of polyethersulfone membranes

J. Biomater. Sci. Polymer Edn, 2000, 11 (10), p. 1085

Hoek EMV, Bhattacharjee S, Elimelech M
Effect of membrane surface roughness on colloid-membrane DLVO interactions
Langmuir, 2003,19, p. 4836

Hsiao BS, Chu B
Functional nanofibers for environmental applications
J.Mater.Chem. 2008,18, p. 5326

Huang ZM, Zhang YZ, Kotaki M, Ramakrishna
A review on polymer nanofibers by electrospinning and their applications in nanocomposites
Compos. Sci Technol., 2003, 63, p. 2223

Huang C, Chen S., Lai C., Reneker D.H., Qiu H., Ye Y., Hou H.
Electrospun polymer nanofiber with small diameters
Nanotechnology, 2006, 17, p.1558

Hutten IM
Handbook of non-woven filter media
Armsterdam, Elsevier 2007

Kato K, Uchida E, Kang ET, Uyama Y, Ikada Y
Polymer surface with graft chains
Prog. Polym. Sci., 2003, 28, p. 209

Kaur S, Kotaki M, Ma Z, Gopal R, Ramakrishna S and Ng SC
Oligosaccharide functionalized nanofibrous membrane
Int. J. Nanoscience, 2006, 5, p. 1

Kaur S, Ma Z, Gopal R, Singh G, Ramakrishna S and Matsuura T.
Plasma-induced graft copolymerization of poly(methacrylic acid) on electrospun poly(vinylidene fluoride) nanofiber membrane
Langmuir, 2007, 23, p. 13085

Kaur S
Surface modification of electrospun PVDF nanofibrous MF membrane
National University of Singapore, Masters Thesis, 2007.

Kaur S, Gopal R, Ng W.J., Ramakrishna S, Matsuura T.
Next Generation Fibrous Media for Water Treatment
MRS bulletin, 33, Jan. 2008, p. 21

Keith S
Handbook of industrial membranes
Oxford : Elsevier Advanced Technology, 1995

Kesting RE
Synthetic polymeric membranes: a structural perspective
Wiley, New York, 2nd ed, 1985

Khayet M, Suk De, Narbaitz RM, Santerre JP, Matsuura T
Study on surface modification by surface modifying macromolecules and its applications in membrane separation processes
J. Appl. Polymer sci., 2003, 898, p. 2902

Kameoka J, Orth R, Yang Y, Czaplewski D, Mathers R, Coates F and Craighead H

Nanotechnology 2003, 14, p. 1124

Kosmider K, Scott J
Polymeric nanofibres exhibit an enhanced air filtration performance

Filtr. Sep., 2002, 39 (6), p. 20

Kim CK, Kim JH, Roh IJ, Kim JJ

The changes of membrane performance with polyamide molecular structure in the reverse osmosis process

J.Membr.Sci. 2000, 165, p. 189

Kroschwitz JI

Concise Encyclopedia of Polymer Science and Engineering

New York: Wiley, 1990

Kiriukhin MY, Collins KD

Dynamic hydration numbers for biologically important ions

Biophys.Chem 2002, 99, p. 155

Kwak S.Y., Jung S.G, Yoon Y.S., Ihm D.W

Details of surface features in aromatic polyamide reverse osmosis membrane characterizes by scanning electron and atomic force microscopy

J. Polym. Sci., Polym. Phys. Ed., 1999, 37, p. 1429

Larson RE, Cadotte JE, Peterson RJ

The FT-30 Seawater Reverse Osmosis Membrane-element Test Results

Desalination, 1981, 38, p. 473

Lee KH, Kim HY, Ra YM and Lee DR

Characterization of nano-structured poly(ε-caprolactone) non-woven mats via electrospinning

Polymer, 2003, 44, p. 1287

Li L, Zhang S, Zhang X , Zheng G

Polyamide thin film composite membranes prepared from 3,4,5-biphenyl triacyl chloride, 3,3,5,5-biphenyl tetraacyl chloride and m-phenylenediamine
J.Membr.Sci., 2007, 289, p. 258

Li L, Zhang S, Zhang X and Zheng G
Polyamide thin film composite membranes prepared from isomeric biphenyl tetraacyl chloride and m-phenylenediamine
J.Membr.Sci., 2008, 315, p. 20

Mark CP
Handbook of Industrial Membrane Technology
Noyes Publications, New Jersey, U.S.A, edited by Mark CP, 1990

Magarvey RH, Outhouse LE
J. Fluid Mechanics, 1962, 13, p. 151

Matsuura T
Synthetic Membranes and Membrane Separation Processes
Publishers, Boca Raton, CRC Press, 1994

Megelski S, Stephens J S, Chase D B and Rabolt J F
Micro- and Nanostructured Surface Morphology on Electrospun Polymer Fibers
Macromolecules 2002, 35, p. 8456

Mit-uppatham C., Nothitanakul M., Supaphol P.
Ultrafine electrospun polyamide-6 fibers:effect of solution conditions on morphology and average fiber diameter
Macromol.Chem.Phys., 2004, 205, p.232

Mulder M

Basic Principles of Membrane Technology
Kluwer Academic, 1996

Norton CL
Methods of and apparatus for producing fibrous or filamentary material
U.S. Patent 2,048,651, 1936

Nunes SP and Peinemann KV
Membrane Technology in the Chemical Industry
Wiley-VCH verlag GmbH, Weinheim, Germany, 2001

Oh NW, Jegal J, Lee KH
Preparation and characterization of nanofiltration composite membranes using polyacrylonitrile. II. Preparation and characterization of polyamide composite membranes.
J.Appl.Polym.Sci., 2001,p. 2729

Park MK, Kim HS , An JH, Kim J
J. Ind. Eng. Chem. 2005, 11, p. 222

Perry RH and Green DW
Perry's Chemical Engineers' Handbook
McGraw-Hill: New York, 1997, 7th ed.

Peters JMH
Rayleighs electrified water drops
Eur. J, Phys., 1980, 1, p. 143

Peterson RJ
Composite reverse osmosis and nanofiltration membranes
J. Membr. Sci. 1993, 83, p. 81

Porter MC, in: Porter MC (Ed.)
Handbook of Industrial Membrane Technology
Noyes Publ., New Jersey, 1990, p. 61

Ramaseshan R, Sundarrajan S, Liu Y, Barhate RS, Lala NL and Ramakrishna S

Functionalized polymer nanofiber membranes for protection from chemical warfare stimulants

Nanotechnology, 2006, 17, p. 2947

Rana D,Matsuura T, Narbaitz RM, Feng C

Development and characterization of novel hydrophilic surface modifying macromolecule for polymeric membranes

J. Membr.Sci. 2005,249, p. 103

Rana D, Matsuura T

Surface Modifications for Antifouling Membranes

Chem. Rev. 2010, 110, p. 2448

Rao AP, Joshu JJ, Trivedi CV, Devmurari VJ

Structure-performance correlation of polyamide thin film composite membrfanes:effect of coating conditions on film formation

J.Membr.Sci., 2003, 211, p.13

Reneker D H, Yarin A L, Fong H and Koombhongse S

Bending instability of electrically charged liquid jets of polymer solutions in electrospinning

J. Appl. Phys. ,2000,87, p. 4531

Ritcharoen W, Supaphol P, Pavasant P

Development of polyelectrolyte multilayer-coated electrospun cellulose acetate fiber mat as composite membranes

European polymer journal, 2008, 44, p. 3963

Roh IJ, Park SY, Kim JJ, Kim CK

Effects of the polyamide molecular structure on the performance of

reverse osmosis membranes
J.Polym.Sci. PartB-Polym.Phys.,1998, 36, p.1821

Sawicka KM, Perena G
Electrospun composite nanofibers for functional applications
J.Nanoparticle Research, 2006, 8, p. 769

Schafer AI, Fane AG, Waite TD
Nanofiltration, Principles and applications
Elsevier Ltd, 2005, p. 43

Seeram R, Fujihara K, Teo WE, Lim TC, Ma Z
An introduction to electrospinning and nanofibers
World scientific publishing, Singapore, 2005

Shenoy S L, Bates W D, Frisch H L and Wnek G E,
Role of chain entanglements on fiber formation during electrospinning of polymer solutions: good solvent, non-specific polymer–polymer interaction limit
Polymer 2005, 46, p. 3372

Singh A, Steely L, Allock HR
Poly[bis(2,2,2-trifluoroethoxy)phosphazene] Superhydrophobic Nanofibers
Langmuir 2005, 21, p.11604

Singh PS, Joshi JJ, Trivedi JJ, Devmurari CV, Rao AP, Ghosh PK
Probing the structural variations of thin film composite RO membranes obtained by coating polyamide over polysulfone membranes of different pore dimensions
J. Membr. Sci. 2006, 278(1-2),p.19

Son W K, Youk J H, Lee T S and Park W H

The effects of solution properties and polyelectrolyte on electrospinning of ultrafine poly(ethylene oxide) fibers
Polymer 2004, 45, p. 2959

Sforca ML, Nunes SP, Peinemann KV
Composite nanofiltration membranes prepared by in situ polycondensation of amines in a poly(ethylene oxide-b-amide) layer
J.Membr.Sci. 1997, 135(2), p. 179

Strathmann H
Membrane separation processes
J.Mem.Sci., 1981, 9, p. 121

Steffens J
Polymeric and ceramic nanofibers
Filtration, 2007, 7(1),p. 26

Suk DE, Pleizer G, Deslandes Y, Matsuura T
Effects of surface modifying macromolecules (SMM) on the properties of polyethersulfone membranes
Desalination, 2002, 149, p.303

Suk DE, Chowdhury G, Matsuura T, Narbaitz RM, Santerre P, Pleizer G, Deslandes Y
Study on the Kinetics of Surface Migration of Surface Modifying Macromolecules in Membrane Preparation
Macromolecules 2002,35, p.3017

Sundarrajan S, Srinivasan KSV
Synthesis, Characterization, and Mechanism of Polymerization of Poly(but-2-ene sulfide)
Macromol. Rapid Commun. 2004, *25*, p.1406

Suthar A and Chase G

Nanofibers in filter media

Chemical Engineer, 2001, 726, p. 26

Sutherland K

Filter media: current developments

Filtration & Separation, 2006, 44 (1), p. 16

Tang Z, Wei J, Yung L, Ji B, Ma H,Qiu C, Yoon K, Wan F, Fang D, Hsiao B, Chu B

UV-cured poly(vinyl alcohol) ultrafiltration nanofibrous membrane based on electrospun nanofiber scaffolds

J. Membr.Sci., 2009, 328, p. 1

Taylor GI

Disintegration of water drops in electric filed

Proceedings of the Royal Society of London Series A- Mathematical and Physical sciences, 1964, 280 (1380) p.383

Tomaschke JE

Amine monomers and their use in preparing interfacially synthesized membranes for reverse osmosis and nanofiltration

US patent 5,922,203, 1999

Thavasi V, Gurdev S, Ramakrishna S

Electrospun nanofibers in energy and environmental applications

Energy Environ. Sci., 2008, 1, p.205

Vogt H

Filtration solutions for medical devices

Filtr. Sep., 2005,42, (7), p. 36

Wannatong L, Sirivat A and Supaphol P

Ultrafine electrospun polyamide-6 fibers:effects of solvent system and emitting electrode polarity on morphology and average fiber diameter
Polym. Int. 2004, 53, p. 1851

Ward G
Nanofibres: media at the nanoscale
Filtr. Sep., 2005, 42 (7), p. 22

Wenzel RN
Resistance of solid surfaces to wetting by water
Ind. Eng. Chem. 1936, 2, p.988

William JM
Method of dispersing fluids
1902, U.S. Patent no.: 705691

Xiao Q, Wang X, Li W, Li Z, Zhang T, Zhang H
Macroporous polymer electrolytes based on PVDF/PEO-b-PMMA block copolymer blends for rechargeable lithium ion battery
J. Membr. Sci. 2009, 334, p.117

Xinhua Z, Kwangsok K, Dufei F, Shaofeng R, Benjamin SH, Benjamin C
Structure and process relationship of electrospun bioabsorbable nanofiber membranes
Polymer, 2002, 43, p.4403

Yoon K, Kim K, W Xuefen, Fang D, Hsia BS, Chu B
High flux ultrafiltration membranes based on electrospun nanofibrous PAN scaffolds and chitosan coating
Polymer, 2006, 47,p. 2434

Yoon K, Hsiao BS, Chu B
Functional nanofibers for environmental applications
J. Mater. Chem., 2008, 18, p. 5326

Yoon K, Hsiao BS, Chu B

High flux nanofiltration membranes based on interfacially polymerized polyamide barrier layer on polyacrylonitrile nanofibrous scaffolds

J. Membr. Sci., 2009, 326, p. 484

Yuan W, Zydney AL

Humic Acid fouling during microfiltration

J. Membr. Sci., 1999, 157, p. 1

Zhao S L, Wu X H, Wang L G and Huang Y,

Electrospinning of ethyl–cyanoethyl cellulose/tetrahydrofuran solutions

J. Appl. Polym. Sci. 2004, 91, p.242

Zhong X H, Kim K S, Fang D F, Ran S F, Hsiao, B. S and Chu B

Structure and process relationship of electrospun bioabsorbable nanofiber membranes

Polymer 2002, 43, p. 4403

Zupancic JJ, Raymond J

Chlorine-resistant semipermeable membranes

US Patent 4661254, 1987